Energy & Environmental Science

ROYAL SOCIETY OF CHEMISTRY

PERSPECTIVE

View Article Online
View Journal | View Issue

Cite this: *Energy Environ. Sci.*, 2020, **13**, 772

Chemical looping beyond combustion – a perspective

Xing Zhu,[ab] Qasim Imtiaz,†[cd] Felix Donat, †[c] Christoph R. Müller *[c] and Fanxing Li *[a]

Received 23rd November 2019,
Accepted 8th January 2020

DOI: 10.1039/c9ee03793d

rsc.li/ees

As a promising approach for carbon dioxide capture, chemical looping combustion has been extensively investigated for more than two decades. However, the chemical looping strategy can be and has been extended well beyond carbon capture. In fact, significant impacts on emission reduction, energy conservation, and value-creation can be anticipated from chemical looping beyond combustion (CLBC). This article aims to demonstrate the versatility and transformational benefits of CLBC. Specifically, we focus on the use of oxygen carriers or redox catalysts for chemical production – a $4 trillion industry that consumes 40.9 quadrillion BTU of energy. Compared to state-of-the-art chemical production technologies, we illustrate that chemical looping offers significant opportunities for process intensification and exergy loss minimization. In many cases, an order of magnitude reduction in energy consumption and CO_2 emission can be realized without the needs for carbon dioxide capture. In addition to providing various CLBC examples, this article elaborates on generalized design principles for CLBC, potential benefits and pitfalls, as well as redox catalyst selection, design, optimization, and redox reaction mechanism.

Broader context

The chemical industry consumes more than 40 quadrillion BTU of energy while emitting 2.5 Gigatons of carbon dioxide each year. Meanwhile, many established chemical processes are extensively optimized, providing limited space for further energy savings and emission reductions. Chemical looping offers exciting new opportunities to the aforementioned challenges through process intensification. Facilitated by a redox catalyst, a rationally designed chemical looping scheme can reduce the number of unit operations and significantly decrease the exergy loss for chemical production. In some cases, the chemical looping strategy can facilitate a chemical conversion that would be otherwise infeasible in a conventional reaction scheme. While a number of chemical looping based chemical production approaches have shown promising results, this concept can be further expanded to a significantly wider sets of products using a variety of feedstock and energy sources. Given the exciting opportunities offered by chemical looping beyond combustion (CLBC) and the emissions and energy demand in the current chemical production practice, the CLBC design principles and redox catalyst selection/optimization strategies covered in this article can provide useful information for researchers in the general areas of chemical looping, catalysis, particle technology, and process intensification.

1. Introduction

Although the term "chemical looping" was first minted by Richter and Knoche in 1983 in the context of reducing exergy loss in fossil fuel combustion,[1] the concept of chemical looping (CL), *i.e.* decomposition of a chemical reaction into multiple sub-reactions facilitated by solid reaction intermediates, was investigated long before that.[2,3] Owing to the pressing demand for carbon emissions reduction,[4,5] chemical looping combustion (CLC) has been studied extensively over the past three decades as a new technology for power generation with integrated CO_2 capture,[6–22] as evidenced by more than 2400 peer-reviewed publications to date (based on the chemical abstracts service). In comparison, research related to chemical looping strategies prior to 1983 was scattered and often dealt with concepts other than power generation and CO_2 capture.[2,23–25] A good example is the commercially implemented steam-iron process for hydrogen production, which was later replaced by methane reforming in the 1930s.[23] However, besides the limitations from the lack of global policies on fighting global warming *via* carbon capture and storage (CCS)-related technologies, the lack of fundamental

[a] *Department of Chemical and Biomolecular Engineering, North Carolina State University, 911 Partners Way, Raleigh, NC 27695-7905, USA. E-mail: fli5@ncsu.edu*
[b] *State Key Laboratory of Complex Nonferrous Metal Resources Clean Utilization, Faculty of Metallurgical and Energy Engineering, Kunming University of Science and Technology, Kunming 650093, China*
[c] *Department of Mechanical and Process Engineering, Laboratory of Energy Science and Engineering, ETH Zurich, Leonhardstrasse 21, 8092, Zurich, Switzerland. E-mail: muelchri@ethz.ch*
[d] *Department of Chemistry and Chemical Engineering, Lahore University of Management Sciences, D.H.A. Lahore Cantt., 54792 Lahore, Pakistan*
† QI and FD contributed equally to the manuscript.

understanding and absence of effective strategies to design and optimize the reaction intermediates, also known as (oxygen) carriers, have largely hindered the research progress in the "pre-CLC" era. We note that the extensive investigation of the CLC technology[26–37] has built up significant background knowledge and fundamental insights for potential breakthroughs in chemical looping applications well beyond combustion and power generation.[24,25,38–51] It is, therefore, not too surprising to see that the extension of the chemical looping strategy has drawn significant attention over the past decade. In fact, journal articles covering such topics increased by nearly 10-fold over this period.

Although there have been quite a few excellent reviews and books covering the topic of chemical looping, they tend to focus on CLC[26–35] and, in some cases, chemical looping reforming (CLR) both with and without being integrated with CO_2 or H_2O splitting.[38–53] A recent review by Zeng *et al.*[21] provided comprehensive discussions of the various aspects of chemical looping including chemical looping for the production of chemicals. However, CLC and CLR related topics were still the primary focus, and many chemical production cases, as summarized in Table 1, have not been covered. Another review by Bayham *et al.*[22] gave an overview of CLC for power production with CO_2 capture and CLR for hydrogen or syngas production with carbon capture. It mainly focused on the potential process configurations (reaction systems and reactor design) and applications. As a highly versatile and effective process intensification strategy, the chemical looping concept can be applied to many applications beyond CO_2 capture and reforming with significant merits in efficiency improvements, emission reduction, and potential cost savings. This article aims to offer a perspective on various potential applications of chemical looping beyond combustion (CLBC) and the generalized design principles for oxygen carrier or redox catalysts in chemical looping processes.

2. The case for chemical looping beyond combustion

2.1. Chemical looping – the general principle

As illustrated in Table 1, chemical looping can take various forms for numerous applications. Generalized schematics and representative reactions of different chemical looping processes are summarized in Fig. 1 and Table 1, respectively. As can be seen, reactive separation facilitated by solid (oxygen, nitrogen, and hydrogen) carrier particles represents an important underlying feature of all chemical looping reactions and processes. In chemical looping processes, oxygen carrier, usually composed of metal oxides, acts as an oxygen reservoir for oxygen donation and regeneration.[21] Nitrogen carrier composed of nitride or nitride–hydride mixed compounds enables the storage and release of N or/and H in the redox cycle for chemical looping ammonia synthesis.[98] In a similar manner, hydride based hydrogen carrier allows the storage and release of hydrogen to participate in in chemical reactions or shift the reaction equilibrium.[106] Although recent research on nitrogen,[98–105,107,108] and hydrogen[106] carriers offer significant new opportunities, the vast majority of the carriers investigated to date are oxygen carrying agents. In order to maintain coherency, we elected to focus exclusively on chemical looping approaches for chemical production using oxygen carriers, also known as redox catalysts. Table 1 summarizes both the key CLBC schemes reported to date and promising CLBC schemes for future investigations. To further illustrate the thermodynamic favorability of the various potential reaction pathways, Fig. 2 summarizes potential reaction pathways and Gibbs free energy changes (ΔG) among various carbon-containing feedstock and products. To maintain consistency, 1 bar oxygen partial pressure (P_{O_2}) was assumed in all cases. Fig. 2 is intended to be used as a screen tool to determine the thermodynamically favorable reactants, products, and CLBC schemes.[49] It is also important to note that while one can anticipate similar trends in relative ease of product formation irrespective to the oxygen carrier used in CLBC, the equilibrium P_{O_2} of oxygen carriers, which is dependent upon both the composition/phase of the redox pair and the reaction temperature, can span more than 20 orders of magnitudes. This large degree of freedom in P_{O_2} and the ability of chemical looping to decouple a single overall reaction into multiple redox steps, provides unique flexibility in "manipulating" the extent and feasibility of certain chemical reactions, as will be illustrated in Section 2.2. Besides redox based CLBC schemes, this article also covers the use of CO_2 sorbents (*i.e.* calcium looping) to enhance the oxygen carrier-based chemical looping approaches, as will be elaborated in Section 4.4.

A typical chemical looping process involving oxygen-carrying agents is composed of two or more reduction and oxidation steps that form a redox loop. In its simplest form, an oxygen carrier or redox catalyst first donates its lattice oxygen under a low oxygen partial pressure environment. The reduced oxygen carrier is subsequently exposed to an oxidant for the replenishment of its lattice oxygen, thereby completing a two-step redox loop. As illustrated in Table 1, the use of oxygen carrier offers significant flexibility and opportunity for process intensification by breaking an overall reaction into sub-reactions because: (i) besides acting as a reactant, the oxygen carrier also acts as a mass separation agent since the looping reactions prevent the mixing among the products from each sub-step; (ii) the carrier's oxygen donation properties can be tailored for improved thermal management of the overall process; and (iii) the reduction or oxidation steps can be further broken into multiple sub-steps.[15,21] When designed properly, an oxygen carrier can be compatible with various oxidizing and reducing agents to facilitate the generation of multiple value-added products with minimal separation requirements.

From a thermodynamic standpoint, the oxygen donation ability of oxygen carriers/redox catalysts can be evaluated by the equilibrium oxygen partial pressure (P_{O_2}) of the reaction $MeO_x \rightarrow MeO_{x-1} + 1/2O_2$.[49] Redox pairs with high P_{O_2}s, which are suitable for chemical looping air separation (CLAS), chemical looping with oxygen uncoupling (CLOU), or CLC, can only be regenerated with air. As applications summarized in Table 1, CLBC can take advantage of redox pairs with a significantly wider range of P_{O_2}s. As such, valuable products can be produced

Table 1 Representative redox schemes for chemical looping beyond combustion. The redox reactions are named from (R1) to (R41)

Feedstock	Products	Product generation	Balance of the loop	Name of the process[a]	Sample oxygen/ nitrogen carriers
Air	Air separation	(R1) $MeO_x \rightarrow MeO_{x-1} + 1/2O_2$	(R2) $MeO_{x-1} + 1/2O_2 \rightarrow MeO_x$	CLAS	CuO,[49] perovskite[54,55]
Methane	Synthesis gas	(R3) $CH_4 + MeO_x \rightarrow MeO_{x-1} + CO + 2H_2$	(R4) $MeO_{x-1} + 1/2O_2 \rightarrow MeO_x$ (R5) $MeO_{x-1} + H_2O \rightarrow MeO_x + H_2$ (R6) $MeO_{x-1} + CO_2 \rightarrow MeO_x + CO$	CLR	NiO,[56,57] FeO_x[58–62] CeO_2,[63–65] perovskite,[66–68] hexaaluminate[69,70]
	Ethylene	(R7) $CH_4 + MeO_x \rightarrow MeO_{x-1} + 1/2C_2H_4 + H_2O$	(R8) $MeO_{x-1} + 1/2O_2 \rightarrow MeO_x$	CL-OCM	Alkali modified Mn, Fe oxides[71,72]
	Benzene	(R9) $2/3CH_4 + MeO_x \rightarrow MeO_{x-1} + 1/9C_6H_6 + H_2O$	(R10) $MeO_{x-1} + 1/2O_2 \rightarrow MeO_x$	CL-DHA	Mo/Zn ZSM-5 + Fe oxide[73,74]
	Methanol	(R11) $CH_4 + MeO_x \rightarrow MeO_{x-1} + CH_3OH$	(R12) $MeO_{x-1} + H_2O \rightarrow MeO_x + H_2$	CL-Selective oxidation	Copper-exchanged zeolites[75,76]
Methanol	Formaldehyde	(R13) $CH_3OH + MeO_x \rightarrow MeO_{x-1} + CH_2O + H_2O$	(R14) $MeO_{x-1} + 1/2O_2 \rightarrow MeO_x$	CL-Selective oxidation	$FeMoO_4$–Fe_2O_3[77]
C_{2+} hydrocarbon	Ethylene oxide	(R15) $C_2H_4 + MeO_x \rightarrow MeO_{x-1} + C_2H_4O$	(R19) $MeO_{x-1} + 1/2O_2 \rightarrow MeO_x$ or (R21) $MeO_{x-1} + CO_2 \rightarrow MeO_x + CO$	CL-Epoxidation	Ag/$SrFeO_3$[78]
	Ethylene	(R16) $C_2H_6 + MeO_x \rightarrow MeO_{x-1} + C_2H_4 + H_2O$		CL-ODH	Alkali modified Mn and Fe oxides[79–83]
	Propylene	(R17) $C_3H_8 + MeO_x \rightarrow MeO_{x-1} + C_3H_6 + H_2O$		CL-ODH	Mn and La perovskite,[84] and VO_x[85]
	Propionaldehyde	(R18) $1/2C_3H_8 + MeO_x \rightarrow MeO_{x1} + 1/2C_3H_6O + 1/2H_2O$		CL-Selective oxidation	—[b]
	Maleic anhydride	(R20) $1/7C_4H_{10} + MeO_x \rightarrow MeO_{x-1} + 1/7C_4H_2O_3 + 4/7H_2O$		CL-Selective oxidation	Vanadium phosphorous oxygen (VPO)[86]
	Butadiene	(R22) $C_4H_8 + MeO_x \rightarrow MeO_{x-1} + C_4H_6 + H_2O$		CL-ODH	—
	Ethylene	(R23) $C_6H_{14} + MeO_x \rightarrow MeO_{x-1} + 3C_2H_4 + H_2O$		CL-Oxidative cracking	Alkali modified Mn and Fe oxides[87]
Aromatic	Styrene	(R24) $C_8H_{10} + MeO_x \rightarrow MeO_{x-1} + C_8H_8 + H_2O$	(R26) $MeO_{x-1} + 1/2O_2 \rightarrow MeO_x$	CL-ODH	—
	Methylstyrene	(R25) $C_9H_{12} + MeO_x \rightarrow MeO_{x-1} + C_9H_{10} + H_2O$			—
Biomass	Synthesis gas	(R27) $C_xH_yO_z + MeO_x \rightarrow MeO_{x-1}$ + synthesis gas	(R28) $MeO_{x-1} + 1/2O_2 \rightarrow MeO_x$	CLR	Fe oxide[44]
H_2O	Hydrogen	(R29) $H_2O + MeO_{x-1} \rightarrow MeO_x + H_2$	(R30) $MeO_x \rightarrow MeO_{x-1} + 1/2O_2$	Thermochemical splitting	Perovskite,[88] CeO_2,[64] Fe oxide[89]
			(R31) $MeO_x + CO \rightarrow CO_2 + MeO_{x-1}$	CL-WGS	Fe oxide[90–92]
CO_2	CO	(R32) $CO_2 + MeO_{x-1} \rightarrow MeO_x + CO$	(R33) $MeO_x \rightarrow MeO_{x-1} + 1/2O_2$	Thermochemical splitting	Perovskite,[67] CeO_2,[93] Fe oxide[94]
			(R34) $MeO_x + H_2 \rightarrow H_2O + MeO_{x-1}$	CL-RWGS	Perovskite,[95] Fe oxide[96,97]
N_2/H_2	NH_3	(R35) $3/2H_2 + MeN_x \rightarrow MeN_{x-1} + NH_3$	(R36) $1/2N_2 + MeN_{x-1} \rightarrow MeN_x$	CL-ammonia synthesis	Transition metal nitride[98]
		(R37) $H_2O + MeN_x \rightarrow MeO + xNH_3 + (1 - 3x/2)H_2$	(R38) $MeO + [2/(4m + n)]C_mH_n \rightarrow Me + [n/(4m + n)]H_2O + [2m/(4m + n)]CO_2$ (R39) $x/2N_2 + Me \rightarrow MeN_x$		Metal nitride/metal oxide/metal[99–101]
		(R40) $3/2H_2 + 1/\beta MeH_\alpha N_\beta \rightarrow 1/\beta MeH_\alpha + NH_3$	(R41) $1/\beta MeH_\alpha + 1/2N_2 \rightarrow 1/\beta MeH_\alpha N_\beta$		Nitrogen-containing hydride/hydride[98–105]

[a] CLAS, chemical looping air separation; CL-OCM, chemical looping oxidative coupling of methane; CL-DHA, chemical looping dehydroaromatization; CL-ODH, chemical looping oxidative dehydrogenation; CL-WGS, chemical looping water–gas shift; CL-RWGS, chemical looping reverse water–gas shift. [b] Exemplary, promising CLBC schemes that has yet to be investigated.

in both the oxygen carrier reduction and re-oxidation steps. In the reduction or oxygen donation step, CLBC can valorize light alkanes, aromatics or biomass into chemicals *via* chemical looping partial oxidation (CLPOx). Although CO_2 and H_2O are the most stable forms of the oxidation products (other than carbonates), many chemical products, including hydrogen, synthesis gas, alkene, aromatic, alcohol, aldehyde, epoxide, or maleic anhydride, are thermodynamically feasible as illustrated in Fig. 2b. The key challenge for high yields towards these partial oxidation products resides in the design of selective redox catalysts to minimize CO_x and other byproduct formation, as will be elaborated in Section 3.2. In the regeneration step, hydrogen can be produced *via* water splitting or CO from CO_2 splitting. Selective hydrogenation reactions can also be carried out during the re-oxidation of tailored redox catalysts. Although the chemical looping cycles can be more complex

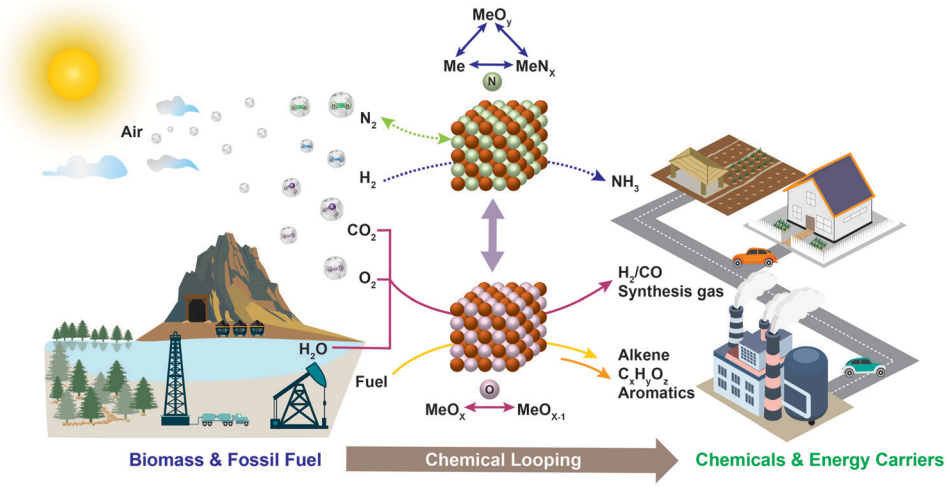

Fig. 1 Schematic illustration of the chemical looping strategy and its potential applications.

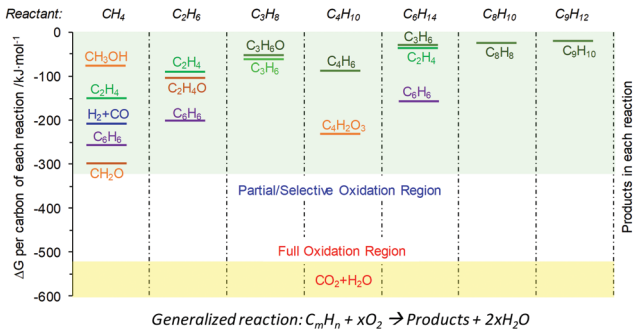

Fig. 2 Normalized reaction Gibbs free energy change (ΔG) per mole of carbon at 700 °C for various potential chemical products from C1–C9 hydrocarbons. Bars with different colors represent the ΔG for the partial oxidation of hydrocarbons to the corresponding products. For consistency, 1 atm gaseous oxygen is assumed to be the oxidant. To calculate ΔG with a specific redox pair as the oxidant (*e.g.* Mn_3O_4/MnO), one can use the corresponding equilibrium oxygen partial pressure (P_{O_2}) of the redox pair at the temperature to account for the oxygen chemical potential change relative to 1 atm O_2.

than conventional processes in the presence of heterogeneous catalysts, they do offer multiple potential advantages from both product selectivity and process efficiency viewpoints, as will be further illustrated in the following sections.

2.2. The case for chemical looping beyond combustion – a second law perspective

As discussed in Section 2.1, a common feature of chemical looping is the ability to facilitate chemical reactions with *in situ* product separation. With separation being the most energy-intensive step in the chemical industry, reactive separation enabled by chemical looping offers excellent opportunities for energy savings and emission reductions. The potential benefits of chemical looping, however, goes well-beyond the simplification of product separations. With strategically designed reaction scheme and intermediates, chemical looping can be intrinsically advantageous over conventional approaches from a second law of thermodynamics perspective. The potential second law (exergy) savings *via* chemical looping result from the following aspects:

a. Exergy savings *via* reactive separation. From a separation standpoint, the redox catalyst in chemical looping acts as a (reactive) mass separation agent, which facilitates feedstock and/or product separation. As such, the driving force (ΔG) for the overall chemical reaction, which is broken down into two or more sub-reactions in chemical looping, can be utilized for separation in an integrated manner. This represents a distinct advantage over conventional separation, in which chemical potential gradients among the various components in a mixture are created *via* extensive cooling or heating (*e.g.* distillation, cryogenic distillation, absorption-stripping, *etc.*) and/or compression (*e.g.* membrane, adsorption, and cryogenic distillation). With tunable thermodynamic properties, the driving forces for sub-reactions (and separation) can also be adjusted in chemical looping to optimize exergy savings. This is exemplified by the partial oxidation (POx) of methane: Under the conventional scheme, synthesis gas is produced from methane in two major steps, that is, cryogenic air separation and methane partial oxidation. Air separation is a thermodynamically uphill process requiring a minimum work input of 6.2 kJ mol^{-1} O_2 for a hypothetical and fully reversible separation process. The actual energy consumption for commercial cryogenic air separation, which requires extensive gas compression, liquefaction, and distillation, is approximately 25 kJ mol^{-1} O_2 (at 1 bar). This corresponds to an exergetic efficiency of ~25%.[109] Even under an idealized scenario,[110] conventional air separation would still lead to an exergy loss of 5.3 kJ mol^{-1} O_2, resulting in a total energy consumption of 11.5 kJ mol^{-1} O_2. As such, conventional methane POx, which consumes gaseous O_2 at a $CH_4:O_2$ stoichiometric ratio of 2 : 1, would consume at least 5.8 kJ of energy in air separation alone for each mole of methane converted. Methane POx, on the other hand, is thermodynamically highly favored with ΔG^0 of −86.7 kJ mol^{-1} of methane converted. Chemical looping POx can take advantage of the large thermodynamic driving force for methane POx and integrate it for air

separation. Using Mn_2O_3 as an example, the two chemical looping sub-reactions are each favored thermodynamically:

$$\text{Sub-reaction 1: } CH_4 + 3Mn_2O_3 \rightarrow CO + 2H_2 + 2Mn_3O_4$$
$$\Delta G_1^0 = -9.8 \text{ kJ mol}^{-1}$$

$$\text{Sub-reaction 2: } 2Mn_3O_4 + 1/2O_2 \rightarrow 3Mn_2O_3$$
$$\Delta G_2^0 = -76.9 \text{ kJ mol}^{-1}$$

$$\text{Overall reaction: } CH_4 + 1/2O_2 \rightarrow CO + 2H_2$$
$$\Delta G^0 = -86.7 \text{ kJ mol}^{-1}$$

As can be seen, the thermodynamic driving force required for air separation is embedded in the chemical looping reactions, thereby eliminating the associated energy consumptions and exergy loss. It is further noted that, even when the chemical looping scheme is used for air separation only, it can be significantly less energy-intensive than cryogenic air separation.[54,55]

b. Exergy savings via in situ conversion of byproducts. The production of value-added chemicals can be intensified by chemical looping, *via* selectively oxidizing the reaction byproducts. As exemplified in Table 1, this principle has been applied to olefin production *via* oxidative coupling of methane, oxidative dehydrogenation, and naphtha oxidative cracking. From a second law standpoint, chemical looping can lead to exergy savings in the following two ways. On one hand, the *in situ* oxidation of byproducts such as hydrogen can compensate for the thermal energy required by endothermic reactions, *e.g.* the non-oxidative coupling of methane or ethane cracking/dehydrogenation. Compared to conventional approaches where hydrocarbon fuels are combusted to neutralize the reaction endothermicity *via* indirect heat transfer through cracker furnaces, *in situ* combustion of hydrogen is intrinsically advantageous due to its lower exergy rate, *i.e.* the ratio between the exergy and enthalpy of a fuel compared to that of hydrocarbons. Fig. 3 illustrates the exergy loss for ideal steam cracking and chemical looping oxidative dehydrogenation (CL-ODH) steps,[111] assuming no heat loss in neither case. When practical factors, such as the temperature difference for indirect heat transfer, are considered, a higher exergy loss can be anticipated for conventional cracking.

A second aspect of exergy savings *via* byproduct oxidation is through enhanced product yields. For instance, steam cracking of both ethane and naphtha are equilibrium-limited.[112] *In situ* combustion of the hydrogen byproduct significantly increases the olefin yield from 50% to nearly 70% in a lab-scale reactor at 850 °C while decreasing the volumetric flow rate of non-condensable product gases by ~40%.[81] The corresponding energy savings in product compression and separation alone correspond to 554 kJ_{th} mol^{-1} of ethylene produced.[113] Due to these reasons, process analyses indicate that the chemical looping approach can lead to more than 80% energy savings for ethane conversion and 50% energy savings for naphtha cracking.[112,113]

c. Ability to circumvent second law limitations by the redox loop. Another potential advantage of dissecting an overall reaction into sub-reactions resides in a higher degree of freedom in terms of thermodynamic characteristics for the individual sub-reactions. Moreover, the operating conditions for each sub-step, *e.g.* temperature and pressure, can be adjusted independently to maximize the product yields from an equilibrium standpoint. A good example of using the chemical looping strategy to circumvent second law limitations of an overall reaction is thermochemical water-splitting to produce hydrogen:

$$H_2O \rightarrow H_2 + 1/2O_2$$

Spontaneous decomposition of water (equilibrium constant, $K \geq 1$) only occurs at ~4100 °C or higher, making thermochemical water-splitting far from practical. This is mainly due to the high reaction enthalpy ($\Delta H^0 = 241.5$ kJ mol^{-1}) and the relatively small reaction entropy ($\Delta S^0 = 43.5$ J K^{-1}). Using the chemical looping principle, however, the overall reaction is broken down into two sub-reactions, as shown in Fig. 4. Take a ceria-based oxygen carrier as an example:

$$\text{Sub-reaction 1: } H_2O + Ce_2O_3 \rightarrow H_2 + 2CeO_2$$
$$\Delta H_1^0 = -126.6 \text{ kJ mol}^{-1}\ \Delta S_1^0 = -82.3 \text{ J K}^{-1}\ \Delta G_1^0 = -104.1 \text{ kJ mol}^{-1}$$

$$\text{Sub-reaction 2: } CeO_2 \rightarrow Ce_2O_3 + 1/2O_2$$
$$\Delta H_2^0 = 368.2 \text{ kJ mol}^{-1}\ \Delta S_2^0 = 125.9 \text{ J K}^{-1}\ \Delta G_2^0 = 333.7 \text{ kJ mol}^{-1}$$

$$\text{Overall reaction: } H_2O \rightarrow H_2 + 1/2O_2$$
$$\Delta H^0 = 241.5 \text{ kJ mol}^{-1}\ \Delta S^0 = 43.5 \text{ J K}^{-1}\ \Delta G^0 = 229.6 \text{ kJ mol}^{-1}$$

Using ceria as the oxygen carrier, the exothermic water-splitting reaction (sub-reaction 1) is favored at lower temperatures[114] but

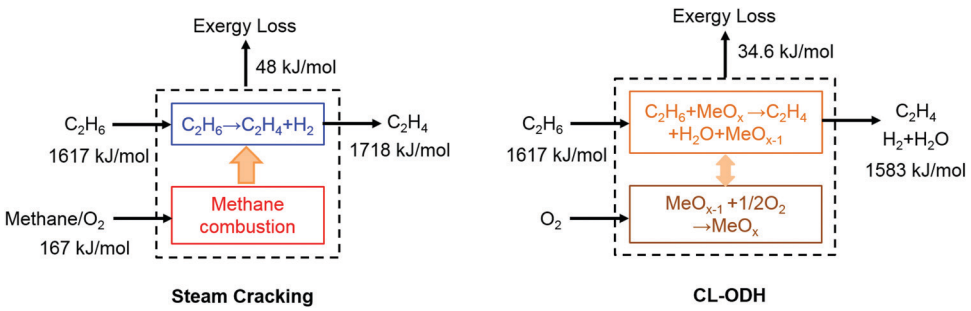

Fig. 3 Availability analysis and exergy loss for idealized steam cracking and chemical looping-oxidative dehydrogenation (CL-ODH) schemes.

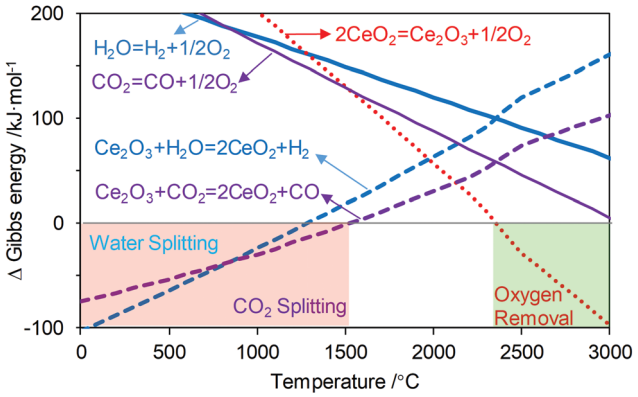

Fig. 4 Ellingham diagram of thermal and chemical looping water and CO_2 splitting. Light green and red regions represent thermodynamically spontaneous ($K \geq 1$) reduction and oxidation reactions, respectively. In practice, a reaction would occur when $K < 1$.

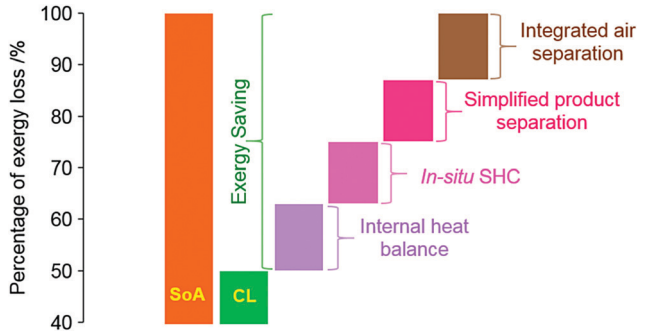

Fig. 5 Schematic illustration of the exergy loss for conventional and chemical looping approaches. SoA: state-of-the-Art (SoA) approaches are typically based on thermal cracking or partial oxidation with oxygen co-feed. SHC refers to selective combustion of hydrogen byproduct, *e.g.* in CL-ODH, chemical looping oxidative coupling of methane (CL-OCM), and chemical looping dehydroaromatization (CL-DHA).

remains favorable up to 1300 °C ($K_{eq} \approx 1$). While the endothermic CeO_2 decomposition reaction is equilibrium-limited at low temperatures, the large entropy term, which increases with temperature, leads to spontaneous decomposition at 2300 °C, or 1800 °C lower than the direct water-splitting temperature (P_{O_2} = 1 bar). While one can argue that 2300 °C is still too high, CeO_2 can be decomposed at much lower temperatures (~1200 °C) in practice by: (i) creating a low P_{O_2} environment through inert purge or vacuum,[115] and/or (ii) inducing oxygen vacancy instead of a phase change. In this case, the chemical looping strategy, which allows "tunable" thermodynamic parameters and operating conditions for sub-reactions, enables an equilibrium-limited chemical reaction, which would otherwise be impossible under reasonable operating temperatures.[116] Using a similar principle, other equilibrium-limited reactions such as CO_2 splitting[117] and thermochemical conversions can also be facilitated by CLBC.[93,98,100,118–121]

d. Tunable exo-/endothermicity of sub-reactions for improved energy integration. Chemical looping would not alter the enthalpy or entropy changes of the overall reaction under (near) isothermal conditions. However, the distributions of the reaction enthalpy/entropy can be modified by varying the type of the oxygen carrier/redox catalyst and the chemical looping sub-reactions. As such, the heat release/demand of individual chemical looping reactors can be adjusted. This additional degree of freedom can enable significantly improved energy integration and hence reduced exergy/energy losses.[122] With an increased understanding of P_{O_2}, phase transition, and catalytic properties for the mixed oxide-based oxygen carriers, the tunabilities of oxygen carriers and hence the corresponding sub-reactions are becoming an increasingly attractive route for efficiency improvements. Fig. 5 summarizes the potential advantages of CLBC over conventional approaches.

2.3 Reasons for CLBC – the practical drivers

Besides the abovementioned thermodynamic "drivers", a strong case can be made for CLBC from a practical standpoint. Commercial implementation of the CLC technology needs to address both technical challenges, in terms of scale-up, and economic challenges, resulting from the low margin of the utility industry and the relatively low economic incentive of the current carbon tax structure.[22,36] A CLC power plant will be more complex and costlier than a standard pulverized coal combustion plant, due to large scale circulating fluidized bed operations, high solids circulation rates, and the need to continuously replenish degraded oxygen carrier particles.[4] Meanwhile, low-cost and long-lifetime oxygen carrier material is required to make CLC cost effective.[4] In addition, concerns over carbon sequestration, a critical downstream step for any carbon capture technology, also limits the wide spread utilization of CLC as a promising carbon capture process.[123–127] CLBC, on the other hand, has the potential to address all the limitations identified above. In contrast to CLC whose economics is likely to be policy driven, CLBC for chemicals production is market driven because the products are of higher value than electric power. As illustrated in Fig. 6, the CLBC concept can be applied to produce chemical products that are significantly more valuable than electricity, thereby increasing the profit margin. In addition, CLBC based on partial oxidation is intrinsically more

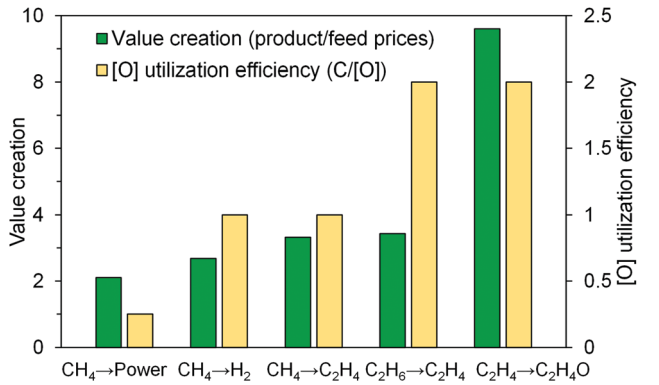

Fig. 6 Valorization and efficiency of oxygen utilization in some typical chemical looping processes.

efficient from an oxygen carrier utilization standpoint. Complete combustion of carbonaceous fuels such as methane consumes a significant amount of lattice oxygen for power generation (four [O] are required for each carbon combusted in CH_4). In comparison, the same amount of lattice oxygen is able to transform eight carbon atoms in ethane into more valuable ethylene products under a CL-ODH scheme (assuming 100% ethylene selectivity whereas ~90% olefin selectivity has been reported experimentally).[79,81,112,128] If oxygen carriers/redox catalysts with identical oxygen storage capacities are used, the CL-ODH plant would correspond to an eight-fold decrease in solids circulation rate compared to a CLC plant with identical feedstock processing capacity on a weight basis. In addition, at least an order of magnitude increase in reaction kinetics was observed for ethane CL-ODH when compared to methane CLC based on the experience at North Carolina State University.[80,81] Considering that ethylene production could significantly increase the gross margin compared to power generation, the "breakeven" plant size for CL-ODH would likely to be one or more order of magnitude smaller than that for CLC from process economics, reaction stoichiometry, and kinetics standpoints. An even stronger case can be made for CLBC of heavier feedstock/products: applying the chemical looping strategy for butane to butadiene, if successful, would lead to a 16 times higher lattice oxygen utilization efficiency than for methane CLC. This simple case study clearly demonstrates the significant advantages of CLBC from process scale up and economic standpoints. Another interesting point to make is that many CLBC processes themselves do not offer the primary benefit of CLC, *i.e.* CO_2 capture, since the target products are chemicals instead of heat (Table 1). However, the process intensification and second law advantages offered by CLBC can still lead to significant CO_2 reductions by producing less CO_2 per unit amount of product generated. A recent study published by Haribal *et al.*[113] indicated that CL-ODH can reduce the CO_2 emissions for ethylene production by 84% when compared to the commercial ethane cracking processes. Such integrated carbon savings without CO_2 capture (except for the removal of a small amount of CO_2 byproducts *via* conventional stripping) eliminates the needs for geological CO_2 sequestration, a potential technical challenge for any CO_2 capture process including CLC.

3. General design strategies for CLBC

3.1 Design considerations for CLBC schemes and limitations

While chemical looping offers various potential advantages as stated in Section 2, it is subjected to a number of limitations, which occasionally are overlooked in CL process analyses. This is somewhat "understandable" considering the complexity of CL processes, which involve dynamic and intertwined gas–solid reactions, *e.g.* the extent of redox catalyst conversion in the reduction step(s) often affects the equilibrium conversion and practical performance of the oxidation step(s). As such, we think it is important to summarize the uniqueness of CLBC as well as its limitations and potential pitfalls in design and analysis of CLBC schemes. Compared to conventional catalytic oxidation or reduction processes, the chemical looping strategy is capable of:

(i) Providing inherently separated product streams to eliminate or alleviate the needs for separation;

(ii) Enhancing process safety by avoiding the direct mixing between a gaseous oxidant (*e.g.* O_2) and reductant (*e.g.* a hydrocarbon);

(iii) Redistributing the overall heat of reaction into two or more steps to simplify heat integration;

(iv) Breaking the "equilibrium barrier" of an overall reaction by carefully selecting redox catalysts, redox pairs[91] and carrying out individual chemical looping steps at substantially different conditions and/or gas–solids contacting modes. For example, the chemical equilibrium limitations in the WGS reaction under a CO–H_2O co-feed mode can be overcome using the chemical looping strategy over a non-stoichiometric mixed oxide, since such an oxide exhibits a large range of equilibrium P_{O_2} as a function of oxygen non-stoichiometry.[91] Metcalfe *et al.*[91] investigated such a scheme using a perovskite ($La_{0.6}Sr_{0.4}FeO_{3-\delta}$) as the oxygen carrier. Using a packed bed reactor operated under a countercurrent contacting mode, a significantly higher overall CO to H_2 conversion (compared to WGS equilibrium conversion) was demonstrated. The unique reactor design and oxygen carrier properties enabled the production of near pure H_2 and CO_2 as separate product streams.

(v) Potentially achieving higher product selectivity by using lattice oxygen as opposed to gaseous oxidants.

However, one must be aware of the following limitations for chemical looping when designing chemical looping schemes or performing process analyses:

(i) The sum of Gibbs free energies of the products from all the chemical looping sub-steps should be smaller than that of the feedstock;

(ii) For a two-step CL process with a single metal/metal oxide redox pair, products from an (oxide) reduction reactor 1 should not be able to oxidize products from an oxidation reactor 2. This principle would apply for both co-currently and countercurrently operated fluidized bed, fixed bed, and moving bed reactors. Using WSG/RWGS reactions[129] as an example, one cannot produce a substantially pure stream of CO_2 or H_2O from reactor 1 while also producing a substantially pure stream of H_2 or CO from reactor 2 if a single redox pair is used. We have to make a choice between a lower CO_2/H_2O yield in reactor 1 and a decreased CO/H_2 yield from reactor 2. Note that this is different from the case illustrated by Metcalfe *et al.*, in which a non-stoichiometric metal oxide was used as the carrier;[91]

(iii) A three-step CL process can allow products from reactor 1 to oxidize products from reactor 2 (since the two reactors and redox pairs do not form a complete loop). However, this is only feasible with an oxidant in step 3 that, when combined with the products from step 2, exhibits a higher equilibrium oxygen partial pressure (P_{O_2}) than do the products from step 1;

(iv) Kinetically, chemical looping reactions are generally much slower than conventional catalytic oxidation/reduction reactions. This is due to the fact that the rates of redox reactions

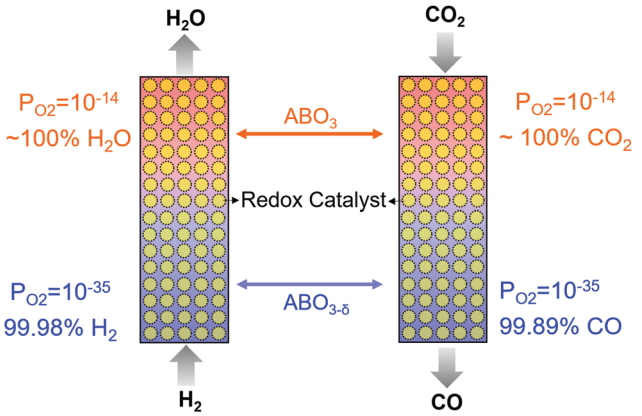

Fig. 7 RWGS in a counter-currently operated two-step chemical looping scheme using ABO_3 perovskite as a redox catalyst at 500 °C.

are limited by the removal and replenishment of lattice oxygen from/to the bulk crystal structure of the redox catalyst. One exception is the CL-ODH operated at thermal cracking temperatures (>700 °C). In that case, the rate of hydrogen combustion by the redox catalysts can often match or exceed the hydrogen generation rate from the cracking reactions.[80,81]

We note that many mixed oxide-based redox catalysts, *e.g.* perovskites, can accommodate significant lattice defects prior to phase transition.[129,130] As such, the redox thermodynamics of these redox catalysts are unique and cannot be categorized as redox pairs. That is, the equilibrium oxygen partial pressure of the oxide is a continuous function of the oxide's (oxygen) vacancy concentration without incurring a distinct phase change.[131] The unique redox properties of these mixed oxides, coupled with counter-current and/or multiple step chemical looping reactor design, can lead to interesting process configurations that are not subjected to limitations (ii) and (iii) presented above. Fig. 7 illustrates a hypothetical case where a mixed oxide redox catalyst with varying equilibrium P_{O_2}s as a function of oxygen storage capacity can be used to break the RWGS equilibrium in a counter-currently operated two-step chemical looping scheme. A comparable effect can be achieved by using more than one redox pairs with different equilibrium P_{O_2}s. In reality, however, one must consider the complex relationships between the oxygen non-stoichiometry of the mixed oxide, which dictates the oxygen mass balance of the redox reactions, and the equilibrium P_{O_2}, which determines the redox thermodynamics, in addition to kinetic and transport effects.

3.2 Oxygen carrier design

3.2.1 Thermodynamic prerequisites and second law guided oxygen carrier selection. Although surface properties of the redox catalysts are essential for their reactivity and product selectivity in CLBC, the redox catalysts need to satisfy certain thermodynamic prerequisites. In terms of partial oxidation reactions, the oxide-based redox catalysts need to provide adequate oxygen chemical potential or equilibrium P_{O_2} to facilitate product generation. Considering the large material design space for redox catalysts, this thermodynamic prerequisite can be used as an effective tool to narrow down the candidate materials. As

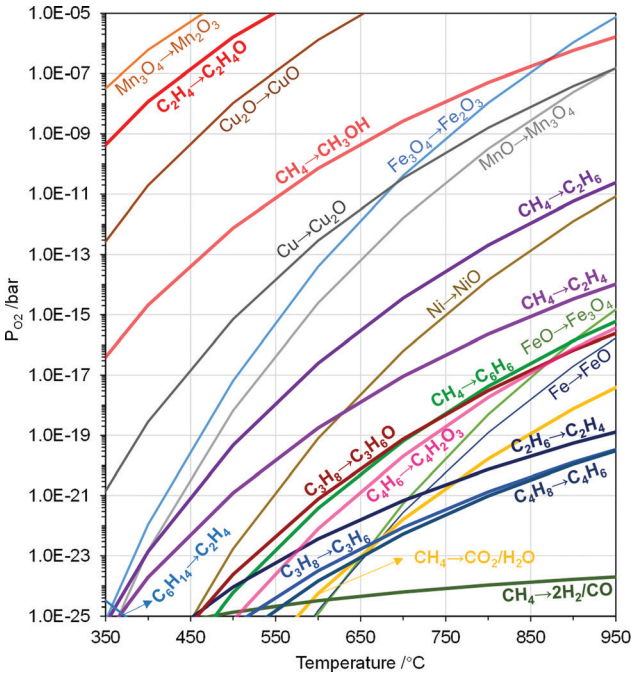

Fig. 8 Modified Ellingham diagram of metal oxide redox and POx reactions. $MeO_x \rightarrow MeO_y$ and hydrocarbons POx reactions correspond to the P_{O_2} when $\Delta G = 0$. Reactions in pathways of $MeO_x \rightarrow MeO_y$ and hydrocarbons POx are given in Table 2.

illustrated in the Ellingham diagram in Fig. 8, one should consider redox pairs above the equilibrium lines of the corresponding POx (selective oxidation) reaction. Taking oxidative coupling of methane (OCM) as an example, it is apparent that redox pairs such as FeO/Fe and Fe_3O_4/FeO should not be considered because they would not be sufficiently "oxidative" to facilitate chemical looping OCM at temperatures ranging from 650 °C to 950 °C. On the other hand, redox catalysts composed of MnO_2/Mn_3O_4 or Mn_3O_4/Mn_2O_3 redox pairs would likely need surface modifications to ensure high selectivities, since their P_{O_2}s are well above that required for OCM. Another thermodynamic consideration for redox pair selection is the upper limit for P_{O_2}. For a CLBC system operated at near atmospheric pressures, practical requirement of >90% O_2 conversion in the air regeneration step would impose an upper limit of 0.02 bar for equilibrium P_{O_2}.

The thermodynamic criteria discussed above are intended for narrowing down the design space of the redox catalysts. Possessing suitable thermodynamic properties alone typically would not ensure high product selectivity. A rare exception is synthesis gas generation. As illustrated in Fig. 2b, synthesis gas is one of the thermodynamically favored oxidation product except for CO_2 and water. As such, synthesis gas selectivity and yield can be optimized by tuning the P_{O_2}s of redox catalysts using Gibbs free energy minimization, as illustrated in a few recent publications.[49,66,67,132] For other POx products with higher Gibbs free energies, however, such a thermodynamically based strategy would not work since the spontaneous decomposition or oxidation of oxygenates to synthesis gas and/or CO_2/H_2O is both kinetically and thermodynamically favored at elevated temperatures.

Aside from being a redox catalyst selection tool, equilibrium P_{O_2}s illustrated in the Ellingham diagram can be used to manage heat distributions among the redox steps involved in CLBC. Due to the endothermicity in the oxygen release step of redox catalysts, a large fraction of the fuel oxidation reactions with redox catalysts in CLBC are endothermic, even though oxidation of a fuel with oxygen would be exothermic. Oxides with higher P_{O_2}s tend to decrease the endothermicity in the fuel oxidation step while decreasing the exothermicity of the redox catalyst re-oxidation step. As such, rationally selected redox pairs can facilitate optimal distribution of the reaction heat in the redox steps to simplify heat integrations. In CLC, a bi-metallic Fe–Cu oxygen carrier composed of CuO and Fe_2O_3 was proposed to shift the endothermic reduction to exothermic or heat neutral.[133,134] This P_{O_2} tuning strategy has also been applied to CLBC, *e.g.* in ethane CL-ODH.[82,83,128]

Redox thermodynamic data for monometallic oxides are readily available, as illustrated in Fig. 8. However, the number of suitable redox pairs are limited when considering the aforementioned thermodynamic criteria. Mixed oxides such as hexaaluminates, spinels, or perovskites, offer significantly increased tunability in terms of redox properties. Moreover, equilibrium P_{O_2}s of many mixed oxides are often variable without incurring phase changes, as discussed in Section 3.1. As such, their multidimensional redox behavior can not be illustrated by a simple redox reaction or a curve in the Ellingham diagram. These unique properties make mixed oxides an intriguing option for CLBC, as illustrated by a number of recent publications.[61,70,135] Among the various mixed oxides, perovskite-type oxides represent a large family of materials that is particularly promising for CLBC due to their highly tunable structural, compositional, and redox properties.[136–138] A recent perspective provided a comprehensive discussion on perovskites as redox catalysts for CLBC.[49]

3.2.2 Surface modifications of redox catalysts. Similar to selective oxidation reactions facilitated by heterogeneous catalysts, a key challenge to redox catalysts in CLBC is to avoid the over-oxidation of desirable products. Recent studies have indicated that surface modifications can be an effective strategy to enhance redox catalysts' activity and/or selectivity.[79–82,128,139] Generally speaking, electrophilic (surface) oxygen species such as O^-, O_2^{2-} (peroxide), and O_2^- (superoxide) are often attributed to non-selective oxidation reactions due to their high activity and electron affinity.[49,140] In comparison, lattice oxygen is often believed to be the "selective" oxygen species in both CLBC and catalytic oxidation reactions involving oxide catalysts. However, such an assignment can be a rather simplistic view since the presence and relative abundance of these oxygen species is not only dependent on the type of oxide but also the reaction conditions and the degree of reduction of the oxide. Recent experimental evidences indicate that lattice oxygen species can be dynamically converted to electrophilic oxygen under chemical looping reaction conditions.[58,139] As such, the abundance of electrophilic oxygen species during the partial oxidation step can be affected by a dynamic balance between: (i) the flux of lattice oxygen from the bulk oxide lattice to the surface; and (ii) the rate of oxygen removal from the surface of the redox catalyst. More facile lattice oxygen flux to the surface would hence allow the transition or relaxation of O^{2-} to electrophilic oxygen especially when such oxygen is bonded with high valency transition metal cations, *e.g.* Fe^{4+} or Mn^{4+}. Therefore, one would anticipate a low product selectivity resulting from the dynamic formation of the electrophilic oxygen species on the surface.

On the other hand, decreased CO_x formation can be achieved by facilitating more facile surface oxygen removal compared to the lattice oxygen flux since the formation of electrophilic oxygen species can be minimized. To ensure a relatively faster surface oxygen removal rate, one can either decelerate the O^{2-} flux or enhance the surface activity of the redox catalyst, as illustrated in Fig. 9. Recent studies have confirmed the effectiveness of both

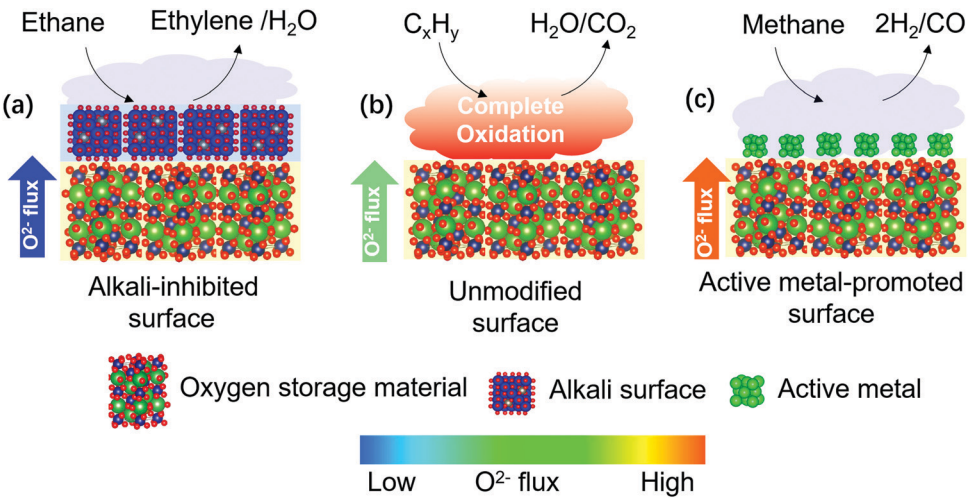

Fig. 9 Schematic illustration of surface modifications of redox catalysts to improve product selectivity by changing the relative rates of surface oxygen removal and bulk O^{2-} flux. The arrows in the three cases (a–c) correspond to the O^{2-} fluxes and the colors correspond to the relative intensity of the O^{2-} fluxes.

approaches. Gao *et al.*[79,128] investigated a $La_xSr_{2-x}FeO_{4-\delta}$-based redox catalyst for CL-ODH of ethane to ethylene. While $La_xSr_{2-x}FeO_{4-\delta}$ promoted the complete combustion of ethane, alkali metal oxide promoters enriched on the surface of the mixed oxide and significantly inhibited the O^{2-} flux from the bulk. As a result, 90% ethylene selectivity was achieved. Besides alkali metal oxide promoters, alkali salt modification also play a similar role to depress O^{2-} flux of the redox catalyst for the selective combustion of hydrogen (SHC) in CL-ODH of ethane to ethylene.[81–83] Enhancement of redox catalyst's surface activity was reported for methane partial oxidation for synthesis gas generation. Shafiefarhood *et al.*[139] reported that impregnating Rh on a $CaMnO_3$-based redox catalyst decreased the methane activation energy on the oxide surface by more than 95%, leading to a decrease in methane conversion temperature by 300 °C and a significantly increased synthesis gas selectivity. Those practices reveal that tuning of the oxygen transfer rate from bulk of a redox catalyst to the catalytically active species on the surface is of great importance for POx. In a redox-involved context, Machida at Kumamoto University found that surface CeO_2 could act as a gateway for oxygen storage in and release from various oxides acting as an oxygen reservoir, such as Fe_2O_3 or $La_2O_2SO_4$.[141–143]

Although the abovementioned strategy for catalyst selectivity optimization has been shown to be effective, we note that it still represents a rather simplified view of the redox catalyst. It would be desirable, from both scientific and engineering standpoints, to determine the active sites and elementary reaction pathways of the chemical looping reactions, but such tasks can be daunting due to the highly dynamic nature of chemical looping reactions. In fact, both the bulk and surface of the redox catalysts can dynamically rearrange throughout the redox cycle.[144] The utilization of modern catalysis and surface science techniques in a few recent studies have already started to reveal fundamental insights on the mechanisms of the redox reactions.[78,128,145–151] However, significant progress still needs to be made to gain additional fundamental insights and this should be a topic of focus for redox catalyst studies within the foreseeable future.

In principle, one can also combine heterogeneous catalysts or active sites with an oxygen storage material to achieve combined catalytic and chemical looping functions. For instance, as will be discussed in Section 4.2.2, Chan *et al.* demonstrated the CL epoxidation of ethylene over $Ag/SrFeO_3$ redox catalyst where Ag acts as the epoxidation catalyst and $SrFeO_3$ acts as the oxygen storage material for oxygen donation.[78] Ethylene was converted to ethylene oxide (with CO_2 and H_2O by products) in the reduction step and the reduced redox catalyst was then replenished with air. Many other CLBC systems can potentially take advantage of such a strategy. Examples include alkane ODH, methane dehydroaromatization, methane oxidative coupling, among others. These topics are discussed in Sections 4.1 and 4.2.

We note that the above discussions are intended to cover the key strategies and the underlying principles for the design of CLBC redox catalysts and reaction schemes. From a practical standpoint, the redox catalyst's activity, available oxygen storage capacity, stability, mechanical strength,[152,153] heat management,[154] cost and environmental risk should all be taken into account to optimize the redox catalyst. The higher margin in the chemical industry over the utility industry can afford significantly higher redox catalyst cost in CLBC. While the raw material cost of some redox catalysts can be high (*e.g.* ceria-based materials), the additional value created for chemical production can potentially accommodate higher redox catalyst costs. Under CLBC schemes, redox catalysts functions similar to heterogeneous catalysts in chemical production processes.[155] It is further noted that a number of CLBC redox catalysts have shown chemical productivities (in terms of weight hourly space velocity) comparable to commercial catalysts.[111] The aforementioned factors should also be considered along with reactor design parameters, operating conditions as well as the reactor/process economics for CLBC process development.

4. CLPOx/CLBC process schemes

4.1 Chemical looping for C_1 valorization

CH_4 is the main constituent of natural gas and an important feedstock for the production of commodity chemicals and liquid fuels.[156] It can be converted into methanol, NH_3 and other higher hydrocarbons either directly *via* a one-step process or indirectly *via* a synthesis gas (a mixture of CO and H_2) intermediate. At present, the only cost-effective route to convert CH_4 into valuable chemicals is *via* synthesis gas.[157] Synthesis gas can be obtained from CH_4 using the following three reactions: steam reforming (R62), dry reforming (R63) and partial oxidation (R49).[158] At the industrial scale, the catalytic steam methane reforming (SMR) is used predominantly to produce synthesis gas. Although SMR is highly optimized, it is a very energy-intensive process and releases large quantities of CO_2 into the atmosphere.[131] To reduce the energy demand of SMR, a part of CH_4 is combusted internally with oxygen or air. The resulting so-called autothermal reforming process enhances CH_4 conversion and reduces CO_2 emissions, but at the expense of lowered synthesis gas yields.[57] Recently, dry reforming of methane (DRM) has received a lot of attention due to its potential to convert two greenhouse gases (*i.e.* CH_4 and CO_2) into an equimolar mixture of CO and H_2 desired for Fischer–Tropsch synthesis.[159,160] Although this concept has many environmental and economic incentives, there is currently no commercial process for DRM. Unlike reforming reactions, methane POx is mildly exothermic allowing for auto-thermal operation at temperatures exceeding 1000 °C. Methane POx can be performed either at elevated temperatures (>1200 °C) without a catalyst or at lower temperatures (<900 °C) in the presence of a platinum group metal (PGM) based catalyst (*e.g.*, Pt, Pd, Rh, Ru, *etc.*).[161,162] Commercial methane POx processes incur a significant efficiency loss due to high operating temperatures. The catalytic route can be costly due to the high cost of the PGM and safety concerns. Both approaches also are challenged by the high cost and energy intensity of pure O_2.

In 2000, Lyon and Cole[163] proposed a chemical looping approach to transfer oxygen from air to a fuel using solid oxygen carriers

Table 2 Reactions for $MeO_x \rightarrow MeO_y$, hydrocarbon partial oxidation, and calcium/carbonate looping reactions illustrated in Fig. 8

Category	Pathway	Reaction
Metal oxide redox pairs	$Mn_3O_4 \rightarrow Mn_2O_3$	(R42) $4Mn_3O_4 + O_2(g) \rightarrow 6Mn_2O_3$
	$MnO \rightarrow Mn_3O_4$	(R43) $6MnO + O_2(g) \rightarrow 2Mn_3O_4$
	$FeO \rightarrow Fe_3O_4$	(R44) $6FeO + O_2(g) \rightarrow 2Fe_3O_4$
	$Cu_2O \rightarrow CuO$	(R45) $2Cu_2O + O_2(g) \rightarrow 4CuO$
	$Cu \rightarrow CuO$	(R46) $2Cu + O_2(g) \rightarrow 2CuO$
	$Ni \rightarrow NiO$	(R47) $2Ni + O_2(g) \rightarrow 2NiO$
Combustion	$CH_4 \rightarrow$ Power	(R48) $1/2CH_4(g) + O_2(g) \rightarrow 1/2CO_2(g) + H_2O(g)$
Partial oxidation/selective oxidation	$CH_4 \rightarrow$ Synthesis gas	(R49) $2CH_4(g) + O_2(g) \rightarrow 2CO(g) + 4H_2(g)$
	$CH_4 \rightarrow CH_3OH$	(R50) $2CH_4(g) + O_2(g) \rightarrow 2CH_3OH(g)$
	$C_2H_4 \rightarrow C_2H_4O$	(R51) $2C_2H_4(g) + O_2(g) \rightarrow 2C_2H_4O(g)$
	$C_3H_8 \rightarrow C_3H_6O$	(R52) $C_3H_8(g) + O_2(g) \rightarrow C_3H_6O(g) + H_2O(g)$
	$C_4H_6 \rightarrow C_4H_2O_3$	(R53) $2/5C_4H_6(g) + O_2(g) \rightarrow 2/5C_4H_2O_3(g) + 4/5H_2O(g)$
Oxidative coupling	$CH_4 \rightarrow C_2H_4$	(R54) $2CH_4(g) + O_2(g) \rightarrow C_2H_4(g) + 2H_2O(g)$
	$CH_4 \rightarrow C_2H_6$	(R55) $4CH_4(g) + O_2(g) \rightarrow 2C_2H_6(g) + 2H_2O(g)$
Oxidative dehydroaromatization (DHA)	$CH_4 \rightarrow C_6H_6$	(R56) $4/3CH_4(g) + O_2(g) \rightarrow 2/9C_6H_6(g) + 2H_2O(g)$
Oxidative dehydrogenation or cracking	$C_2H_6 \rightarrow C_2H_4$	(R57) $2C_2H_6(g) + O_2(g) \rightarrow 2C_2H_4(g) + 2H_2O(g)$
	$C_3H_8 \rightarrow C_3H_6$	(R58) $2C_3H_8(g) + O_2(g) \rightarrow 2C_3H_6(g) + 2H_2O(g)$
	$C_4H_8 \rightarrow C_4H_6$	(R59) $2C_4H_8(g) + O_2(g) \rightarrow 2C_4H_6(g) + 2H_2O(g)$
	$C_6H_{14} \rightarrow C_2H_4$	(R60) $2C_6H_{14}(g) + O_2(g) \rightarrow 6C_2H_4(g) + 2H_2O(g)$
	$C_6H_{14} \rightarrow C_3H_6$	(R61) $2C_6H_{14}(g) + O_2(g) \rightarrow 4C_3H_6(g) + 2H_2O(g)$
Reforming	$CH_4 \rightarrow$ Synthesis gas	(R62) $CH_4(g) + H_2O(g) \rightarrow 3H_2(g) + CO(g)$
		(R63) $CH_4(g) + CO_2(g) \rightarrow 2H_2(g) + 2CO(g)$
Methane cracking	$CH_4 \rightarrow H_2$	(R64) $CH_4(g) \rightarrow C(s) + 2H_2(g)$
Dehydroaromatization	$CH_4 \rightarrow C_6H_6$	(R65) $6CH_4(g) \rightarrow C_6H_6(g) + 9H_2(g)$
Anaerobic conversion	$CH_4 \rightarrow CH_3OH$	(R66) $CH_4(g) + H_2O(g) \rightarrow CH_3OH(g) + H_2(g)$
Super-dry reforming	$CH_4/CO_2 \rightarrow CO/H_2O$	(R67) $CH_4(g) + 3CO_2(g) \rightarrow 4CO(g) + 2H_2O(g)$
Calcium/carbonate looping	$CaO \leftrightarrow CaCO_3$	(R68) $CaO(s) + CO_2(g) \leftrightarrow CaCO_3(s)$
		(R69) $CH_4(g) + 2H_2O(g) + CaO \rightarrow CaCO_3(s) + 4H_2(g)$
		(R70) $2CH_4(s) + 4CuO(s) + 4NiO(s) + CaCO_3(s) \rightarrow CaO(s) + 4Cu(s) + 4Ni(s) + 3CO_2(g) + 4H_2O(g)$
RWGS	$CO_2/H_2 \rightarrow CO/H_2O$	(R71) $CO_2(g) + H_2(g) \rightarrow CO(g) + H_2O(g)$
Methanol oxidation	$CH_3OH \rightarrow CH_2O$	(R72) $2CH_3OH(g) + O_2(g) \rightarrow 2CH_2O(g) + 2H_2O(g)$

for a number of applications such as pollution control, production of inert gases, delivery of heat to endothermic reactions, *etc.* Since then various chemical looping cycles have been proposed to address the limitations of conventional CH_4 conversion processes (see in Table 2). Sections 4.1.1 and 4.1.2 provide a brief summary of the chemical looping approaches related to indirect and direct CH_4 conversion routes, respectively.

4.1.1 CL methane conversion to synthesis gas. Compared to conventional CH_4 reforming processes that utilize gaseous oxidants, the two-step chemical looping approach, schematized in Fig. 10, relies on the lattice oxygen of a solid oxygen carrier to partially oxidize CH_4 *via* (R3).[63,164,165] A subsequent re-oxidation step then replenishes the lattice oxygen. If air is used in the regeneration step to re-oxidize the reduced oxygen carrier, *via* (R4), the overall reaction is methane POx and hence the chemical looping cycle is also referred to as CL-methane POx.[166] Unlike the conventional methane POx reaction (R49), the chemical looping route does not require pure oxygen, thereby eliminating the need of an energy- and cost-intensive air separation unit (ASU). Further, the actual CH_4 conversion step using lattice oxygen (when the oxygen carrier is reduced) is endothermic. Depending upon the thermodynamic characteristics of the oxygen carrier, it can also be re-oxidized using H_2O,[167,168] see (R5), resulting in the so-called CL-SMR.[64,169] Here, two separate streams of synthesis gas (with a $CO:H_2$ ratio of 1 : 2) and high-purity H_2 are produced inherently, thus intensifying the production of high-purity H_2 from CH_4. It is noted here that CL-SMR would become the CL-WGS process if CO instead of CH_4 were used to reduce the oxygen carrier.[42,96,170,171] Both CL-SMR and CL-WGS are also referred to as CL-water-splitting processes.[47,172] Recently the CL-DRM cycle, in which CO_2 is used to regenerate the oxygen carrier (*via* (R6)), has been proposed to maximize the conversion of CO_2, captured from various emission sources, to CO.[96,162,167,173–175] The modified CL-methane POx coupled with H_2O–CO_2 splitting[176] for the oxygen carrier regeneration allows the production of syngas with identical compositions in both the reduction and regeneration steps.[121,177,178]

The oxygen carriers used in the above-mentioned chemical looping processes are often called redox catalysts because they simultaneously act as an oxygen donor (*i.e.* as a reactant) and as a catalyst. NiO, Fe_2O_3, CeO_2, spinel and certain perovskite-based oxides possess suitable thermodynamic properties that permit their use as redox catalysts for chemical looping conversion of CH_4 to synthesis gas.[41,179–184] Among various oxygen carriers, Ni-based oxygen carriers are particularly attractive for CLR owing to their high catalytic activity for CH_4 reforming.[56,185–191] NiO possesses a low selectivity towards synthesis gas, but as NiO reduces to Ni the selectivity towards synthesis gas increases.[56] However, Ni is highly prone to deactivation *via* carbon deposition under low oxygen partial pressures[187] and the formation of sulfides in the presence of feedstock containing sulfur species.[192]

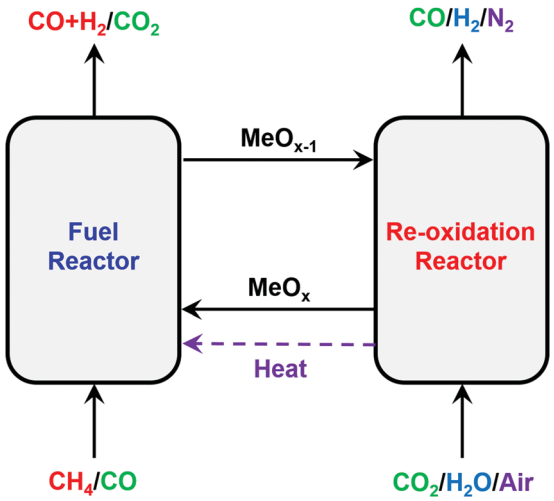

Fig. 10 Schematic and reaction schemes of different CL cycles for conversion of CH_4 to synthesis gas.

Moreover, Ni is a known carcinogenic, thus possessing significant health and safety risks.[193] Fe-Based redox catalysts are also very promising for CL-methane POx owing to their suitable thermodynamic properties for both CH_4 reforming and H_2O/CO_2 splitting, low cost and minimal environmental impact.[90,194] However, compared to Ni-based oxygen carriers, Fe-based redox catalysts possess a low reactivity with CH_4 and a low selectivity towards synthesis gas.[195] Because of their high activity and thermal stability, La-based perovskites with Fe, Mn, or Co as B-site cations have been widely investigated in recent years for CL-methane POx and CL-SMR.[58–60,64,66,88,89,139,179,196–198] As mentioned above, the structural and compositional tailoring of the redox catalysts can open up extensive possibilities for improvements of CLR processes. Since the objective of this part of the perspective is not to present a comprehensive review of the redox catalysts used for CLR, we briefly summarize some of the strategies that have been demonstrated to enhance the reactivity and selectivity of redox catalysts in the following sections.

Stabilization by a mixed conductive support. The redox catalysts typically comprise of a primary metal oxide as an oxygen reservoir and an inert support to stabilize the metal oxide. The appropriate combinations of oxygen carriers and supports can potentially increase the selectivity of synthesis gas and reduce catalyst deactivation.[199] For example, it has been demonstrated that the use of a mixed conductive support (such as $La_{0.8}Sr_{0.2}FeO_{3-\delta}$ or $Ca_{0.8}Sr_{0.2}Ti_{0.8}Ni_{0.2}O_3$) enables fast solid state O^{2-} and electron/hole exchange[92,131,200] between the metal oxide crystallites and the surface of oxygen carrier particle, thereby allowing effective oxygen removal and restoration during reactions (R3) and (R4).[201,202] Importantly, supports that promote the outwards diffusion of active metal should be avoided because such supports can potentially deactivate the redox catalysts *via* surface enrichment and agglomeration of the active metal oxide crystallites.[203]

Core–shell architecture. The spatial distribution of support in an oxygen carrier particle also significantly affects its activity and selectivity.[204] For example, Shafiefarhood *et al.*[59] demonstrated that an Fe_2O_3@$La_xSr_{1-x}FeO_3$ (LSF) core–shell material was 10–200 times more active, selective and resistant to carbon formation than composite iron oxide-based materials comprising inert (Al_2O_3 and $MgAl_2O_4$), ionic-conductive (YSZ), and mixed-conductive (LSF) supports. Neal *et al.*[58,60] and Shafiefarhood *et al.*[205] investigated the mechanism for CH_4 partial oxidation over an Fe_2O_3@LSF core–shell material and found four distinct regimes, *viz.* (i) full oxidation of CH_4 to CO_2, (ii) competing full oxidation to CO_2 and partial oxidation to CO, (iii) partial oxidation of CH_4 to CO, and (iv) CH_4 decomposition. During deep oxidation in region (i) "loose" lattice oxygen from the iron oxide core transports and evolves into surface oxygen species. In region (ii), both selective and non-selective (*i.e.* loose) oxygen species compete for CH_4 oxidation, with O^{2-} flux and overall oxygen availability determining the product ratio. In region (iii), dissociatively adsorbed CH_x species are partially oxidized by O^{2-} species on the surface, resulting in an increase in metallic iron species along with a decrease in the concentration of oxygen surface species. Coke formation in region (iv) results from the depletion of O^{2-} in the iron oxide core and CH_4 decomposition over metallic iron precipitated from the LSF lattice. Transient pulse studies showed that oxygen anion conduction and/or its evolution to electrophilic surface oxygen species is the rate-limiting step in all the reduction regions of interest.[205] Oxygen atoms maintain a modified Mars–van Krevelen (MvK) mechanism throughout the reaction, while the mechanism of CH_4 oxidation changes from the Eley–Rideal in region (i) to a Langmuir–Hinshelwood-like mechanism in region (iii). These findings indicate that redox catalyst architectures that inhibit the formation of non-selective surface oxygen species while maintaining a steady supply of lattice oxygen to the surface can potentially lead to an improved performance for CL-methane POx.

Use of promotors. Ni- and Fe-based oxygen carriers have a high catalytic activity for the decomposition of CH_4, *via* (R64). Promotion of redox catalysts with a transition metal that is inactive for the dissociation of CH_4, *e.g.* Cu, Ag, or Au, can suppress the formation of carbon during the CH_4 reforming step.[206] In this regard, Imtiaz *et al.*[207] demonstrated that doping of Fe_2O_3 with CuO significantly lowers its propensity for coke deposition in a CH_4 atmosphere. The high resistance to carbon deposition of Cu modified oxygen carriers was found to be due to the (partial) coverage of surface Fe with Cu. Some transition metals (*e.g.* Ru, Rh, Ir, *etc.*) can expedite the dissociation of C–H bonds in CH_4[206] and can therefore enhance the reforming activity of redox catalysts. Shafiefarhood *et al.*[139] reported a significant improvement in the performance of Rh-promoted $CaMnO_3$ and $La_2Ce_2O_7$ redox catalysts for CH_4 reforming. It was found that a higher concentration of CH_x species on the surface of Rh-promoted catalysts accelerates the extraction of facile oxygen resulting in an enhanced O^{2-} conduction through the bulk of the redox catalyst. Therefore, a higher redox activity and synthesis gas selectivity was observed for Rh promoted redox catalysts at temperatures as low as

500 °C than for pristine catalysts. Similar findings were reported by Palchelva *et al.*[208] for Rh promoted $La_{0.8}Sr_{0.2}(Fe_{0.8}Co_{0.2})_{1-x}Ga_xO_3$, which showed a 40% enhancement in CO selectivity for methane conversion at 600 °C. Noble metals, modification with CeO_2 nanoparticles can also improve the oxygen storage capacity and mobility in perovskite[68] or iron oxides,[63,64,141,209] which in turn can enhance the availability of lattice oxygen for the methane POx to synthesis gas.

4.1.2 CL methane to chemicals. The selective oxidation of CH_4 to value-added chemicals has been studied extensively, but no significant breakthroughs have been achieved that would enable commercial adoption. A key reason lies in the thermodynamic limitations: CH_4 is more favorably converted to CO_2 and H_2O than to C_1 oxygenates or C_{2+} hydrocarbons, as evident when comparing the Gibbs free energy changes for the respective reactions (Fig. 2b).[210] In consequence, the reactions must be controlled kinetically through suitable catalysts.[211] Even if CH_4 is converted successfully to the desired products, these products tend to be more reactive than CH_4 and can get oxidized readily to CO_x, thus lowering the overall yield.

For CL-based CH_4 partial oxidation, gaseous O_2 is substituted by lattice oxygen. This eliminates the expensive air separation, ensures safer operation and inhibits non-selective oxidation reactions in the gas phase when carried out at high temperatures.[212,213] In addition, the use of lattice oxygen is also shown to potentially benefit the product selectivity.[214,215] Challenges in the design of suitable redox catalysts relate to the following aspects of CL-based CH_4 oxidation processes:[213] (i) CL would likely to require higher operating temperature than co-feed which may negate the selectivity benefit of using lattice oxygen, and (ii) the surface and bulk of the CL redox catalyst tend to undergo notable changes during the redox reactions, which makes maintaining a high product selectivity challenging. Below we briefly discuss several CH_4 conversion schemes that were shown to be feasible in chemical looping mode.

Oxidative coupling. The oxidative coupling of methane (OCM) is a method proposed in the early 1980s to convert CH_4 directly into ethane and ethylene according to reactions (R55) and (R54) at temperatures >600 °C.[216] The exothermic reactions can be carried out either in "normal" catalytic fashion where oxygen is co-fed with CH_4, or in a cyclic redox (chemical looping) operation expressed by reactions (R7) and (R8).[212,217,218] For either mode, an upper limit of 25–30% yield for C_{2+} hydrocarbon products has been supposed based on mechanistic considerations,[215,217,219] which is near the yields required for economic competitiveness.[220–222] Various engineering means have been suggested to improve yields, but no breakthroughs have been achieved to date.[213,223,224] It is worth noting that early studies by Atlantic Richfield company, which operated a 12 year program on OCM focusing on the redox mode, reported an approximately 10% higher C_{2+} selectivity under the chemical looping mode compared to the conventional catalytic route.[215]

The OCM reaction occurs *via* a complex mechanism including coupled heterogeneous and homogeneous steps (depending on the catalyst) and is initiated by breaking one of the four equivalently strong C–H bonds of the methane molecule to form methyl radicals.[224,225] The low yields for C_{2+} hydrocarbons obtained so far are largely due to secondary oxidation reactions of these reactive products with oxygen weakly bound to the surface of the catalyst and with oxygen in the gas phase, forming a significant amount of CO_x.[71,222,226,227] More recently, the upper yield limit for C_{2+} products in the absence of gas phase reactions was estimated to be as high as 60% at elevated pressure, which could possibly be achieved *via* chemical looping.[225,228] Experiments with doped-Mg_6MnO_8 and $Mn/Na_2WO_4/SiO_2$, a catalyst previously shown to attain single pass C_{2+} product yields of ~25% in co-feed mode,[229,230] gave C_{2+} product yields of 23.2% and 25%, respectively under a chemical looping mode.[231–234] In these studies, the selectivity toward the coupling reaction was high, but the H_2 molecules formed through the dehydrogenation reaction of ethane competed with CH_4 molecules for reacting with activated oxygen on the surface of the catalyst, resulting in a decreasing rate of CH_4 activation and consequently lower C_{2+} yields than expected.[222] Hence, improving the activity of the redox catalysts without negatively affecting their selectivity is one important task. In addition, the reaction conditions (*e.g.* temperature and pressure) probably need to be revised to surpass C_{2+} product yields of 30%.[235] The importance of dopants in Mg_6MnO_8 was highlighted recently,[234] and it was found that Li-doping-induced oxygen vacancies reduce the adsorption energy of methyl radicals and increase the C–H activation barrier, resulting in an increased selectivity towards C_{2+}. For doped Na_2WO_4 on SiO_2-supported MO_x catalysts (where M = V, Cr, Mn, Fe, Co or Zn) it was found previously that their performance is correlated with their electrical conductivity.[236]

Non-oxidative dehydroaromatization. Non-oxidative dehydroaromatization (DHA) is a promising route to produce C_6H_6 directly from CH_4. Conversion of CH_4 to C_6H_6 *via* reaction (R65) was first reported in 1993 using a ZSM-5 zeolite modified with Mo or Zn.[237] Since then, a wide range of metals and zeolites have been investigated for DHA of CH_4, but Mo-modified ZSM-5-based catalysts still remain the most effective.[238,239]

Despite being a potentially attractive pathway to selectively produce high-value aromatics, CH_4 DHA has not yet been commercialized due to the following reasons: Firstly, CH_4 DHA (R65) is endothermic and limited by the thermodynamic equilibrium. From Fig. 11, it can be seen that the amount of C_6H_6 produced is only significant at high temperatures (*i.e.* >600 °C). Secondly, the inevitable decomposition of CH_4 (R64) under reaction conditions not only lowers the equilibrium yield of C_6H_6 substantially but also causes coking and catalyst deactivation.[241] Consequently, C_6H_6 selectivity is typically between 60–80% at CH_4 conversions of ~10%, corresponding to net C_6H_6 yields of <10% under conditions of practical interest.[239] Several strategies have been proposed to overcome these barriers, *e.g.* the use of membrane reactors to remove H_2 produced during reaction[242] or the periodic regeneration of the coked catalyst.[73] Recently, a CL approach was suggested to potentially address all three limitations of conventional CH_4 DHA process as following (Fig. 11):[145] (i) the reactive separation

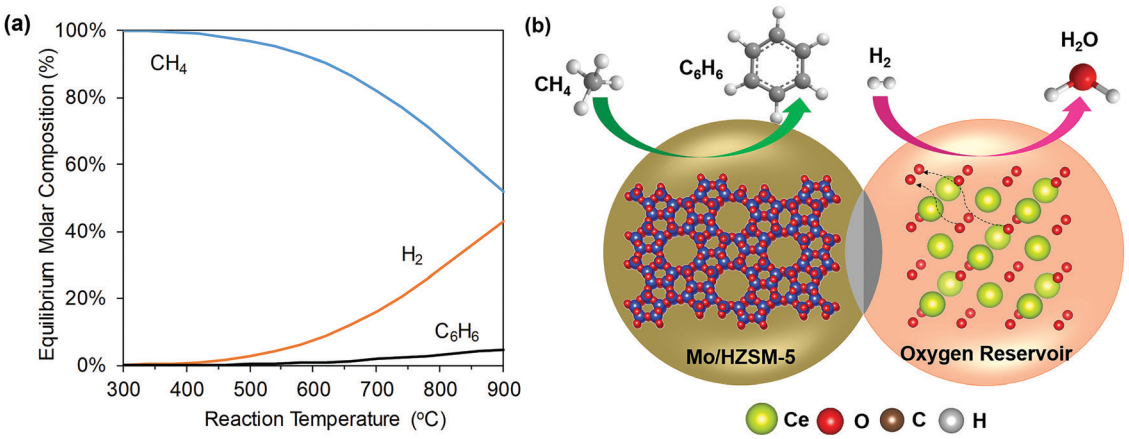

Fig. 11 (a) Equilibrium product composition of CH_4 DHA as a function of reaction temperature. (b) A potential configuration of methane CL-DHA process (the air regeneration step is not shown).[240]

of H_2 from the products of DHA reaction to enhance the equilibrium CH_4 conversion and C_6H_6 yield, (ii) heat generation by selective H_2 combustion to decrease the overall heat demand, and (iii) *in situ* steam generation to reduce coking. However, care must be taken because excessive presence of steam can negatively affect catalyst selectivity. Moreover, re-oxidation requirements for CL may affect the active MoC_x species on Mo/ZSM-5. Using Mo/HZSM-5 (as the DHA catalyst) and $Ce_{0.9}Gd_{0.1}O_y$ (as the SHC redox catalyst) in a composite bed, an approximately three times higher aromatics yield was demonstrated compared to the conventional process employing only Mo/HZSM-5 without periodic regeneration with oxygen.[145]

Besides the two-step approach, Brady *et al.*[240] proposed a four-step approach for CL-DHA. In the first step, DHA reaction is performed on a Mo/H-ZSM-5 catalyst at 700 °C to obtain a mixture of CH_4, C_6H_6 and H_2. Subsequently, H_2 present in the DHA effluent is combusted selectively using Fe_3O_4. The H_2O produced in step two is then removed using a high-temperature water adsorbent, *e.g.* Zeolite 5A, which can be regenerated using a temperature swing. Finally, the reduced oxygen carrier is re-oxidized back to Fe_3O_4 using steam. To increase the conversion of CH_4 and the yield of C_6H_6, the effluent from step three is fed again to the DHA unit in the subsequent cycle. Brady *et al.*[240] demonstrated each of these above steps. Based on extrapolation, the upper limit of aromatics yield for such a process was estimated to be ~43%.[240] However, an integrated CL-DHA process under such a multi-step scheme has yet to be demonstrated. Furthermore, the oxidation of Fe to Fe_3O_4 with steam is thermodynamically limited. It is also to be noted that the regeneration of Fe with water instead of air renders the overall process endothermic. The use of water for regeneration by Brady *et al.*[240] may have been (partially) motivated by the lack of H_2 combustion selectivity of Fe_2O_3. Although this CL-enhanced DHA scheme is quite innovative, it could be simplified while accounting for the aforementioned design considerations. For this, other SHC redox catalysts with higher H_2 combustion selectivities should be considered in addition to iron oxides.[83,145]

Direct conversion of CH_4 to CH_3OH. Direct conversion of CH_4 to CH_3OH (and/or formaldehyde) *via* (R50) is thermodynamically feasible. However, despite over a century of research the development of such a process remains a challenge owing to (i) a large energy barrier associated with the activation of the C–H bonds of CH_4, and (ii) a lower stability of CH_3OH than CH_4, resulting in further oxidation of CH_3OH to CO_2.[243] Consequently, CH_3OH is currently produced on a commercial scale from synthesis gas derived from coal or CH_4.[244]

To date, no heterogeneous catalyst exists that can activate CH_4 according to reaction (R50) while simultaneously inhibiting CH_3OH oxidation at practical yields.[245] Interestingly, in nature monooxygenase (MMO) enzymes convert CH_4 selectively into CH_3OH at ambient temperature.[246] The active sites in these enzymes, *i.e.* binuclear iron and copper centers, can be mimicked using zeolite frameworks. However, so far with Fe and Cu-based zeolites a high selectivity for CH_3OH is only achievable at very low CH_4 conversions ($<0.1\%$).[247,248] The low CH_3OH yields of the direct aerobic conversion of CH_4 to CH_3OH process is a thermodynamic feature that cannot be overcome by the choice of catalyst. Nonetheless, this thermodynamic constraint can be circumvented by using a CL approach and soft oxidants such as H_2O or N_2O.[75,76,249–251] For example, using a Cu-exchanged mordenite zeolite, Sushkevich *et al.*[252,253] reported an anaerobic CL process based on the reaction (R66) to avoid the over-oxidation of CH_3OH. In the proposed three-step process, the Cu-exchanged mordenite zeolite was first activated at 400 °C in a flow of either dry O_2 or He, followed by exposure to CH_4 at 200 °C and 7 bar to form methoxy species. Subsequently, the methoxy species were desorbed in the form of CH_3OH under a flow of a H_2O/He mixture. Once the desorption step was complete, the second reaction cycle was started by heating the zeolite again to 400 °C under a flow of dry O_2 or He. This process resulted in a normalized CH_3OH production rate of ~20 μmole CH_3OH $g_{catalyst}^{-1}$ h^{-1} (based on a cycle time of 6.7 h) with a selectivity of 97%, which is considerably higher than the CH_3OH production rate of 1.81 μmole CH_3OH $g_{catalyst}^{-1}$ h^{-1} reported for a continuous process using O_2 as the oxidant.[254]

4.2 Chemical looping for C_{2+} valorization

4.2.1 ODH of light alkanes. As illustrated in Section 2, the chemical looping strategy has been explored to intensify the production of ethylene,[111] an important commodity chemical with a worldwide production capacity exceeding 150 million tonnes per year.[255] Compared to the well-established, yet energy- and carbon-intensive ethane (and naphtha) cracking processes, the CL-ODH approach (Fig. 12) has the potential to reduce the energy consumption and CO_2 emissions for ethylene production by as much as 87%.[113] The significant process intensification of CL-ODH is enabled by: (i) built-in air separation *via* chemical looping; (ii) higher ethane conversion with autothermal operations *via* the *in situ* oxidation of hydrogen; and (iii) simplified downstream product separation due to the higher ethylene yield and the combustion of hydrogen.[256] We note that extensive research has been conducted for catalytic ethane ODH in the presence of gaseous oxygen,[257–260] but with limited success,[261,262] The key challenges for catalytic ODH resides in the cost of oxygen, safety issues related to the oxygen/ethane co-feed, the lack of catalysts with high activity and selectivity, and the complexity for the removal of oxygenate byproducts. To date, no suitable ODH catalysts have been identified to achieve sufficiently high olefin yields (~70%) such that ODH could replace the commercial steam cracking processes.[263,264] Moreover, most of ODH reactions were carried out at very low ethane partial pressures (<0.1 bar) due to safety concerns. In contrast, CL-ODH avoids direct contact between ethane and oxygen, provides integrated oxygen separation, and has demonstrated superior olefin yields (>70%)[265] at practical ethane partial pressures (≥0.8 bar). In principle, the same CL-ODH strategy can be applied to other light alkanes such as propane and butane. The following discussions provide a brief account of the chemical looping studies related to ethane and propane conversion to light olefins.

The chemical looping operations illustrated in Fig. 12 can be realized by two types of redox catalysts with distinct functions.[266] The Type I redox catalysts function primarily as SHC materials. Using Type I catalysts, ethylene production is realized by a combination of dehydrogenation (DH) or cracking reaction (for olefin and hydrogen production) and SHC reaction (for the *in situ* oxidation of the hydrogen byproduct, reaction (R16)). In comparison, Type II redox catalysts catalyze ethane ODH reactions while donating their active lattice oxygen.

Type I: SHC redox catalysts. While it could be argued that Type II redox catalysts are more desirable due to their multi-functionality, Type I redox catalysts could offer better flexibility since they can be tuned independently for various operating conditions and reactor configurations. For instance, SHC redox catalysts have been explored to enhance both DH and thermal cracking reactions with a temperature range varying from 450 to 900 °C.[82,83]

The use of SHC to enhance catalytic DH reactions (Route a in Fig. 12) was proposed in the late 1990s by Imai *et al.*[267,268] in the context of propane dehydrogenation. While both co-feeding oxygen[269] and redox mode operation using lattice oxygen[269] were investigated, the latter was surmised to be superior based on both experimental data and reactor simulations.[268,270,271] Resulting from their significant potential, various oxides were explored as SHC redox catalysts in the temperature range of 550–800 °C. Representative materials showing high (>90%) SHC selectivities, defined as the conversion of the hydrogen divided by the conversion of all combustible species, include Sb_2O_4, In_2O_3, WO_3, Bi_2O_3, $PbCrO_4$, doped ceria, ion-exchanged ZSM-5, *etc.*[268,269,272–277] Bi, In, Pb, and Sb oxides often suffer from a poor redox stability owing to relatively low melting temperatures of their reduced states. Ceria doped with W, Bi, Cr or Pb, were found to be stable in the temperature range 500–600 °C with selectivities of up to 98% for hydrogen combustion in the presence of C_2 and C_3 hydrocarbons and oxygen storage capacities as high as 2 wt%.[273,278–282] Mn- and La-containing perovskites also showed a high SHC selectivity and stability in the presence of C_3 hydrocarbons at 550 °C.[84] It is noted, however, that the SHC selectivity tends to decrease with increasing temperature due to the lower activation energy for hydrogen combustion compared to hydrocarbon oxidation. Therefore, these early SHC studies focusing mostly on operating temperatures <650 °C were exclusively geared towards dehydrogenation applications in combination with a DH catalyst such as supported PGM (*e.g.* Pt) and chromium oxides.[259,278,283]

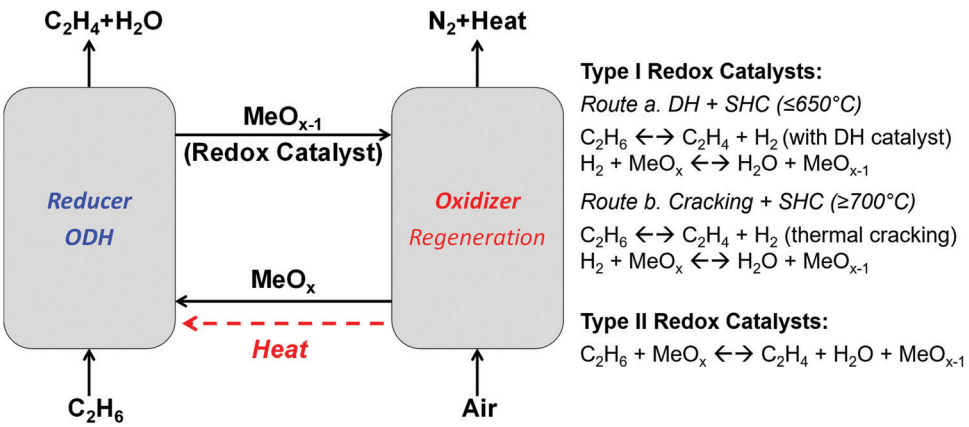

Fig. 12 Schematic of CL-ODH, redox catalyst types, and reaction schemes. Ethane is used as an example for light alkanes for illustration purpose.

Another challenge with the DH and SHC concept resides in the incompatibility of the catalysts and their operating conditions. While physical and chemical interactions between the catalysts themselves can be avoided by spatially separating them (*e.g.* in a packed bed with alternating DH catalyst and SHC redox catalyst layers), active sites and dominating reaction pathways on DH catalysts can be affected by the steam generated from the SHC material. For instance, steam can lead to undesirable reforming reactions on PGM-containing catalysts. For oxide-based DH catalysts, steam (or air during the regeneration step) can affect the oxidation state of the active metal, induce changes in the surface compositions, and hence negatively affecting the DH performance. Except for very few studies,[269] the aforementioned studies used hydrogen and a hydrocarbon mixture (*e.g.* hydrogen, ethane, and ethylene) to evaluate the redox catalysts' SHC performances. The incompatibility issues between DH and SHC have largely been unaddressed to date. Development of DH catalysts that are stable under redox conditions and in the presence of steam is therefore the key to apply the DH + SHC approach for CL-ODH.

SHC redox catalysts can also be integrated with thermal cracking reactions (Route b in Fig. 12). Unlike surface-catalyzed DH reactions, thermal cracking proceeds *via* gas-phase radical reactions and so steam generated by SHC would not negatively affect cracking reactions. Under this approach, the CL-ODH reactions proceed *via* parallel gas-phase and surface pathways, *i.e.* hydrogen generated from gas phase cracking reactions is selectively combusted on the surface of the redox catalysts.[80,269] In some cases, the redox catalyst surface can also function as a radical initiator to enhance the gas phase reactions (*i.e.* surface-initiated homogeneous reactions).[87] It is noted that the initiation of radicals from alkanes typically requires temperatures close to or higher than 700 °C. While such a temperature range is not uncommon for CLC, the inverse relationship between SHC selectivity and reaction temperature for most oxide redox catalysts dictates that many of the SHC catalysts reported for DH + SHC, which are geared towards operating at 650 °C or lower, would not be compatible with thermal cracking reactions. The high operating temperature can also be challenging for oxides or metals with low melting points or high vapor pressures. To address these challenges, Dudek *et al.*[83] investigated a number of Mn-containing redox catalysts including $CaMnO_3$, $SrMnO_3$, and Mg_6MnO_8 for selective hydrogen combustion using hydrogen and ethylene mixtures at temperatures up to 850 °C. The effect of promoters was also studied by impregnating Na_2WO_4 on each of these oxides. In general, Na_2WO_4 was effective in inhibiting the formation of CO_x, but negatively affected the redox activity of the mixed oxide. The operating temperature windows, *i.e.* the optimal temperature ranges with a high activity and selectivity towards hydrogen combustion, for the six redox catalysts investigated ranged between 550 and 850 °C. The large and tunable operating temperature window opens up the potential opportunity for integration of a SHC redox catalyst with thermal cracking. The effectiveness of CL-ODH under thermal cracking conditions was confirmed with Na_2WO_4 promoted Mn–Mg and Mn–Si oxides.[284] Resulting from their high activity and high temperature SHC selectivity, ethylene yields up to 68% were demonstrated with CO_x selectivities as low as 1.9%. Negligible coking was observed in these studies. This is not surprising considering the redox catalysts' high activity for lattice oxygen donation, which can actively inhibit coke formation. Na_2WO_4 was important for obtaining a high olefin selectivity since it enriches on the oxide surface and suppresses the deep oxidation of hydrocarbons.[285] In the case of the Mg_6MnO_8 system, a mixed oxide with a cation deficient rocksalt structure, near surface Mn^{4+} was suppressed by more than 85%.[80,81] Further characterizations by low energy ion scattering (LEIS), *in situ* XRD, and differential scanning calorimetry indicated that the Na_2WO_4 is likely to form a molten layer on the oxide surface under the operating conditions and thus acts as a physical blocker to suppress surface catalyzed C–H bond activation.[286] The corresponding process analysis further highlighted the advantages of CL-ODH of ethane over steam cracking.[113] These include higher single-pass yields, a reduction in the total energy demand by >80% and a reduction in CO_2 emissions by >80%. Importantly, CL-ODH is self-sufficient from a process heat requirement point of view, making it a highly efficient and low emission technology ideal for distributed systems.

Type II: ODH redox catalysts. Many heterogeneous catalysts used in conventional ethane ODH (where oxygen is co-fed with the ethane) are redox-active.[287] In the presence of gaseous oxygen (or, as was shown recently, mild oxidants such as steam),[288] the reaction proceeds through a MvK mechanism[289] in which ethane is activated and dehydrogenated by surface metal-oxide species, thereby reducing the metal oxide and creating oxygen vacancies. The vacancies on the surface are subsequently replenished by gaseous oxygen, which is dissociated and incorporated at surface sites different from the ODH reaction sites.[290–292] The overall reaction is therefore facilitated by the migration of oxygen anions through the lattice and/or on the surface. The most common redox-active heterogeneous catalysts for ODH of light alkanes are based on vanadium oxide[293–295] with different supports, such as alumina,[296–299] alumina modified with zirconia[300,301] or silica.[302–305] Nickel oxides[306,307] and cobalt oxides[308,309] have also been examined.

Since a key characteristic for the MvK mechanism is that the overall reaction can be carried out under a "swing mode", *i.e.* separating the reduction and oxidation into two sequential steps identical to chemical looping operations, it is not surprising that many of the redox-active oxide catalysts can act as redox catalysts in CL-ODH schemes. For example, Hossain and de Lasa developed a number of cyclically stable VO_x/γ-alumina-based catalysts for the CL-ODH of ethane in a continuous fluidized bed process consisting of an ODH reactor and a catalyst regenerator.[298,299,310] Ethylene selectivities ranging from 80–90% at temperatures between 550–600 °C were reported. The corresponding ethane conversions, however, were relatively low (<10%).[300,311,312] The same class of catalysts was also used for the CL-ODH of propane in the simulated fluidized bed process and propylene selectivities of >90% were obtained at up to 25% conversion of propane.[313–315] The good performance of the most promising

redox catalyst, VO_x/CaO–γ-Al_2O_3, was attributed to an intermediate acidity of the catalyst and moderate active site–support interactions.[85] Encouraging results for ethane CL-ODH were also obtained with Mo-based redox catalysts, which gave ethylene selectivties of 93–95% and conversion up to 66.5% at 600 °C.[297,316] The oxygen storage capacity of these Mo-based redox catalysts was relatively low (<0.4 wt%), resulting in a decreasing conversion of ethane with time. Nonetheless, in a continuously operating riser reactor system, an ethane conversion of 12% at ethylene selectivities >90% was obtained with a mixed Mo–Te–V–Nb oxide supported on γ-Al_2O_3 when the contact time of ethane feed and redox catalysts was 1–2 s at 500–575 °C.[317] The same authors also showed that the performance of Mo-based redox catalysts is strongly affected by the support material (Al_2O_3, Ga_2O_3 or Y_2O_3), leading to an increased ethane conversion and ethylene selectivity with a decrease in the content of MoO_3; the best results were obtained with 5 wt% MoO_3 on alumina, giving 90% selectivity for ethylene at an ethane conversion of 30%.[318,319] Novotny *et al.*[284] investigated the effect of impregnating MoO_3 onto an α-Fe_2O_3-based redox catalyst, which improved the oxygen storage capacity from 0.28 wt% to 0.62 wt%. A MoO_3 and $Fe_2(MoO_4)_3$ enriched surface layer was formed upon calcination. At 600 °C, the ethylene selectivity was as high as 62% while CO_2 formation was suppressed when compared to pure α-Fe_2O_3. Supported chromium oxide catalysts are widely used in catalytic dehydrogenation,[320] *e.g.* the commercial CATOFIN® process. Chromium oxides were also shown to perform reasonably well in CL-ODH of propane with potential use in a moving bed process.[321–323] The oxygen storage capacity was determined to be crucial for the performance of the redox catalyst, and slightly higher oxygen capacities (up to ~0.5 wt%) resulted in higher yields of propylene (~46% at 630 °C).[324] More recently, Chen *et al.* used to use Mo–V–O mixed oxides as the redox catalyst for CL-ODH of propane to propylene.[325] Attractive propylene yield (89% propylene selectivity at 36% pro-pane conversion) over 100 redox cycles was obtained at 500 °C due to the tailored bulk lattice oxygen *via* atomic-scale doping of Mo in the redox catalyst. Although promising results were obtained from these redox catalysts, the toxicity of Cr and V and thermal stabilities of Mo and V oxides could affect their practical applicability especially in circulating bed systems.

Aside from the redox-active oxides commonly found in heterogeneous DH and ODH catalysts, alkali metal-promoted, Ruddlesden–Popper structured, $La_xSr_{2-x}FeO_{4-\delta}$ redox catalyst was recently shown to be active for CL-ODH of ethane.[79,128] Up to 90% ethylene selectivity and 61% conversion were observed at 700 °C, with near 100% H_2O selectivity. An important finding from this study was that electrophilic surface oxygen species (such as O^- and O_2^-), which limit the selectivity of the ODH reaction and account for the deep oxidation of the alkanes and olefins, can be suppressed by enrichment of alkali metal oxide on the surface of the redox catalyst. A thin layer of Li_2O on the surface likely served as a barrier to inhibit the outward diffusion of O^{2-} and its evolution into electrophilic oxygen species on the surface.

A common challenge with these Type II ODH redox catalysts is the lack of oxygen storage capacity. Most of the redox catalysts reported to date exhibit <1 wt%, and in many cases <0.5 wt%, oxygen storage capacity. As noted above, the utilization of lattice oxygen in CL-ODH is significantly more efficient than that in CLC. For instance, combusting one mole of propane under CLC consumes ten moles of lattice oxygen whereas under CL-ODH it consumes only one. The order of magnitude increase in oxygen utilization efficiency make these low capacity redox catalysts potentially feasible for industrial applications, provided that high olefin selectivity, redox activity, and stability are demonstrated. Another challenge is the trade-off between conversion and selectivity especially in many of the V- and Mo-based redox catalysts, *i.e.* higher alkane conversion (*e.g.* by increasing the residence time) often leads to a significantly decreased olefin selectivity. This could result from the re-adsorption of the olefin products and/or the presence of distinct active sites for selective and non-selective reactions. In-depth understanding of the active sites and reaction pathways would be crucial for rational optimization of the redox catalysts. Although a large body of literature is available on conventional, catalytic ODH systems, the exact mechanisms for many redox-active ODH catalysts are still under debate.[259,326] The dynamic nature of redox catalysts undergoing chemical looping reactions also makes mechanistic investigation on CL-ODH even more challenging than catalytic ODH. Therefore, further investigation on the mechanistic aspects of the redox catalysts is an important, yet challenging task. Although we did not separately discuss ethane and propane CL-ODH in this section, we note that propane (and C_{4+}) is significantly less stable than ethane. The tendency for C–C bond cleavage makes it more difficult to develop highly selective redox catalysts for CL-ODH of propane and C_{4+} to olefins. Thus, a redox catalyst optimized for CL-ODH of ethane may not automatically be applicable for propane and C_{4+} conversion.

4.2.2 Epoxidation of olefins. The epoxidation of olefins (R51) is another example for oxidation reactions where yields are generally low due to the non-selective oxidation of the educts and the epoxides; yet, these catalytic reactions are of enormous relevance for the chemical industry.[327]

So far, only the epoxidation of ethylene has been realized industrially using molecular oxygen as the sole oxidant.[328] The selectivity to ethylene oxide is typically in the range of 85–90% at ~10% ethylene conversion with optimized silver-based catalysts.[329–331] A chemical looping approach was recently explored to undertake the epoxidation reaction by substituting co-fed molecular oxygen with lattice oxygen (Fig. 13).[78] Here, Ag (15 wt%) was impregnated onto the perovskite $SrFeO_3$ that possesses an oxygen storage capacity of up to ~2 wt%. The main rationale for selecting $SrFeO_3$ was its excellent ability to spontaneously release O_2 at relatively low temperatures.[136] The authors proposed that oxygen was transported from subsurface $SrFeO_3$ to the surface of the redox catalyst and thus formed oxygen adatoms on the silver surface. The vital role of atomic oxygen adsorbed on the silver surface for catalyzing the oxidation of ethylene has been discussed extensively in the literature,[331,332] as well as the availability of subsurface oxygen to achieve a high ethylene oxide selectivity.[333] Furthermore, it was found in

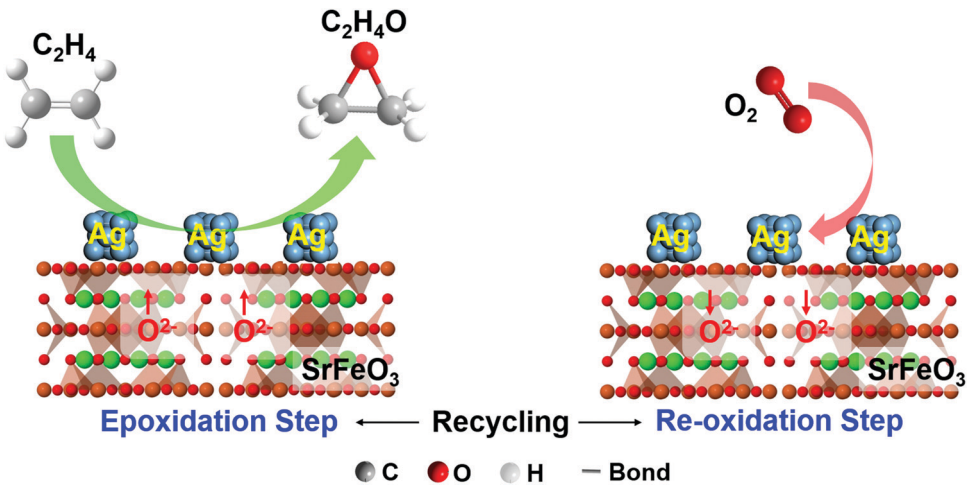

Fig. 13 The reaction mechanism of chemical looping epoxidation using a silver-modified $SrFeO_{3-\delta}$ redox catalyst.

previous studies that higher selectivities could be obtained with low surface area supports,[334,335] a characteristic of most redox catalysts used in chemical looping applications. The selectivities and conversions reported by Chan *et al.*[78] were, however, very low (the ethylene oxide selectivity was <20% and the ethylene conversion was <4% at 270 °C). Previous work showed that the dispersion of Ag, the morphology and temperature treatment of the support all affect, besides operational parameters, the performance of the catalyst.[336–338] It is also possible that the exposed surface of $SrFeO_3$ is largely responsible for non-selective oxidation reactions and the activity of the oxide substrate to catalyze non-selective oxidation reactions should not be overlooked. Another challenge observed by Chan *et al.* was the low rate of oxidation when the redox catalyst was regenerated in air, causing a gradual loss in oxygen capacity.[78] A similar problem was reported for vanadium phosphorous oxide redox catalysts, as will be discussed in Section 4.2.3. The problem was overcome by modifying the $SrFeO_3$ with 5 mol% CeO_2, which also improved the cyclic stability and ultimately gave 60% selectivity towards ethylene oxide at 10% ethylene conversion.[339] The authors proposed that CeO_2 may have acted as oxygen gateway (see Section 3.2.2) and thus improved the re-oxidation of the redox catalyst. The challenge for further improvement will thus be to find oxygen storage materials with sufficient reduction/regeneration activities at temperatures <300 °C while suppressing over-oxidation of ethylene. Despite the relatively low reaction temperatures of 200–280 °C typically employed for the epoxidation of ethylene, Ag-based catalysts tend to deactivate owing to the sintering of the silver particles,[340–342] and this may be even more problematic when the redox catalysts are regenerated in an exothermic oxidation reaction.

In principle, the chemical looping epoxidation approach can certainly also be applied to the selective oxidation of propylene, where it was shown recently that mixed metal oxides are catalytically active in a conventional oxygen co-fed mode. For a mixed MoO_3/Bi_2SiO_5 catalysts supported on SiO_2, propylene oxide selectivities of 55% were reported at a propylene conversion of 22% at 400 °C for a diluted feed with a molar ratio of O_2/C_3H_6 of 4 : 1,[343] whereas high formation rates of propylene oxide were observed for a RuO_2/CuO catalyst supported on SiO_2.[344] Using a copper–manganese mixed metal oxide catalyst, Seubsai *et al.*[345] found selectivities >30% towards propylene oxide at up to 1.5% propylene conversion at 300 °C. These catalyst systems are structurally and chemically similar to typical chemical looping redox catalysts, indicating the potential for future work in this field.

4.2.3 Maleic anhydride production. ODH in a redox mode was demonstrated commercially by DuPont for the oxidation of *n*-butane to maleic anhydride to produce maleic acid (R53).[86,346] Up to 6500 kg h^{-1} of maleic acid were produced using a vanadium phosphorous oxide (VPO) redox catalyst in a circulating fluidized bed reactor operated at ~400 °C.[347] The process was developed over a period of more than ten years, as summarized by Contractor, also highlighting the challenges associated with redox catalyst and reactor design.[348,349] Selectivity of near 80% was claimed at a conversion of 40%.[327] Nevertheless, the plant was shut down in the early 2000s, partially owing to economic reasons related to a rapidly changing market situation for different raw materials and intermediates,[350] but also owing to problems with catalyst loss through attrition[351] and deteriorating oxidation kinetics of the VPO catalyst, which resulted in a gradual loss in oxygen capacity during operation such that O_2 had to be co-fed.[352] We also note that the oxygen capacity of the VPO redox catalyst was rather low to begin with, corresponding to merely a few monolayers of lattice oxygen near the catalyst surface.[353,354]

4.3 Chemical looping involving liquid and solid fuels

4.3.1 Liquid fuels driven processes. The CLBC approach can readily be extended to liquid hydrocarbons. In fact, it has been successfully employed to reform various liquid fuels, such as alcohols (*e.g.* methanol or ethanol),[355–362] glycerol,[363] waste cooking oil,[364] liquid alkanes (*e.g.* dodecane),[365] kerosene,[366] heavy oil,[365] and biomass tar.[367–370] In addition to reforming, liquid fuels can also decompose or completely oxidize in the fuel reactor. For example, Ochoa *et al.*[359] explored the nature of the surface species and gaseous products formed during

reduction of different spinel mixed oxides using ethanol. It was found that ethanol always first dehydrogenates to acetaldehyde on the surface of the spinel. Subsequently, depending upon the spinel composition, acetaldehyde (i) partially oxidizes to acetates (Ni-based spinel), (ii) decomposes to CO and CH_4 (Co-based spinel), or (iii) completely oxidizes to CO_2 and H_2O (Fe-based spinel). The design criteria of redox catalysts and operating conditions for liquid fuels driven chemical looping processes are similar to those of the gaseous hydrocarbon-based chemical looping processes. However, special care must be taken when using viscous liquids such as tar or heavy oil to avoid their condensation upstream and/or downstream of the fuel reactor. Similar to Type II ODH process, the chemical looping approach has been applied for the oxidative cracking of naphtha. Process simulations indicate that over 50% energy and CO_2 savings can be achieved *via* the chemical looping route.[112] Using perovskite-based redox catalysts, Dudek *et al.*[87] demonstrated close to 70% olefin selectivity with a CO_x selectivity as low as 0.3%.

4.3.2 Solid fuels driven processes. Owing to the slow rates of solid-solid reactions, using solid fuels directly for CLBC is challenging. Therefore, solid fuels (such as biomass or coal) are typically gasified in a separate unit and the resulting synthesis gas is fed to the chemical looping process designed for gaseous fuels.[371–374] To avoid dilution of the synthesis gas with N_2, the gasification reaction needs to be carried out with pure O_2 or a mixture of O_2 and steam/CO_2. Therefore, an air separation unit would be required. Several strategies to extend CLBC to solid fuels are summarized below:

(i) The solid fuel can be gasified *in situ* in the presence of a redox catalyst using steam or CO_2 as the fluidizing gas. This strategy not only eliminates the need for a separate gasification unit but also enhances the rate of gasification.[375,376] However, owing to the inherently slow nature of the gasification reaction, it is difficult to achieve complete gasification of the solid fuel *in situ*.

(ii) Depending upon their thermodynamic characteristics, certain oxygen carriers can undergo spontaneous decomposition at high temperatures to release molecular oxygen.[377,378] The use of such oxygen carriers allows the direct combustion of a solid fuel *via* a gas–solid reaction, *i.e.* without an intermediate gasification step. This process configuration, typically referred to as chemical looping with oxygen uncoupling (CLOU), significantly increases the rate of fuel oxidation, thereby allowing the complete combustion of the solid fuel. Furthermore, instead of fully oxidizing the solid fuel it is also possible to gasify it by controlling the partial pressure of oxygen released by the redox catalyst.[379]

(iii) Recently, it has been proposed to use molten oxygen carriers or reaction system for CL-methane POx, CLC, and CL separation to circumvent the challenges associated with the solid-based chemical looping systems, such as carbon deposition, thermal sintering and low reaction rates.[380] Wang *et al.*[381] proposed a molten slat alkali carbonate based CL-methane POx system for the coproduction of synthesis gas and metallic Zn. The molten reaction system enables to intensify heat and mass transfer during the cyclic redox, increasing the energy utilization efficiency. Sarafraz *et al.*[382–384] investigated the thermodynamic feasibility of using liquid oxygen carriers for the partial oxidation of fuel to synthesis gas and identified Cu, Pb and Sb as the most promising candidates. Upham *et al.*[385] demonstrated a molten bromide-oxide based chemical looping for the reactive separation of HBr in a halogen-based natural gas conversion. Nickel-alkali bromide and oxide were switched in molten reactor for the conversion of HBr to Br through the MeBr/MeO redox pair. Although the use of molten redox catalysts avoids the aforementioned issues and enhances the rate of reaction, it also introduces new challenges such as evaporation or solidification of liquid oxygen carriers, continuous circulation of liquid metals/oxides, large pressure drops across the reactors, *etc.*

(iv) For solid fuels with high volatile contents, *e.g.* biomass or low-rank coal, it is possible that a redox catalyst can be used to generate value-added products *via* pyrolysis-type of processes – an area that has not been investigated extensively by the chemical looping community.[44,386] It is noted that pyrolysis products with less oxygenates are typically desired, which may conflict with typical chemical looping operations.

4.4 Synergy between oxide and calcium/carbonate looping

CaO-Based sorbents, often in the form of naturally-occurring lime, are used widely in applications such as flue gas desulfurization[387–389] and sorption-enhanced steam methane reforming (SE-SMR) to produce H_2.[390–393] In SE-SMR, CO_2 is removed continuously in the WGS reaction step, thus shifting the equilibrium to the product side according Le Chatelier's principle.[394] The H_2 yield can thereby be increased to $\sim$97 vol% at 550 °C.[395] The WGS reaction is relevant also in gasification reactions, and generally in schemes where mixtures of CO, CO_2, H_2 and H_2O co-exist at high temperature, and so sorbents for CO_2 are conventionally used.[396] Lately, CaO-based sorbents have also gained considerable attention for carbonate looping (CaL),[397–405] a post-combustion CO_2 capture technique.[402,406] A key advantage of using CaO for the sorption of CO_2 is its high theoretical uptake of 0.78 g CO_2 per g CaO, according to reaction (R68) in Table 2. The carbonation reaction is exothermic whereas the reverse reaction, known as the calcination reaction, is endothermic, giving a stream of concentrated CO_2.[407] Carbonate and oxide (chemical) looping processes can be combined to improve efficiencies of both processes, as discussed below.

4.4.1 Reaction schemes

Chemical looping with sorbent enhancement for heat-neutral sorbent regeneration. Besides permitting higher yields of H_2 in the SE-SMR/gasification scheme, the exothermic carbonation reaction can provide a large amount of heat for the strongly endothermic methane reforming or the gasification reaction. Meanwhile, the regeneration of the sorbent *via* the highly endothermic calcination reaction is critical and requires high reaction temperatures (>750 °C). Performing the calcination reaction in the presence of an exothermic reaction would balance the heat requirements. Such exothermic reaction could be the oxidation of a reduced oxygen carrier, as suggested by Lyon and Cole,[163,408] *e.g.* the simultaneous oxidation of the

Ni-based reforming catalyst. However, a relatively high ratio of Ni to $CaCO_3$ (>0.75) would be required to balance the heats of reaction, resulting in an increase in the catalyst cost, and the CO_2 produced is diluted with N_2 when air is used for the re-oxidation of Ni. In addition, the oxidation of the reforming catalyst at high temperature is likely to promote its sintering and deactivation.

Chemical looping with sorbent enhancement for CO_2 capture. The simultaneous oxidation and calcination reactions eliminate the benefit of CaO-based sorbents to produce a pure stream of CO_2. In CaO-based CO_2 capture architectures, the calcination reaction can be performed in a reactor operated in an oxy-fuel mode, where the heat is provided by combusting additional fuel (*e.g.* natural gas) in an atmosphere containing O_2 diluted with CO_2.[409–411] Replacing molecular oxygen with an oxygen carrier that reduces in an exothermic reaction while fully combusting the fuel would enable both the balancing of the endothermicity of the calcination reaction and generating a pure stream of CO_2.[412] A few redox pairs, *e.g.* CuO/Cu or Mn_2O_3/Mn_3O_4, can be reduced exothermally with CH_4 and other hydrocarbons.[39] This feature can be applied to integrate the heat released from the CLC reduction step with the endothermic calcination step to produce concentrated CO_2. A reaction scheme where CuO-based chemical looping combustion is combined with SE-SMR is shown in Fig. 14a and at least three reactors are required to obtain separate streams of H_2 and CO_2.[413]

For carbonate looping as a CO_2 capture technique, heat integration is vital to be economically competitive with other CO_2 capture techniques. In analogy to the SE-SMR process, CuO-based oxygen carriers have mostly been investigated to render the heat exothermic during the exothermic calcination step.[414–417]

Unlike the CLC reduction step that is often endothermic, the regeneration step is always exothermic for monometallic oxides. Therefore, integration of the heat released in the CLC regeneration step with the sorbent calcination step can also result in concentrated CO_2 if a heat transfer agent is used to avoid direct contact between the air (in the regeneration step and the oxidizer) and CO_2 (from calcination in the calciner). Both ALSTOM and General Electric proposed and investigated such schemes (details on these two processes have been summarized by Fan[122]). In ALSTOM's Hybrid Combustion–Gasification Process for hydrogen generation, a $CaSO_4$ oxygen carrier is employed to generate the heat for the calcination of the CaO sorbent. Instead of oxidizing the oxygen carrier in the vicinity of the $CaCO_3$, bauxite is used to transfer the heat from the oxidation reactor to the calcination reactor. Similarly, General Electric's Fuel-Flexible Advanced Gasification–Combustion Process also adopted CLC reactions to provide the heat for calcination. In this case, an iron oxide-based oxygen carrier was used as the heat transfer agent.

Sorption-enhanced methane reforming coupled with chemical looping conversion schemes. The thermodynamic properties of some oxygen carriers permit the splitting of CO_2 or H_2O to produce CO or H_2 upon oxidation (see Section 4.1.1). Since the rate of reduction of many oxygen carriers, *e.g.* Fe_2O_3, with primary fuels such as CH_4 is low, it was proposed to convert CH_4 first to a synthesis gas over a catalysts (*e.g.* Ni; in analogy to the dry reforming of methane (DRM)) and use the synthesis gas to reduce the oxygen carrier.[94,418] Depending on the oxidant used (CO_2 or H_2O) for the subsequent regeneration of the oxygen carrier, CO or H_2 can readily be produced.

This reaction concept can be extended by adding a CaO-based sorbent (Fig. 14b).[419,420] Analogously to SE-SMR, the heat of sorption from the carbonation reaction (reaction (R68)) balances the endothermic reforming and reduction reactions. In the following oxidation step, CO_2 is released from the sorbent and oxidizes the oxygen carrier while producing CO. The chemical looping concept, where in theory three moles of CO_2 per mole CH_4 are converted to four moles of CO, has been termed super-dry reforming of methane (R67). Importantly, in such a process the formation of an equilibrium mixture of CO_2, CO, H_2O and H_2 is circumvented during the

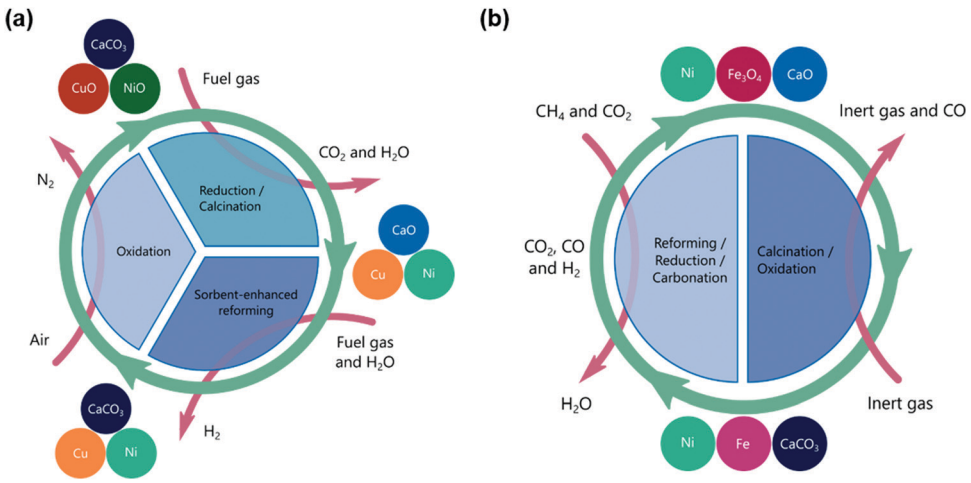

Fig. 14 (a) Reaction scheme with three reactors where CuO-based chemical looping combustion is integrated into the SE-SMR process. (b) Reaction scheme of the super-dry reforming of methane with two reactors, in which the reforming catalyst (Ni) is spatially separated from the oxygen carrier (Fe_3O_4) and the CO_2 sorbent.

reforming step, thus avoiding a loss in CO yield through the RWGS reaction (R71). So far, the process has been demonstrated by mixing different materials, *viz.* CaO supported on Al_2O_3 as CO_2 sorbent, Fe_2O_3 supported on $MgAl_2O_4$ as oxygen carrier, and NiO supported on $MgAl_2O_4$ as the CH_4 reforming catalyst, rather than multifunctional redox catalysts. While the theoretical advantages over conventional dry-reforming of CH_4 are apparent, there is still scope for improvement (besides improving the materials used). For example, it was proposed to run the process isothermally. Equilibrium thermodynamics dictate that the release of CO_2 from the CO_2 sorbent requires very low CO_2 partial pressures and for that, an inert gas would likely be needed in the oxidation step (where Fe is oxidized by the CO_2 released from the sorbent). This will inevitably dilute the product gas CO. The product gas CO is diluted further with CO_2 because the conversion of CO_2 to CO over Fe is thermodynamically limited and the ratio of CO/CO_2 in the product gas will decrease further as the Fe-based oxygen carrier is oxidized *via* FeO to Fe_3O_4.

4.4.2 Material design. The performance and function of CaO-based sorbents can be further improved by doping with active oxides,[414,421,422] addition of supports,[423] acid modifications,[424,425] and morphology control.[421,426] One of the most studied combined oxide and carbonate looping schemes is CuO-based chemical looping combustion coupled with SE-SMR.[427–430] In this process, at least three materials are required: A catalyst for the reforming of CH_4, a sorbent for CO_2, and CuO as the oxygen carrier that can be reduced by various fuels in an exothermic reaction. If CH_4 is used as the fuel, the Cu/Ca ratio needs to be >3.1 to achieve thermally neutral conditions in the calcination step based on the enthalpies of reaction at 900 °C. However, this figure varies somewhat and is subject to the process design, the type of fuel (*e.g.* using CO as the fuel, the ratio would be 1.3) and the heat management strategy.[431,432]

Three active components make the design of suitable, ''trifunctional'' materials rather challenging;[433] current research thus focuses largely on the development and optimization of separate particle systems[434–436] or bi-functional Ca–Cu[422,437–440] or Ca–Ni[441–443] composites and uses commercially available Ni-based catalyst particles.[444,445] The CO_2 capture capacity of the CaO-based sorbents is linked strongly with the available surface area, which is known to decay due to sintering when the sorbents undergo cycling of carbonation and calcination.[446–448] Producing stable particles with a porous CaO structure in the vicinity of low surface area CuO in a Ca–Cu composite material requires appropriate support materials, *e.g.* MgO[449] or $Ca_{12}Al_{14}O_{33}$.[450] Recent works[405,414,451] at ETH Zürich have shown how such support materials function as structural stabilizers at the microscopic level and how subtle phase transitions affect the cyclic performance of the CaO-sorbents (Fig. 15). Another recent study

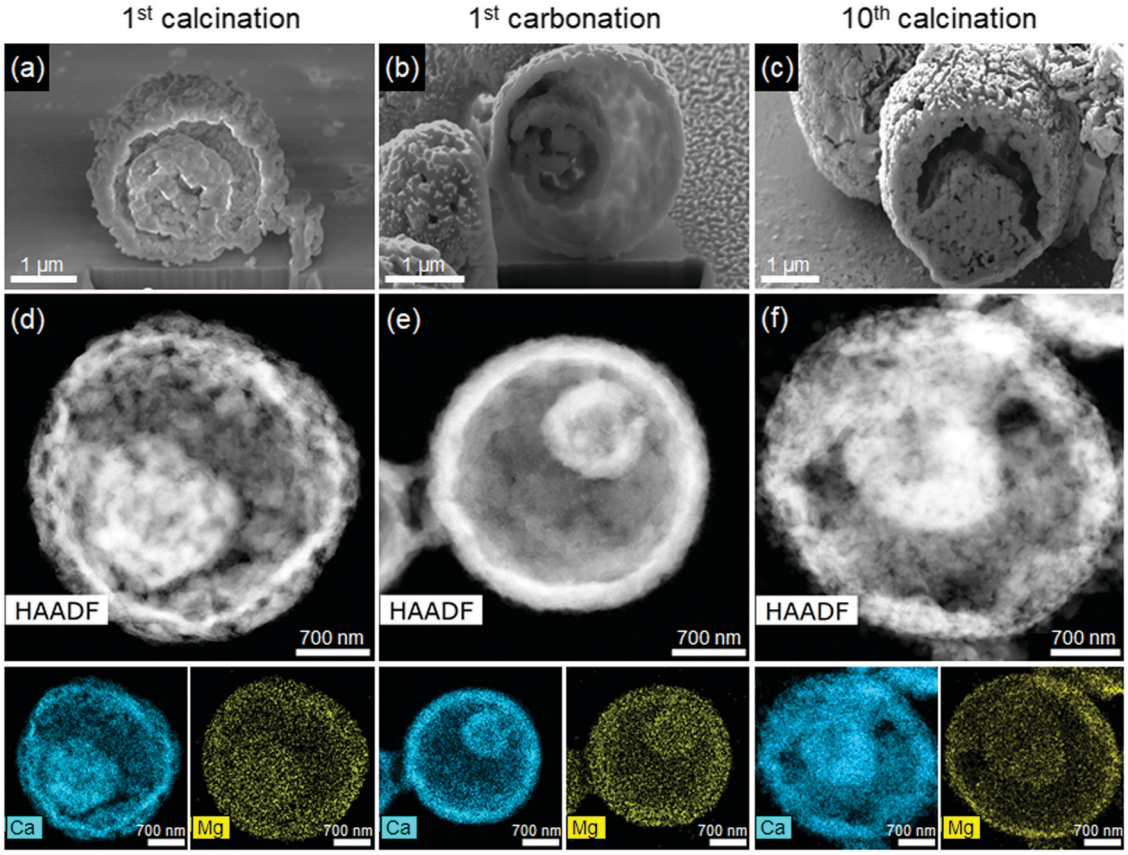

Fig. 15 Morphological changes during cyclic operation of a Ca–Mg mixed oxide-based sorbent. (a–c) SEM imges of FIB cross-sections. (d–f) HAADF-STEM images with EDX maps of Ca and Mg at different stages of CO_2 capture/regeneration cycles. Scale bars: 1 μm for (a–c) and 700 nm for (d–f).[451]

reported an interesting phase transition based approach to effectively enhance sorbent stability for the hydrogen production from bio-glycerol.[452]

Conventional design strategies aim to limit the mobility of active species and their growth by using inert support materials that act as physical barriers.[199] New approaches have shown that the active species in a sorbent or redox catalyst may well be mobile, but their self-diffusion is limited if the simultaneous formation of a new phase with the active species is thermodynamically more preferred.[453] For example, Dang *et al.*[452] demonstrated that calcium cobalt, a layered bi-functional material acting as both sorbent and catalyst for the sorbent enhanced reforming of glycerol could effectively be stabilized because the components $CaCO_3$ and CoO homogenized into calcium cobalt on an atomic level in every calcination stage of the cyclic process instead of remaining segregated and sintering. Well-ordered structures, such as layered oxides, spinels or perovskites are particularly suitable for such approaches.[452,454]

For reaction schemes such as the super-dry reforming of methane, catalyst and oxygen storage material are usually separated spatially.[455] Work by Hosseini *et al.* demonstrated that both the reforming of methane through the catalyst and the reduction of the oxygen storage material can be realized by the same redox catalyst particle provided it is designed carefully in a core–shell structure.[456]

5. Summary and perspective

The chemical and petrochemical industry generates an annual revenue in excess of $4 trillion while consuming 40.9 quadrillion BTU of energy and emitting 2.5 Gigatons of CO_2 (2014 numbers provided by IEA).[457] The significant energy intensity and CO_2 emissions associated with this important industrial sector offer excellent opportunities for process intensification, energy conservation, emission reduction, as well as profitability enhancement. We believe that CLBC represents a promising new frontier in chemical reaction engineering, catalysis, and particle technology to address the aforementioned challenges and opportunities. As discussed in Section 2, the unique advantages of CLBC largely reside in its ability to significantly improve a chemical (and energy) conversion process from a thermodynamic second law standpoint: a strategically designed CLBC scheme, when coupled with tailored oxygen carrier or redox catalyst, can significantly reduce process exergy loss and/or facilitate chemical transitions that would otherwise be impossible under a conventional scheme. From an economic standpoint, reactive separation enabled by oxygen carriers in CLBC offers excellent potential to simplify conventional processes and to reduce the number of unit operations. With the continued technical progress in CLC, a promising carbon capture technology that addresses the carbon intensive, $1.4 trillion power generation sector, we argue that chemical looping beyond combustion offers equally and perhaps even more exciting opportunities due to their potential for more efficient lattice oxygen utilization, higher product value, and relative ease for scale-up compared to full scale utility plants.

Although CLBC has attracted increasing attentions over the past 5–10 years, we note this emerging research area is far from being adequately explored particularly considering its significant complexity and excellent potential. From scientific and engineering standpoints, CLBC represents an "ultimate" multidisciplinary and multiscale challenge that requires expertise in various areas including, but not limited to, chemical looping, heterogeneous catalysis, material science, particle technology, reaction and reactor engineering, and process and system engineering. This is due to the uniquely intertwined nature of CLBC. For instance, redox catalyst performance cannot be treated in an isolated manner since it is significantly affected by reactor design and gas–solids contacting patterns as well as the multi-step redox scheme configuration. Meanwhile, the redox catalyst can undergo significant changes in its surface and bulk properties within a CLBC cycle that exceeds complexities typically observed in heterogeneous catalysts. Such complexities, while daunting, are closely associated with the unique advantages CLBC has to offer. They can and should be addressed through continued research *via* interdisciplinary efforts. From a practical standpoint, redox catalysts with high stability and satisfactory long-term performance are critical for CLBC. Moreover, reactor designs that facilitate suitable redox catalyst particle circulation, gas–solids contacting patterns, residence time distributions, and heat integration between multiple reactors are important to enable these promising CLBC technologies.

This article aims to cover all the CLBC schemes to the best of our knowledge. Although a number of promising approaches such as oxidative dehydrogenation of light alkanes and alkene epoxidation are under investigation, significantly greater opportunities still exist both within and beyond these CLBC topics. From a reaction chemistry standpoint, the chemical looping approach is analogous to the MvK mechanism commonly encountered in catalytic oxidation reactions. As illustrated in Fig. 16, CLBC carries out catalytic oxidation cycles *via* a step-wise MvK with macroscopic spatial or temporal separation of the lattice oxygen removal and replenishment events. This is in contrast with conventional MvK, where the catalytic cycle is completed on the surface of an oxide catalyst under steady-state operations. The step-wise operations in CLBC offers both significant advantages (reactive separation, process intensification, and energy/cost reduction) and potential challenges (surface and/or phase changes of the redox catalytic under redox cycles). Considering their similarities, it would not be unreasonable to anticipate catalytic reactions operated under MvK mechanism to be potentially suitable candidates for CLBC. Table 3 summarizes a number of such candidate reactions. Compared to the limited CLBC reactions investigated to date, a significantly number of potential reactions are yet to be explored. In addition, the regeneration step in CLBC, which was demonstrated to be effective for H_2 and CO production *via* CO_2/H_2O splitting, could be investigated for hydrogenation or carbonylation reactions. Carriers other than oxygen, *e.g.* nitrogen

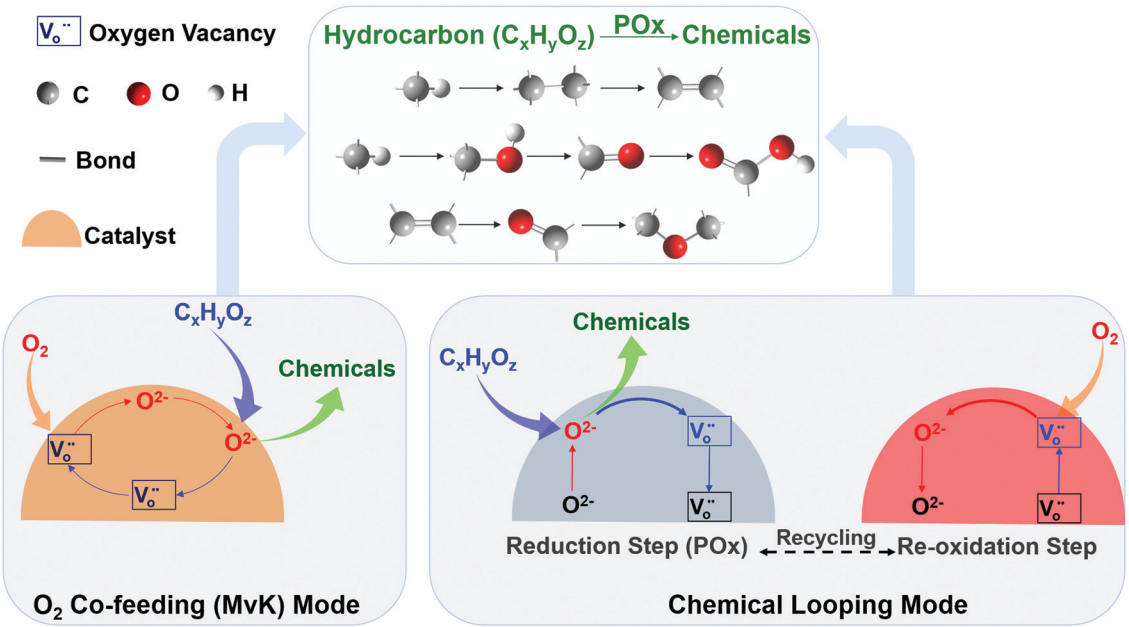

Fig. 16 Comparison of O_2 co-feeding (MvK) and chemical looping modes for partial oxidations and their applications on conversions of hydrocarbon to chemicals (transformation between alkane, alkene, alcohol, aldehyde, ketone, acid, and aromatics).

Table 3 Partial oxidation reactions facilitated by oxide catalysts *via* the Mars van Krevelen mechanism. The overall oxidation reactions are numbered from (R73) to (R111) and these reactions can potentially be realized by CLBC

Feedstock	Products	Reaction	Heterogeneous catalysts
Methane	Formaldehyde	(R73) $CH_4 + 2CO_2 \rightarrow CH_2O + 2CO + H_2O$	V_2O_5/SiO_2[458]
Methanol	Formaldehyde	(R74) $CH_3OH + 1/2O_2 \rightarrow CH_2O + H_2O$	$Fe_2(MoO_4)_3$[459,460]
	Methyl formate	(R75) $2CH_3OH + O_2 \rightarrow HCOOCH_3 + 2H_2O$	V_2O_5/TiO_2,[461] SnO_2–MoO_3[462]
Ethanol	Acetic acid	(R76) $C_2H_5OH + O_2 \rightarrow CH_3COOH + H_2O$	V_2O_5/TiO_2[463]
	Acetaldehyde	(R77) $C_2H_5OH + 1/2O_2 \rightarrow CH_3CHO + H_2O$	
1,2-Ethanediol	Ethanedial	(R78) $C_2H_6O_2 + O_2 \rightarrow C_2H_2O_2 + 2H_2O$	P-Doped Fe–Mo mixed oxide[464]
Propane	Acrolein	(R79) $C_3H_8 + 3/2O_2 \rightarrow C_3H_4O + 2H_2O$	$NiMoO_4/MoO_3/Te_2MoO_7/P_2O_5$[465]
	Acrylic acid	(R80) $C_3H_8 + 2O_2 \rightarrow C_3H_4O_2 + 2H_2O$	$NiMoO_4/MoO_3/Te_2MoO_7/P_2O_5$[465]
Propene	Acrolein	(R81) $C_3H_6 + O_2 \rightarrow C_3H_4O + H_2O$	Fe–Sb mixed oxide,[466] V_2O_5/Nb_2O_5[467]
	Acrylonitrile	(R82) $C_3H_6 + NH_3 + 3/2O_2 \rightarrow C_3H_3N + 3H_2O$	Fe–Sb mixed oxide[466]
	1,5-Hexadiene	(R83) $2C_3H_6 + 1/2O_2 \rightarrow C_6H_{10} + H_2O$	$Bi_2M_{0.1}V_{0.9}O_{5.35}$ (M = Cu or Co)[468]
	Acrylic acid	(R84) $C_3H_6 + 3/2O_2 \rightarrow C_3H_4O_2 + H_2O$	As_2O_3–Nb_2O_5–MoO_3[469]
Butane	1-Butene	(R85) $C_4H_{10} + 1/2O_2 \rightarrow C_4H_8 + H_2O$	VO_x/Al_2O_3,[470] VO_x/Mg–Al spinel,[470]
	1,3-Butadiene	(R86) $C_4H_{10} + O_2 \rightarrow C_4H_6 + 2H_2O$	VO_x/Mg–Al hydrotalcite,[470] VMgO,[470] $Mg_3(VO_4)_2$–MgO,[471] $Mg_2V_2O_7$,[471] $(VO)_2P_2O_7$[471]
	Acetic acid	(R87) $C_4H_{10} + 5/2O_2 \rightarrow 2CH_3COOH + H_2O$	V_2O_5/TiO_2[472]
1-Butene	1,3-Butadiene	(R88) $C_4H_8 + 1/2O_2 \rightarrow C_4H_6 + H_2O$	VO_x/Al_2O_3,[470] VO_x/Mg–Al spinel,[470] VO_x/Mg–Al hydrotalcite,[470] VMgO,[470] USb_3O_{10},[473] $USbO_5$,[473] MO_3/SiO_2 (M = Cr, Mo or W)[474]
Cyclopentene	Glutaraldehyde	(R89) $C_5H_8 + O_2 \rightarrow C_5H_6O_2$	WO_3/SiO_2[475]
Ethyl lactate	Ethyl pyruvate	(R90) $C_5H_{10}O_3 + 1/2O_2 \rightarrow C_5H_8O_3 + H_2O$	Mesoporous VO_x/TiO_2[476]
Cyclohexane	Cyclohexanone	(R91) $C_6H_{12} + 1/2O_2 \rightarrow C_6H_{10}O + H_2O$	$Mn_{0.5}Ce_{0.5}O_x$[477]
	Cyclohexanol	(R92) $C_6H_{12} + 1/2O_2 \rightarrow C_6H_{12}O$	
Glucose	Lactic acid	(R93) $C_6H_{12}O_6 + O_2 \rightarrow C_3H_6O_3 + 3CO_2 + 3H_2O$	$LaCoO_3$[478]
5-Hydroxymethyl-furfural	2,5-Furandicarboxylic acid	(R94) $C_6H_6O_3 + 3/2O_2 \rightarrow C_6H_4O_5 + H_2O$	Co–Mn mixed oxide[479]
Benzene	Maleic acid	(R95) $C_6H_6 + 9/2O_2 \rightarrow C_4H_4O_4 + 2CO_2 + 2H_2O$	V_2O_5–MoO_3[480]
Toluene	Benzaldehyde	(R96) $C_7H_8 + O_2 \rightarrow C_7H_6O + H_2O$	V_2O_5/TiO_2,[481] V_2O_5–MoO_3/TiO_2[481]
	Benzoic acid	(R97) $C_7H_8 + 3/2O_2 \rightarrow C_7H_6O_2 + H_2O$	V_2O_5/TiO_2,[481] V_2O_5–MoO_3/TiO_2[481]
Benzyl alcohol	Benzaldehyde	(R98) $C_7H_8O + 1/2O_2 \rightarrow C_7H_6O + H_2O$	Au/CeO_2[482]
p-Cresol	*p*-Hydroxybenzyl alcohol	(R99) $C_7H_8O + 1/2O_2 \rightarrow C_7H_8O_2$	MWCNT–Mn_3O_4 composite[483]
Ethylbenzene	Styrene	(R100) $C_8H_{10} + 1/2O_2 \rightarrow C_8H_8 + H_2O$	$Mn_xTi_{1-x}O_2$ (x = 0–0.15)[484]
o-Xylene	Phthalic anhydride	(R101) $C_8H_{10} + 3O_2 \rightarrow C_8H_4O_3 + 3H_2O$	V_2O_5[485]
Naphthalene	Phthalic anhydride	(R102) $C_{10}H_8 + 9/2O_2 \rightarrow C_8H_4O_3 + 2CO_2 + 2H_2O$	V_2O_5-Based catalysts[486]

Table 3 (*continued*)

Feedstock	Products	Reaction	Heterogeneous catalysts
Amines	Imines	(R103) R/R′-CH_2-NH_2 + O_2 → R-CH = NH-CH_2-R/R′ + H_2O (R = aryl, R′ = alkyl)	*Meso*-Cs/MnO_x[487]
Methyl bromide	Bromine	(R104) $2CH_3Br + 7/2O_2 \rightarrow 2CO_2 + 3H_2O + Br_2$	Amorphous MnO_x[488]
1,2-Dichlorobenzene	Chlorine	(R105) $C_6H_4Cl_2 + 7O_2 \rightarrow 6CO_2 + 2H_2O + Cl_2$	Ru/Co_3O_4[489]
Formaldehyde	Carbon dioxide	(R106) $CH_2O + O_2 \rightarrow CO_2 + H_2O$	Au/α-MnO_2[490]
Benzene	Carbon dioxide	(R107) $C_6H_6 + 15/2O_2 \rightarrow 6CO_2 + 3H_2O$	MCo_2O_4 (M = Cu, Ni or Mn)[491]
Toluene	Carbon dioxide	(R108) $C_7H_8 + 9O_2 \rightarrow 7CO_2 + 4H_2O$	$LaMnO_3$,[492] $La_{0.9}Sr_{0.1}MnO_3$,[492] $La_{0.9}Sr_{0.1}Mn_{0.9}Fe_{0.1}O_3$,[492] Ag, Pt or Pd doped CoAl layered double hydroxide[493]
Ammonia	Nitrogen	(R109) $2NH_3 + 3/2O_2 \rightarrow N_2 + 3H_2O$	Fe_2O_3,[494] Cr_2O_3,[494] CeO_2[494]
	Nitric oxide	(R110) $NH_3 + 5/4O_2 \rightarrow NO + 3/2H_2O$	Fe_2O_3,[494] Cr_2O_3,[494] CeO_2[494]
Hydrogen sulfide	Sulfur	(R111) $H_2S + 1/2O_2 \rightarrow 1/nS_n + H_2O$	$La_{1-x}Ce_xFeO_3$ (x = 0, 0.2, 0.4, 0.6 and 0.8),[495] Cu–V and Cu–V–Mo mixed oxides[496]

carriers, also offer exciting potential for chemical syntheses. Aside from these, significant progress still needs to be made towards in-depth understanding of redox reaction mechanisms, catalyst design and optimizations, reactor and process design and operations, as well as process scale up for the existing CLBC approaches. To summarize, we believe that CLBC represents a largely uncharted and extraordinarily exciting area of research and potential applications.

Conflicts of interest

Authors have no conflict of interest to declare.

Acknowledgements

This work was supported by the U.S. National Science Foundation (Award No. CBET-1604605 and CBET CBET-1510900), US Department of Energy (Award No. FE0031521 and RAPID Subaward DE-EE0007888-05-6) and the Kenan Institute for Engineering, Technology and Science at NC State University. The Scholarship provided by the State Key Laboratory of Complex Nonferrous Metal Resources Clean Utilization at Kunming University of Science and Technology is gratefully acknowledged. F. D and C. R. M. acknowledge the Swiss Office of Energy and the European Commission for financial support (BFE SI/501590-01 and ACT Grant Agreement No. 691712 under the Horizon 2020 programme).

References

1 H. J. Richter and K. F. Knoche, *Efficiency and Costing*, American Chemical Society, 1983, ch. 3, vol. 235, pp. 71–85.
2 A. Messerschmitt, Process of Producing Hydrogen, *US Pat.*, US971206A, 1910.
3 H. Lane, Process for the production of hydrogen, *US Pat.*, US1078686A, 1913.
4 M. Bui, C. S. Adjiman, A. Bardow, E. J. Anthony, A. Boston, S. Brown, P. S. Fennell, S. Fuss, A. Galindo, L. A. Hackett, J. P. Hallett, H. J. Herzog, G. Jackson, J. Kemper, S. Krevor, G. C. Maitland, M. Matuszewski, I. S. Metcalfe, C. Petit, G. Puxty, J. Reimer, D. M. Reiner, E. S. Rubin, S. A. Scott, N. Shah, B. Smit, J. P. M. Trusler, P. Webley, J. Wilcox and N. Mac Dowell, *Energy Environ. Sci.*, 2018, **11**, 1062–1176.
5 E. J. B. Anthony, *Coal in the 21st Century: Energy Needs, Chemicals and Environmental Controls*, The Royal Society of Chemistry, 2018, pp. 198–215.
6 M. Ishida, D. Zheng and T. Akehata, *Energy*, 1987, **12**, 147–154.
7 M. Ishida and H. Jin, *Energy*, 1994, **19**, 415–422.
8 M. Ishida and H. Jin, *Ind. Eng. Chem. Res.*, 1996, **35**, 2469–2472.
9 H. Jin and M. Ishida, *Int. J. Hydrogen Energy*, 2001, **26**, 889–894.
10 P. Gupta, L. G. Velazquez-Vargas, F. Li and L.-S. Fan, Proc. – Annu. Int. Pittsburgh Coal Conf., 2006, 23rd, 37.33/31-37.33/38.
11 F. He, H. Wang and Y. Dai, *J. Nat. Gas Chem.*, 2007, **16**, 155–161.
12 F. Li and L.-S. Fan, *Energy Environ. Sci.*, 2008, **1**, 248–267.
13 L.-S. Fan and F. Li, *Ind. Eng. Chem. Res.*, 2010, **49**, 10200–10211.
14 L.-S. Fan, L. Zeng and S. Luo, *AIChE J.*, 2015, **61**, 2–22.
15 L.-S. Fan, *Cambridge Series in Chemical Engineering*, Cambridge University Press, 2017.
16 C. Chung, L. Qin, V. Shah and L.-S. Fan, *Energy Environ. Sci.*, 2017, **10**, 2318–2323.
17 S. Bhavsar, M. Najera, A. More and G. Veser, *Reactor and Process Design in Sustainable Energy Technology*, ed. F. Shi, Elsevier, Amsterdam, 2014, pp. 233–280.
18 L. C. Buelens, H. Poelman, G. B. Marin and V. V. Galvita, *Ind. Eng. Chem. Res.*, 2019, **58**, 16235–16257.
19 T. Mattisson, M. Keller, C. Linderholm, P. Moldenhauer, M. Rydén, H. Leion and A. Lyngfelt, *Fuel Process. Technol.*, 2018, **172**, 1–12.
20 G. Veser and C. R. Müller, *Energy Technol.*, 2016, **4**, 1127–1129.
21 L. Zeng, Z. Cheng, J. A. Fan, L.-S. Fan and J. Gong, *Nat. Rev. Chem.*, 2018, **2**, 349–364.
22 S. C. Bayham, A. Tong, M. Kathe and L.-S. Fan, *Wiley Interdiscip. Rev.: Energy Environ.*, 2016, **5**, 216–241.
23 Development of the steam-iron process for hydrogen production, 1979.

24 S. Bhavsar, M. Najera, R. Solunke and G. Veser, *Catal. Today*, 2014, **228**, 96–105.
25 Q. Wang, J. Guo and P. Chen, *J. Energy Chem.*, 2019, **36**, 25–36.
26 M. M. Hossain and H. I. de Lasa, *Chem. Eng. Sci.*, 2008, **63**, 4433–4451.
27 H. Jin, H. Hong and T. Han, *Chin. Sci. Bull.*, 2009, **54**, 906–919.
28 L.-S. Fan, L. Zeng, W. Wang and S. Luo, *Energy Environ. Sci.*, 2012, **5**, 7254–7280.
29 Q. Imtiaz, D. Hosseini and C. R. Mueller, *Energy Technol.*, 2013, **1**, 633–647.
30 A. Lyngfelt, *Appl. Energy*, 2014, **113**, 1869–1873.
31 P. Wang, N. Means, D. Shekhawat, D. Berry and M. Massoudi, *Energies*, 2015, **8**, 10605–10635.
32 M. Matzen, J. Pinkerton, X. Wang and Y. Demirel, *Int. J. Greenhouse Gas Control*, 2017, **65**, 1–14.
33 J. Li, H. Zhang, Z. Gao, J. Fu, W. Ao and J. Dai, *Energy Fuels*, 2017, **31**, 3475–3524.
34 T. Gauthier, M. Yazdanpanah, A. Forret, B. Amblard, A. Lambert and S. Bertholin, *Powder Technol.*, 2017, **316**, 3–17.
35 T. Song and L. Shen, *Int. J. Greenhouse Gas Control*, 2018, **76**, 92–110.
36 A. Lyngfelt, A. Brink, Ø. Langørgen, T. Mattisson, M. Rydén and C. Linderholm, *Int. J. Greenhouse Gas Control*, 2019, **88**, 38–56.
37 Z. Haibo, T. Xin, M. Jinchen, S. Mingze, W. Baowen and M. Daofeng, *Int. J. Greenhouse Gas Control*, 2020, **93**, 102898.
38 A. Thursfield, A. Murugan, R. Franca and I. S. Metcalfe, *Energy Environ. Sci.*, 2012, **5**, 7421–7459.
39 J. Adanez, A. Abad, F. Garcia-Labiano, P. Gayan and L. F. de Diego, *Prog. Energy Combust. Sci.*, 2012, **38**, 215–282.
40 B. Moghtaderi, *Energy Fuels*, 2012, **26**, 15–40.
41 M. Tang, L. Xu and M. Fan, *Appl. Energy*, 2015, **151**, 143–156.
42 G. Voitic and V. Hacker, *RSC Adv.*, 2016, **6**, 98267–98296.
43 L. Protasova and F. Snijkers, *Fuel*, 2016, **181**, 75–93.
44 X. Zhao, H. Zhou, V. S. Sikarwar, M. Zhao, A.-H. A. Park, P. S. Fennell, L. Shen and L.-S. Fan, *Energy Environ. Sci.*, 2017, **10**, 1885–1910.
45 P. T. Krenzke, J. R. Fosheim and J. H. Davidson, *Sol. Energy*, 2017, **156**, 48–72.
46 J. Hu, V. V. Galvita, H. Poelman and G. B. Marin, *Materials*, 2018, **11**, 1187.
47 M. Luo, Y. Yi, S. Wang, Z. Wang, M. Du, J. Pan and Q. Wang, *Renewable Sustainable Energy Rev.*, 2018, **81**, 3186–3214.
48 Z. Cheng, L. Qin, J. A. Fan and L.-S. Fan, *Engineering*, 2018, **4**, 343–351.
49 X. Zhu, K. Li, L. Neal and F. Li, *ACS Catal.*, 2018, **8**, 8213–8236.
50 A. Mishra and F. Li, *Curr. Opin. Chem. Eng.*, 2018, **20**, 143–150.
51 S. Laassiri, *Alternative Catalytic Materials: Carbides, Nitrides, Phosphides and Amorphous Boron Alloys*, The Royal Society of Chemistry, 2018, pp. 120–132.
52 J. A. Medrano, A. Helmi, V. Spallina, M. van Sint Annaland and F. Gallucci, *Membrane Engineering for the Treatment of Gases: Volume 2: Gas-separation Issues Combined with Membrane Reactors (2)*, The Royal Society of Chemistry, 2018, vol. 2, pp. 30–57.
53 D. S. Baser, S. G. Nadgouda, A. S. Joshi and L. S. Fan, *Ind. Eng. Chem. Res.*, 2019, **58**, 16407–16416.
54 J. Vieten, B. Bulfin, F. Call, M. Lange, M. Schmucker, A. Francke, M. Roeb and C. Sattler, *J. Mater. Chem. A*, 2016, **4**, 13652–13659.
55 J. Dou, E. Krzystowczyk, A. Mishra, X. Liu and F. Li, *ACS Sustainable Chem. Eng.*, 2018, **6**, 15528–15540.
56 F. X. Chiron, G. S. Patience and S. Rifflart, *Chem. Eng. Sci.*, 2011, **66**, 6324–6330.
57 L. Silvester, A. Antzara, G. Boskovic, E. Heracleous, A. A. Lemonidou and D. B. Bukur, *Int. J. Hydrogen Energy*, 2015, **40**, 7490–7501.
58 L. M. Neal, A. Shafiefarhood and F. Li, *ACS Catal.*, 2014, **4**, 3560–3569.
59 A. Shafiefarhood, N. Galinsky, Y. Huang, Y. Chen and F. Li, *ChemCatChem*, 2014, **6**, 790–799.
60 L. Neal, A. Shafiefarhood and F. Li, *Appl. Energy*, 2015, **157**, 391–398.
61 C. Huang, J. Wu, Y.-T. Chen, M. Tian, A. I. Rykov, B. Hou, J. Lin, C.-R. Chang, X. Pan, J. Wang, A. Wang and X. Wang, *Commun. Chem.*, 2018, **1**, 55.
62 C. Lu, K. Li, H. Wang, X. Zhu, Y. Wei, M. Zheng and C. Zeng, *Appl. Energy*, 2018, **211**, 1–14.
63 K. Li, H. Wang, Y. Wei and D. Yan, *Appl. Catal., B*, 2010, **97**, 361–372.
64 X. Zhu, Y. Wei, H. Wang and K. Li, *Int. J. Hydrogen Energy*, 2013, **38**, 4492–4501.
65 J. R. Fosheim, B. J. Hathaway and J. H. Davidson, *Energy*, 2019, **169**, 597–612.
66 V. P. Haribal, F. He, A. Mishra and F. Li, *ChemSusChem*, 2017, **10**, 3402–3408.
67 J. Zhang, V. Haribal and F. Li, *Sci. Adv.*, 2017, **3**, e1701184.
68 Y. Zheng, K. Li, H. Wang, D. Tian, Y. Wang, X. Zhu, Y. Wei, M. Zheng and Y. Luo, *Appl. Catal., B*, 2017, **202**, 51–63.
69 Q. Shen, F. Huang, M. Tian, Y. Zhu, L. Li, J. Wang and X. Wang, *ACS Catal.*, 2019, **9**, 722–731.
70 Y. Zhu, W. Liu, X. Sun, X. Ma, Y. Kang, X. Wang and J. Wang, *AIChE J.*, 2018, **64**, 550–563.
71 S. Parishan, E. Nowicka, V. Fleischer, C. Schulz, M. G. Colmenares, F. Rosowski and R. Schomäcker, *Catal. Lett.*, 2018, **148**, 1–17.
72 W. Riedel, L. Thum, J. Möser, V. Fleischer, U. Simon, K. Siemensmeyer, A. Schnegg, R. Schomäcker, T. Risse and K.-P. Dinse, *J. Phys. Chem. C*, 2018, **122**, 22605–22614.
73 N. Kosinov, F. J. Coumans, E. Uslamin, F. Kapteijn and E. J. Hensen, *Angew. Chem. Int. Ed.*, 2016, **55**, 15086–15090.
74 C. Brady, B. Murphy and B. Xu, *ACS Catal.*, 2017, **7**, 3924–3928.
75 T. Sheppard, C. D. Hamill, A. Goguet, D. W. Rooney and J. M. Thompson, *Chem. Commun.*, 2014, **50**, 11053–11055.
76 V. L. Sushkevich, D. Palagin, M. Ranocchiari and J. A. van Bokhoven, *Science*, 2017, **356**, 523–527.
77 R. Blume, M. Hävecker, S. Zafeiratos, D. Techner, A. Knop-Gericke, R. Schlögl, L. Gregoratti, A. Barinov and

M. Kiskinova, in *Nanostructured Catalysts: Selective Oxidations*, ed. C. Hess and R. Schlögl, The Royal Society of Chemistry, 2011, pp. 248–265.
78 M. S. C. Chan, E. Marek, S. A. Scott and J. S. Dennis, *J. Catal.*, 2018, **359**, 1–7.
79 Y. Gao, L. M. Neal and F. Li, *ACS Catal.*, 2016, **6**, 7293–7302.
80 L. M. Neal, S. Yusuf, J. A. Sofranko and F. Li, *Energy Technol.*, 2016, **4**, 1200–1208.
81 S. Yusuf, L. M. Neal and F. Li, *ACS Catal.*, 2017, **7**, 5163–5173.
82 S. Yusuf, L. Neal, V. Haribal, M. Baldwin, H. H. Lamb and F. Li, *Appl. Catal., B*, 2018, **232**, 77–85.
83 R. B. Dudek, Y. Gao, J. Zhang and F. Li, *AIChE J.*, 2018, **64**, 3141–3150.
84 J. Beckers, R. Drost, Z. I. Van, P. F. Collignon and G. Rothenberg, *ChemPhysChem*, 2010, **9**, 1062–1068.
85 A. A. Ayandiran, I. A. Bakare, H. Binous, S. Al-Ghamdi, S. A. Razzak and M. M. Hossain, *Catal. Sci. Technol.*, 2016, **6**, 5154–5167.
86 D. K. Hood and O. M. Musa, *Handbook of Maleic Anhydride Based Materials*, 2016, pp. 3–55.
87 R. B. Dudek, X. Tian, M. Blivin, L. M. Neal, H. Zhao and F. Li, *Appl. Catal., B*, 2019, **246**, 30–40.
88 F. He and F. Li, *Energy Environ. Sci.*, 2015, **8**, 535–539.
89 F. He, J. Trainham, G. Parsons, J. S. Newman and F. Li, *Energy Environ. Sci.*, 2014, **7**, 2033–2042.
90 A. Murugan, A. Thursfield and I. Metcalfe, *Energy Environ. Sci.*, 2011, **4**, 4639–4649.
91 I. S. Metcalfe, B. Ray, C. Dejoie, W. Hu, C. de Leeuwe, C. Dueso, F. R. García-García, C.-M. Mak, E. I. Papaioannou, C. R. Thompson and J. S. O. Evans, *Nat. Chem.*, 2019, **11**, 638–643.
92 C. Dueso, C. Thompson and I. Metcalfe, *Appl. Energy*, 2015, **157**, 382–390.
93 D. Arifin and A. W. Weimer, *Sol. Energy*, 2018, **160**, 178–185.
94 V. V. Galvita, H. Poelman, C. Detavernier and G. B. Marin, *Appl. Catal., B*, 2015, **164**, 184–191.
95 B. J. Hare, D. Maiti, S. Ramani, A. E. Ramos, V. R. Bhethanabotla and J. N. Kuhn, *Catal. Today*, 2019, **323**, 225–232.
96 M. Wenzel, L. Rihko-Struckmann and K. Sundmacher, *Chem. Eng. J.*, 2018, **336**, 278–296.
97 N. V. R. A. Dharanipragada, L. C. Buelens, H. Poelman, E. De Grave, V. V. Galvita and G. B. Marin, *J. Mater. Chem. A*, 2015, **3**, 16251–16262.
98 G. Wenbo, G. Jianping, W. Peikun, W. Qianru, C. Fei, P. Qijun, Z. Weijin, L. Lin and C. Ping, *Nat. Energy*, 2018, **3**, 1067–1075.
99 R. Michalsky, B. J. Parman, V. Amanor-Boadu and P. H. Pfromm, *Energy*, 2012, **42**, 251–260.
100 Y. Wu, G. Jiang, H. Zhang, Z. Sun, Y. Gao, X. Chen, H. Liu, H. Tian, Q. Lai, M. Fan and D. Liu, *Chem. Commun.*, 2017, **53**, 10664–10667.
101 Y. Gao, Y. Wu, Q. Zhang, X. Chen, G. Jiang and D. Liu, *Int. J. Hydrogen Energy*, 2018, **43**, 16589–16597.
102 R. Michalsky, A. M. Avram, B. A. Peterson, P. H. Pfromm and A. A. Peterson, *Chem. Sci.*, 2015, **6**, 3965–3974.
103 I. AlShibane, A. Daisley, J. S. J. Hargreaves, A. L. Hector, S. Laassiri, J. L. Rico and R. I. Smith, *ACS Sustainable Chem. Eng.*, 2017, **5**, 9214–9222.
104 S. Laassiri, C. D. Zeinalipour-Yazdi, C. R. A. Catlow and J. S. J. Hargreaves, *Appl. Catal., B*, 2018, **223**, 60–66.
105 J. S. J. Hargreaves and D. McKay, *J. Mol. Catal. A: Chem.*, 2009, **305**, 125–129.
106 N. A. A. Rusman and M. Dahari, *Int. J. Hydrogen Energy*, 2016, **41**, 12108–12126.
107 R. Michalsky, P. H. Pfromm and A. Steinfeld, *Interface Focus*, 2015, **5**, 20140084.
108 J. G. Chen, R. M. Crooks, L. C. Seefeldt, K. L. Bren, R. M. Bullock, M. Y. Darensbourg, P. L. Holland, B. Hoffman, M. J. Janik, A. K. Jones, M. G. Kanatzidis, P. King, K. M. Lancaster, S. V. Lymar, P. Pfromm, W. F. Schneider and R. R. Schrock, *Science*, 2018, **360**, eaar6611.
109 A. Darde, R. Prabhakar, J.-P. Tranier and N. Perrin, *Energy Procedia*, 2009, **1**, 527–534.
110 R. L. Cornelissen and G. G. Hirs, *Energy Convers. Manage.*, 1998, **39**, 1821–1826.
111 L. M. Neal, V. P. Haribal and F. Li, *iScience*, 2019, **19**, 894–904.
112 V. P. Haribal, Y. Chen, L. Neal and F. Li, *Engineering*, 2018, **4**, 714–721.
113 V. P. Haribal, L. M. Neal and F. Li, *Energy*, 2017, **119**, 1024–1035.
114 Z. Zhao, M. Uddi, N. Tsvetkov, B. Yildiz and A. F. Ghoniem, *J. Phys. Chem. C*, 2016, **120**, 16271–16289.
115 N. Gokon, T. Suda and T. Kodama, *Energy*, 2015, **90**, 1280–1289.
116 C. L. Muhich, B. D. Ehrhart, V. A. Witte, S. L. Miller, E. N. Coker, C. B. Musgrave and A. W. Weimer, *Energy Environ. Sci.*, 2015, **8**, 3687–3699.
117 Z. Zhao, M. Uddi, N. Tsvetkov, B. Yildiz and A. F. Ghoniem, *Phys. Chem. Chem. Phys.*, 2017, **19**, 25774–25785.
118 J. R. Scheffe and A. Steinfeld, *Mater. Today*, 2014, **17**, 341–348.
119 C. L. Muhich, B. D. Ehrhart, I. Al-Shankitit, B. J. Ward, C. B. Musgrave and A. W. Weimer, *Wiley Interdiscip. Rev.: Energy Environ.*, 2016, **5**, 261–287.
120 C. Agrafiotis, M. Roeb and C. Sattler, *Renewable Sustainable Energy Rev.*, 2015, **42**, 254–285.
121 C. Ruan, Z.-Q. Huang, J. Lin, L. Li, X. Liu, M. Tian, C. Huang, C.-R. Chang, J. Li and X. Wang, *Energy Environ. Sci.*, 2019, **12**, 767–779.
122 L.-S. Fan, *Chemical Looping Systems for Fossil Energy Conversions*, Wiley, 2010.
123 Z. Sarshar, F. Kleitz and S. Kaliaguine, *Energy Environ. Sci.*, 2011, **4**, 4258–4269.
124 F. Li, Z. Sun, S. Luo and L.-S. Fan, *Energy Environ. Sci.*, 2011, **4**, 876–880.
125 F. Li, S. Luo, Z. Sun, X. Bao and L.-S. Fan, *Energy Environ. Sci.*, 2011, **4**, 3661–3667.
126 S. Wang, G. Wang, F. Jiang, M. Luo and H. Li, *Energy Environ. Sci.*, 2010, **3**, 1353–1360.
127 Q. Song, W. Liu, C. D. Bohn, R. N. Harper, E. Sivaniah, S. A. Scott and J. S. Dennis, *Energy Environ. Sci.*, 2013, **6**, 288–298.

128 Y. Gao, F. Haeri, F. He and F. Li, *ACS Catal.*, 2018, **8**, 1757–1766.
129 D. Maiti, B. J. Hare, Y. A. Daza, A. E. Ramos, J. N. Kuhn and V. R. Bhethanabotla, *Energy Environ. Sci.*, 2018, **11**, 648–659.
130 A. Mishra, T. Li, F. Li and E. E. Santiso, *Chem. Mater.*, 2019, **31**, 689–698.
131 A. Thursfield, A. Murugan, R. V. Franca and I. S. Metcalfe, *Energy Environ. Sci.*, 2012, **5**, 7421–7459.
132 F. Donat, Y. Xu and C. R. Müller, *Energy Technol.*, 2020, DOI: 10.1002/ente.201900655.
133 W. Benincosa, R. Siriwardane, H. Tian and J. Riley, *Appl. Energy*, 2017, **203**, 522–534.
134 F. He, N. Galinsky and F. Li, *Int. J. Hydrogen Energy*, 2013, **38**, 7839–7854.
135 I. Teknetzi, P. Nessi, V. Zaspalis and L. Nalbandian, *Int. J. Hydrogen Energy*, 2017, **42**, 26231–26242.
136 C. Y. Lau, M. T. Dunstan, W. Hu, C. P. Grey and S. A. Scott, *Energy Environ. Sci.*, 2017, **10**, 818–831.
137 A. H. Bork, E. Povoden-Karadeniz and J. L. M. Rupp, *Adv. Energy Mater.*, 2017, **7**, 1601086.
138 M. Kubicek, A. H. Bork and J. L. M. Rupp, *J. Mater. Chem. A*, 2017, **5**, 11983–12000.
139 A. Shafiefarhood, J. Zhang, L. M. Neal and F. Li, *J. Mater. Chem. A*, 2017, **5**, 11930–11939.
140 X. P. Dai, R. J. Li, C. C. Yu and Z. P. Hao, *J. Phys. Chem. B*, 2006, **110**, 22525–22531.
141 M. Machida, T. Kawada, H. Fujii and S. Hinokuma, *J. Phys. Chem. C*, 2015, **119**, 24932–24941.
142 D. Zhang, T. Kawada, F. Yoshioka and M. Machida, *ACS Omega*, 2016, **1**, 789–798.
143 M. Machida, M. Ueno, T. Omura, S. Kurusu, S. Hinokuma, T. Nanba, O. Shinozaki and H. Furutani, *Ind. Eng. Chem. Res.*, 2017, **56**, 3184–3193.
144 Z. Zhao, M. Uddi and A. F. Ghoniem, *Combust. Flame*, 2019, **207**, 71–88.
145 Y. Zhang and H. Jiang, *Chem. Commun.*, 2018, **54**, 10343–10346.
146 N. S. Yüzbasi, A. M. Kierzkowska, Q. Imtiaz, P. M. Abdala, A. Kurlov, J. L. M. Rupp and C. R. Müller, *J. Phys. Chem. C*, 2016, **120**, 18977–18985.
147 Q. Imtiaz, P. M. Abdala, A. M. Kierzkowska, W. van Beek, S. Schweiger, J. L. M. Rupp and C. R. Müller, *Phys. Chem. Chem. Phys.*, 2016, **18**, 12278–12288.
148 Q. Imtiaz, A. Kurlov, J. L. M. Rupp and C. R. Müller, *ChemSusChem*, 2015, **8**, 2055–2065.
149 J. W. Bennett, X. Huang, Y. Fang, D. M. Cwiertny, V. H. Grassian and S. E. Mason, *J. Phys. Chem. C*, 2019, **123**, 6450–6463.
150 N. S. Yüzbasi, P. M. Abdala, Q. Imtiaz, S. M. Kim, A. M. Kierzkowska, A. Armutlulu, W. van Beek and C. R. Müller, *Phys. Chem. Chem. Phys.*, 2018, **20**, 12736–12745.
151 K. J. Warren and J. R. Scheffe, *J. Phys. Chem. C*, 2019, **123**, 13208–13218.
152 T. Hatanaka and Y. Yukihiro, *Powder Technol.*, 2019, **356**, 974–979.
153 Y. De Vos, M. Jacobs, P. Van Der Voort, I. Van Driessche, F. Snijkers and A. Verberckmoes, *Chem. Eng. J.*, 2017, **309**, 824–839.
154 K. Li, X. Cheng, N. Li, X. Zhu, Y. Wei, K. Zhai and H. Wang, *J. Mater. Chem. A*, 2017, **5**, 24232–24246.
155 H. Bahzad, N. Shah, N. M. Dowell, M. Boot-Handford, S. M. Soltani, M. Ho and P. S. Fennell, *Int. J. Hydrogen Energy*, 2019, **44**, 21251–21263.
156 K. Aasberg-Petersen, I. Dybkjær, C. V. Ovesen, N. C. Schjødt, J. Sehested and S. G. Thomsen, *J. Nat. Gas Sci. Eng.*, 2011, **3**, 423–459.
157 A. I. O. Suarez, Á. Szécsényi, E. J. M. Hensen, J. Ruiz-Martínez, E. A. Pidko and J. Gascon, *ACS Catal.*, 2016, **6**, 2965–2981.
158 S. Arora and R. Prasad, *RSC Adv.*, 2016, **6**, 108668–108688.
159 B. Abdullah, N. A. Abd Ghani and D.-V. N. Vo, *J. Cleaner Prod.*, 2017, **162**, 170–185.
160 S. M. Kim, P. M. Abdala, T. Margossian, D. Hosseini, L. Foppa, A. Armutlulu, W. van Beek, A. Comas-Vives, C. Copéret and C. Müller, *J. Am. Chem. Soc.*, 2017, **139**, 1937–1949.
161 B. C. Enger, R. Lødeng and A. Holmen, *Appl. Catal., A*, 2008, **346**, 1–27.
162 V. P. Haribal, X. Wang, R. Dudek, C. Paulus, B. Turk, R. Gupta and F. Li, *Adv. Energy Mater.*, 2019, 1901963.
163 R. K. Lyon and J. A. Cole, *Combust. Flame*, 2000, **121**, 249–261.
164 S. Bhavsar and G. Veser, *RSC Adv.*, 2014, **4**, 47254–47267.
165 D. Li, R. Xu, Z. Gu, X. Zhu, S. Qing and K. Li, *Energy Technol.*, 2019, DOI: 10.1002/ente.201900925.
166 H. C. Mantripragada and G. Veser, *Energy Technol.*, 2020, DOI: 10.1002/ente.201900580.
167 D. R. Barcellos, M. D. Sanders, J. Tong, A. H. McDaniel and R. P. O'Hayre, *Energy Environ. Sci.*, 2018, **11**, 3256–3265.
168 D. Hosseini, F. Donat, S. M. Kim, L. Bernard, A. M. Kierzkowska and C. R. Müller, *ACS Appl. Energy Mater.*, 2018, **1**, 1294–1303.
169 X. Zhu, K. Li, Y. Wei, H. Wang and L. Sun, *Energy Fuels*, 2014, **28**, 754–760.
170 B. J. Hare, D. Maiti, Y. A. Daza, V. R. Bhethanabotla and J. N. Kuhn, *ACS Catal.*, 2018, **8**, 3021–3029.
171 M. Wenzel, N. V. R. Aditya Dharanipragada, V. V. Galvita, H. Poelman, G. B. Marin, L. Rihko-Struckmann and K. Sundmacher, *J. CO2 Util.*, 2017, **17**, 60–68.
172 S. Bock, R. Zacharias and V. Hacker, *RSC Adv.*, 2019, **9**, 23686–23695.
173 S. M. Kim, P. M. Abdala, M. Broda, D. Hosseini, C. Copéret and C. Müller, *ACS Catal.*, 2018, **8**, 2815–2823.
174 J. Hu, V. V. Galvita, H. Poelman, C. Detavernier and G. B. Marin, *Appl. Catal., B*, 2019, **247**, 86–99.
175 D. Kang, M. Lee, H. S. Lim and J. W. Lee, *Fuel*, 2018, **215**, 787–798.
176 A. Farooqui, A. Bose, D. Ferrero, J. Llorca and M. Santarelli, *J. CO2 Util.*, 2018, **27**, 500–517.
177 Y. Chen, X. Zhu, K. Li, Y. Wei, Y. Zheng and H. Wang, *ACS Sustainable Chem. Eng.*, 2019, **7**, 15452–15462.
178 A. Farooqui, F. Di Tomaso, A. Bose, D. Ferrero, J. Llorca and M. Santarelli, *Energy Convers. Manage.*, 2019, **186**, 200–219.
179 A. Mishra, N. Galinsky, F. He, E. E. Santiso and F. Li, *Catal. Sci. Technol.*, 2016, **6**, 4535–4544.

180 O. Vozniuk, N. Tanchoux, J. M. M. Millet, S. Albonetti, F. Di Renzo and F. Cavani, *Spinel Mixed Oxides for Chemical-Loop Reforming: From Solid State to Potential Application*, 2019.
181 T. Li, R. S. Jayathilake, D. D. Taylor and E. E. Rodriguez, *Chem. Commun.*, 2019, **55**, 4929–4932.
182 D. Zeng, Y. Qiu, S. Peng, C. Chen, J. Zeng, S. Zhang and R. Xiao, *J. Mater. Chem. A*, 2018, **6**, 11306–11316.
183 M. Guo, Z. Cheng, Y. Liu, L. Qin, J. Goetze, J. A. Fan and L.-S. Fan, *Catal. Today*, 2019, DOI: 10.1016/j.cattod.2019.06.016.
184 Y. Kang, M. Tian, C. Huang, J. Lin, B. Hou, X. Pan, L. Li, A. I. Rykov, J. Wang and X. Wang, *ACS Catal.*, 2019, **9**, 8373–8382.
185 A. Antzara, E. Heracleous, L. Silvester, D. B. Bukur and A. A. Lemonidou, *Catal. Today*, 2016, **272**, 32–41.
186 M. Johansson, T. Mattisson, A. Lyngfelt and A. Abad, *Fuel*, 2008, **87**, 988–1001.
187 A. More, C. J. Hansen and G. Veser, *Catal. Today*, 2017, **298**, 21–32.
188 A. More, S. Bhavsar and G. Veser, *Energy Technol.*, 2016, **4**, 1147–1157.
189 S.-K. Otto, K. Kousi, D. Neagu, L. Bekris, J. Janek and I. Metcalfe, *ACS Appl. Energy Mater.*, 2019, **2**, 7288–7298.
190 J. Huang, W. Liu, Y. Yang and B. Liu, *ACS Catal.*, 2018, **8**, 1748–1756.
191 D. Hosseini, F. Donat, P. M. Abdala, S. M. Kim, A. M. Kierzkowska and C. R. Müller, *ACS Appl. Mater. Interfaces*, 2019, **11**, 18276–18284.
192 H. Tian, T. Simonyi, J. Poston and R. Siriwardane, *Ind. Eng. Chem. Res.*, 2009, **48**, 8418–8430.
193 A. R. Oller, M. Costa and G. Oberdöster, *Toxicol. Appl. Pharmacol.*, 1997, **143**, 152–166.
194 R. D. Solunke and G. T. Veser, *Ind. Eng. Chem. Res.*, 2010, **49**, 11037–11044.
195 S. K. Wilke and D. C. Dunand, *Acta Mater.*, 2019, **162**, 90–102.
196 K. Zhao, F. He, Z. Huang, G. Wei, A. Zheng, H. Li and Z. Zhao, *Appl. Energy*, 2016, **168**, 193–203.
197 F. He, X. Li, K. Zhao, Z. Huang, G. Wei and H. Li, *Fuel*, 2013, **108**, 465–473.
198 M. S. S. Khine, L. Chen, S. Zhang, J. Lin and S. P. Jiang, *Int. J. Hydrogen Energy*, 2013, **38**, 13300–13308.
199 Y. Saito, F. Kosaka, N. Kikuchi, H. Hatano and J. Otomo, *Ind. Eng. Chem. Res.*, 2018, **57**, 5529–5538.
200 X.-Y. Wu and A. F. Ghoniem, *Prog. Energy Combust. Sci.*, 2019, **74**, 1–30.
201 N. L. Galinsky, Y. Huang, A. Shafiefarhood and F. Li, *ACS Sustainable Chem. Eng.*, 2013, **1**, 364–373.
202 W. C. Cho, J. K. Lee, G. D. Nam, C. H. Kim, H.-S. Cho and J. H. Joo, *Appl. Energy*, 2019, **239**, 644–657.
203 N. L. Galinsky, A. Shafiefarhood, Y. G. Chen, L. Neal and F. X. Li, *Appl. Catal., B*, 2015, **164**, 371–379.
204 S. Ma, S. Chen, M. Zhu, Z. Zhao, J. Hu, M. Wu, S. Toan and W. Xiang, *Int. J. Hydrogen Energy*, 2019, **44**, 6491–6504.
205 A. Shafiefarhood, J. C. Hamill, L. M. Neal and F. Li, *Phys. Chem. Chem. Phys.*, 2015, **17**, 31297–31307.
206 M. S. Liao and Q. E. Zhang, *J. Mol. Catal. A: Chem.*, 1998, **136**, 185–194.
207 Q. Imtiaz, N. S. Yuzbasi, P. M. Abdala, A. M. Kierzkowska, W. van Beek, M. Broda and C. R. Muller, *J. Mater. Chem. A*, 2016, **4**, 113–123.
208 R. Palcheva, U. Olsbye, M. Palcut, P. Rauwel, G. Tyuliev, N. Velinov and H. H. Fjellvåg, *Appl. Surf. Sci.*, 2015, **357**, 45–54.
209 H. Li, K. Li, H. Wang, X. Zhu, Y. Wei, D. Yan, X. Cheng and K. Zhai, *Appl. Surf. Sci.*, 2016, **390**, 513–525.
210 J. L. G. Fierro, *Catal. Lett.*, 1993, **22**, 67–91.
211 S. Arndt, G. Laugel, S. Levchenko, R. Horn, M. Baerns, M. Scheffler, R. Schlogl and R. Schomacker, *Catal. Rev.*, 2011, **53**, 424–514.
212 Y. Amenomiya, V. I. Birss, M. Goledzinowski, J. Galuszka and A. R. Sanger, *Catal. Rev.*, 1990, **32**, 163–227.
213 E. V. Kondratenko and B. Manfred, Oxidative Coupling of Methane, *Handbook of Heterogeneous Catalysis*, 2008, DOI: 10.1002/9783527610044.hetcat0152.
214 K. Tabata, Y. Teng, T. Takemoto, E. Suzuki, M. A. Bañares, M. A. Peña and J. L. G. Fierro, *Catal. Rev.*, 2002, **44**, 1–58.
215 A. M. Gaffney, C. A. Jones, J. J. Leonard and J. A. Sofranko, *J. Catal.*, 1988, **114**, 422–432.
216 G. E. Keller and M. M. Bhasin, *Chem. Informationsdienst*, 1982, **73**, 9–19.
217 J. A. Labinger, *Catal. Lett.*, 1988, **1**, 371–375.
218 J. S. Lee and S. T. Oyama, *Catal. Rev.*, 1988, **30**, 249–280.
219 Y. S. Su, J. Y. Ying and W. H. Green Jr, *J. Catal.*, 2003, **218**, 321–333.
220 A. E. Bishop, K. Sekiya, M. J. Salahuddin, J. H. Steel, M. Hedges, T. Domoto, R. Fischer-Colbrie, H. Winkler, M. A. Ghatei and S. R. Bloom, *ChemCatChem*, 2011, **3**, 1935–1947.
221 E. V. Kondratenko and M. Baerns, *Catalysis of Oxidative Methane Conversions*, 2011, ch. 3, pp. 35–55.
222 S. Parishan, P. Littlewood, A. Arinchtein, V. Fleischer and R. Schomäcker, *Catal. Today*, 2018, **311**, 40–47.
223 A. Cruellas, T. Melchiori, F. Gallucci and M. V. S. Annaland, *Catal. Rev.: Sci. Eng.*, 2017, **59**, 234–294.
224 E. V. Kondratenko and M. Baerns, *Focus on Catalysts*, 2012, 8.
225 B. Beck, V. Fleischer, S. Arndt, M. G. Hevia, A. Urakawa, P. Hugo and R. Schomäcker, *Catal. Today*, 2014, **228**, 212–218.
226 I. Kim, G. Lee, H. Bin Na, J. M. Ha and J. C. Jung, *Mol. Catal.*, 2017, **435**, 13–23.
227 V. Fleischer, R. Steuer, S. Parishan and R. Schomacker, *J. Catal.*, 2016, **341**, 91–103.
228 V. Fleischer, P. Littlewood, S. Parishan and R. Schomäcker, *Chem. Eng. J.*, 2016, **306**, 646–654.
229 Z. C. Jiang, H. Gong and S. B. Li, *Stud. Surf. Sci. Catal.*, 1997, **112**, 481–490.
230 S. Pak, P. Qiu and J. H. Lunsford, *J. Catal.*, 1998, **179**, 222–230.
231 V. Fleischer, P. Littlewood, S. Parishan and R. Schomacker, *Chem. Eng. J.*, 2016, **306**, 646–654.
232 E. Y. Chung, W. K. Wang, S. G. Nadgouda, D. S. Baser, J. A. Sofranko and L. S. Fan, *Ind. Eng. Chem. Res.*, 2016, **55**, 12750–12764.
233 V. Fleischer, U. Simon, S. Parishan, M. G. Colmenares, O. Gorke, A. Gurlo, W. Riedel, L. Thum, J. Schmidt,

T. Risse, K. P. Dinse and R. Schomacker, *J. Catal.*, 2018, **360**, 102–117.
234 Z. Cheng, D. S. Baser, S. G. Nadgouda, L. Qin, J. A. Fan and L.-S. Fan, *ACS Energy Lett.*, 2018, **3**, 1730–1736.
235 S. Parishan, P. Littlewood, A. Arinchtein, V. Fleischer and R. Schomacker, *Catal. Today*, 2018, **311**, 40–47.
236 A. Malekzadeh, A. Khodadadi, M. Abedini, M. Amini, A. Bahramian and A. K. Dalai, *Catal. Commun.*, 2001, **2**, 241–247.
237 L. Wang, L. Tao, M. Xie, G. Xu, J. Huang and Y. Xu, *Catal. Lett.*, 1993, **21**, 35–41.
238 Z. R. Ismagilov, E. V. Matus and L. T. Tsikoza, *Energy Environ. Sci.*, 2008, **1**, 526–541.
239 J. J. Spivey and H. Graham, *Chem. Soc. Rev.*, 2014, **43**, 792–803.
240 C. Brady, B. M. Murphy and B. Xu, *ACS Catal.*, 2017, **7**, 3924–3928.
241 J. Gao, Y. Zheng, J.-M. Jehng, Y. Tang, I. E. Wachs and S. G. Podkolzin, *Science*, 2015, **348**, 686–690.
242 R. W. Borry, E. C. Lu, Y. H. Kim and E. Iglesia, *Natural Gas Conversion V*, 1998, vol. 119, pp. 403–410.
243 A. A. Latimer, A. Kakekhani, A. R. Kulkarni and J. K. Nørskov, *ACS Catal.*, 2018, **8**, 6894–6907.
244 T. Lunkenbein, F. Girgsdies, T. Kandemir, N. Thomas, M. Behrens, R. Schlögl and E. Frei, *Angew. Chem., Int. Ed.*, 2016, **128**, 12900–12904.
245 M. Ravi and M. Ranocchiari, *Angew. Chem. Int. Ed.*, 2017, **56**, 16464.
246 A. C. Rosenzweig, C. A. Frederick, S. J. Lippard and P. Nordlund, *Nature*, 1993, **366**, 537–543.
247 K. T. Dinh, M. M. Sullivan, P. Serna, R. J. Meyer, M. Dinca and Y. Roman-Leshkov, *ACS Catal.*, 2018, **8**, 8306–8313.
248 A. R. Kulkarni, Z. J. Zhao, S. Siahrostami, J. K. Norskov and F. Studt, *Catal. Sci. Technol.*, 2018, **8**, 114–123.
249 B. Ipek and R. F. Lobo, *Chem. Commun.*, 2016, **52**, 13401–13404.
250 S. Grundner, M. A. C. Markovits, G. Li, M. Tromp, E. A. Pidko, E. J. M. Hensen, A. Jentys, M. Sanchez-Sanchez and J. A. Lercher, *Nat. Commun.*, 2015, **6**, 7546.
251 J.-P. Lange, V. L. Sushkevich, A. J. Knorpp and J. A. van Bokhoven, *Ind. Eng. Chem. Res.*, 2019, **58**, 8674–8680.
252 V. L. Sushkevich, D. Palagin, M. Ranocchiari and J. A. van Bokhoven, *Science*, 2017, **358**, eaan5970.
253 L. Artiglia, V. L. Sushkevich, D. Palagin, A. J. Knorpp, K. Roy and J. A. van Bokhoven, *ACS Catal.*, 2019, **9**, 6728–6737.
254 K. Narsimhan, K. Iyoki, K. Dinh and Y. Roman-Leshkov, *ACS Cent. Sci.*, 2016, **2**, 424–429.
255 P. Atkins, T. Overton and J. Rourke, *Shriver and Atkins' Inorganic Chemistry*, Oxford University Press, 2009.
256 L. Neal, V. Haribal, J. McCaig, H. H. Lamb and F. Li, *J. Adv. Manuf. Proc.*, 2019, **1**, e10015.
257 F. Cavani and F. Trifiro, *Catal. Today*, 1995, **24**, 307–313.
258 M. A. Banares, *Catal. Today*, 1999, **51**, 319–348.
259 J. J. H. B. Sattler, J. Ruiz-Martinez, E. Santillan-Jimenez and B. M. Weckhuysen, *Chem. Rev.*, 2014, **114**, 10613–10653.
260 O. O. James, S. Mandal, N. Alele, B. Chowdhury and S. Maity, *Fuel Process. Technol.*, 2016, **149**, 239–255.
261 F. Cavani, N. Ballarini and A. Cericola, *Catal. Today*, 2007, **127**, 113–131.
262 C. A. Gartner, A. C. van Veen and J. A. Lercher, *ChemCatChem*, 2013, **5**, 3196–3217.
263 S. Agouram, A. Dejoz, F. Ivars, I. Vázquez, J. M. López Nieto and B. Solsona, *Fuel Process. Technol.*, 2014, **119**, 105–113.
264 T. Ren, M. Patel and K. Blok, *Energy*, 2006, **31**, 425–451.
265 US Pat., 2017/0313637 A1, 2015.
266 Y. Gao, L. Neal, D. Ding, W. Wu, C. Baroi, A. M. Gaffney and F. Li, *ACS Catal.*, 2019, 8592–8621.
267 J. G. Tsikoyiannis, D. L. Stern and R. K. Grasselli, *J. Catal.*, 1999, **184**, 77–86.
268 R. K. Grasselli, D. L. Stern and J. G. Tsikoyiannis, in *Studies in Surface Science and Catalysis*, ed. A. Corma, F. V. Melo, S. Mendioroz and J. L. G. Fierro, Elsevier, 2000, vol. 130, pp. 773–778.
269 R. K. Grasselli, D. L. Stern and J. G. Tsikoyiannis, *Calcif. Tissue Int.*, 1999, **189**, 1–7.
270 D. Creaser, B. Andersson, R. R. Hudgins and P. L. Silveston, *J. Catal.*, 1999, **182**, 264–269.
271 E. A. D. Graaf, G. Zwanenburg, G. Rothenberg and A. Bliek, *Org. Process Res. Dev.*, 2005, **9**, 397–403.
272 L. M. van der Zande, E. A. de Graaf and G. Rothenberg, *Adv. Synth. Catal.*, 2002, **344**, 884–889.
273 E. A. de Graaf, A. Andreini, E. J. M. Hensen and A. Bliek, *Appl. Catal., A*, 2004, **262**, 201–206.
274 J. Beckers and G. Rothenberg, *Green Chem.*, 2009, **11**, 1550.
275 C.-H. Lin, K.-C. Lee and B.-Z. Wan, *Appl. Catal., A*, 1997, **164**, 59–67.
276 L. Late, W. Thelin and E. A. Blekkan, *Appl. Catal., A*, 2004, **262**, 63–68.
277 M. S. C. Chan, H. G. Baldovi and J. S. Dennis, *Catal. Sci. Technol.*, 2018, **8**, 887–897.
278 J. Beckers, A. F. Lee and G. Rothenberg, *Adv. Synth. Catal.*, 2009, **351**, 1557–1566.
279 J. Beckers and G. Rothenberg, *Dalton Trans.*, 2009, 5673–5682.
280 J. H. Blank, J. Beckers, P. F. Collignon and G. Rothenberg, *ChemPhysChem*, 2007, **8**, 2490–2497.
281 G. Rothenberg, E. A. de Graaf and A. Bliek, *Angew. Chem., Int. Ed.*, 2003, **42**, 3366–3368.
282 J. H. Blank, J. Beckers, P. F. Collignon, F. Clerc and G. Rothenberg, *Chemistry*, 2007, **13**, 5121–5128.
283 E. A. D. Graaf, G. Rothenberg, P. J. Kooyman, A. Andreini and A. Bliek, *Appl. Catal., A*, 2005, **278**, 187–194.
284 P. Novotny, S. Yusuf, F. X. Li and H. H. Lamb, *Catal. Today*, 2018, **317**, 50–55.
285 S. Yusuf, V. Haribal, D. Jackson, L. Neal and F. Li, *Appl. Catal., B*, 2019, **257**, 117885.
286 S. Yusuf, L. Neal, Z. Bao, Z. Wu and F. Li, *ACS Catal.*, 2019, **9**, 3174–3186.
287 C. Zhao and J. A. Lercher, *ChemCatChem*, 2012, **4**, 64–68.
288 H. Saito, H. Seki, Y. Hosono, T. Higo, J. G. Seo, S. Maeda, K. Hashimoto, S. Ogo and Y. Sekine, *J. Phys. Chem. C*, 2019, **123**, 26272–26281.

289 P. Mars and D. W. V. Krevelen, *Chem. Eng. Sci.*, 1954, **3**, 41–59.
290 R. Grabowski, *Catal. Rev.*, 2006, **48**, 199–268.
291 R. Schlöl, *Angew. Chem. Int. Ed.*, 2015, **54**, 3465–3520.
292 D. Arne, S. C. Reinhard and A. T. Bell, *Phys. Chem. Chem. Phys.*, 2009, **11**, 6119–6124.
293 N. Ballarini, A. Battisti, F. Cavani, A. Cericola, C. Cortelli, M. Ferrari, F. Trifirò and P. Arpentinier, *Appl. Catal., A*, 2006, **307**, 148–155.
294 D. Creaser, B. Andersson, R. R. Hudgins and P. L. Silveston, *Chem. Eng. Sci.*, 1999, **54**, 4437–4448.
295 O. Rubio, J. Herguido and M. Menéndez, *Chem. Eng. Sci.*, 2003, **58**, 4619–4627.
296 I. A. Bakare, S. A. Mohamed, S. Al-Ghamdi, S. A. Razzak, M. M. Hossain and H. I. de Lasa, *Chem. Eng. J.*, 2015, **278**, 207–216.
297 S. N. Khadzhiev, N. Y. Usachev, I. M. Gerzeliev, V. P. Kalinin, V. V. Kharlamov, E. P. Belanova, A. V. Kazakov, S. A. Kanaev and T. S. Starostina, *Pet. Chem.*, 2015, **55**, 640–644.
298 S. Al-Ghamdi, M. Volpe, M. M. Hossain and H. de Lasa, *Appl. Catal., A*, 2013, **450**, 120–130.
299 A. Qiao, V. N. Kalevaru, J. Radnik, A. Düvel, P. Heitjans, A. S. H. Kumar, P. S. S. Prasad, N. Lingaiah and A. Martin, *Ind. Eng. Chem. Res.*, 2014, **53**, 18711–18721.
300 A. H. Elbadawi, M. S. Ba-Shammakh, S. Al-Ghamdi, S. A. Razzak, M. M. Hossain and H. I. de Lasa, *Chem. Eng. Sci.*, 2016, **145**, 59–70.
301 A. H. Elbadawi, M. S. Ba-Shammakh, S. Al-Ghamdi, S. A. Razzak and M. M. Hossain, *Chem. Eng. J.*, 2016, **284**, 448–457.
302 N. Ballarini, F. Cavani, M. Ferrari, R. Catani and U. Cornaro, *J. Catal.*, 2003, **213**, 95–102.
303 N. Ballarini, F. Cavani, A. Cericola, C. Cortelli, M. Ferrari, F. Trifirò, R. Catani and U. Cornaro, *Stud. Surf. Sci. Catal.*, 2004, **147**, 649–654.
304 N. Ballarini, F. Cavani, A. Cericola, C. Cortelli, M. Ferrari, F. Trifirò, G. Capannelli, A. Comite, R. Catani and U. Cornaro, *Catal. Today*, 2004, **91**, 99–104.
305 K. Fukudome, N. O. Ikenaga, T. Miyake and T. Suzuki, *Catal. Sci. Technol.*, 2011, **1**, 987–998.
306 D. Delgado, B. Solsona, A. Ykrelef, A. Rodríguez-Gómez, A. Caballero, E. Rodríguez-Aguado, E. Rodríguez-Castellón and J. M. López Nieto, *J. Phys. Chem. C*, 2017, **121**, 25132–25142.
307 Z. Zhang, J. Ding, R. Chai, G. Zhao, Y. Liu and Y. Lu, *Appl. Catal., A*, 2018, **550**, 151–159.
308 R. Koirala, R. Buechel, S. E. Pratsinis and A. Baiker, *Appl. Catal., A*, 2016, **527**, 96–108.
309 Z. Li, A. W. Peters, A. E. Platero-Prats, J. Liu, C. W. Kung, H. Noh, M. R. DeStefano, N. M. Schweitzer, K. W. Chapman, J. T. Hupp and O. K. Farha, *J. Am. Chem. Soc.*, 2017, **139**, 15251–15258.
310 S. A. Al-Ghamdi, M. M. Hossain and H. I. de Lasa, *Ind. Eng. Chem. Res.*, 2013, **52**, 5235–5244.
311 M. Y. Khan, S. Al-Ghamdi, S. A. Razzak, M. M. Hossain and H. de Lasa, *Mol. Catal.*, 2017, **443**, 78–91.
312 A. H. Elbadawi, M. S. Ba-Shammakh, S. Al-Ghamdi, S. A. Razzak, M. M. Hossain and H. I. de Lasa, *Chem. Eng. Res. Des.*, 2017, **117**, 733–745.
313 J. Moreira, S. Al-Ghamdi and H. D. Lasa, *Ind. Eng. Chem. Res.*, 2014, **53**, 15317–15332.
314 A. H. I. d. L. Samira Rostom, *Ind. Eng. Chem. Res.*, 2017, **56**, 13109–13124.
315 M. M. Hossain, *Ind. Eng. Chem. Res.*, 2017, **56**, 4309–4318.
316 S. N. Khadzhiev, N. Y. Usachev, I. M. Gerzeliev, E. P. Belanova, V. P. Kalinin, V. V. Kharlamov, A. V. Kazakov, S. A. Kanaev, T. S. Starostina and A. Y. Popov, *Pet. Chem.*, 2015, **55**, 651–654.
317 I. M. Gerzeliev, A. Y. Popov and V. A. Ostroumova, *Pet. Chem.*, 2016, **56**, 724–729.
318 N. Y. Usachev, I. M. Gerzeliev, V. V. Kharlamov, V. P. Kalinin, E. P. Belanova, S. A. Kanaev, A. V. Kazakov and T. S. Starostina, *Pet. Chem.*, 2016, **56**, 841–845.
319 N. Y. Usachev, I. M. Gerzeliev, E. P. Belanova, A. V. Kazakov, V. P. Kalinin, V. V. Kharlamov, S. A. Kanaev and T. S. Starostina, *Pet. Chem.*, 2016, **56**, 846–851.
320 B. M. Weckhuysen and R. A. Schoonheydt, *Catal. Today*, 1999, **51**, 223–232.
321 K. H. Kang, T. H. Kim, W. C. Choi, Y. K. Park, U. G. Hong, D. S. Park, C. J. Kim and I. K. Song, *Catal. Commun.*, 2015, **72**, 68–72.
322 T. H. Kim, M. Y. Gim, J. H. Song, W. C. Choi, Y.-K. Park, U. G. Hong, D. S. Park and I. K. Song, *Catal. Commun.*, 2017, **97**, 37–41.
323 S. Sim, S. Gong, J. Bae, Y.-K. Park, J. Kim, W. C. Choi, U. G. Hong, D. S. Park, I. K. Song, H. Seo, N. Y. Kang and S. Park, *Mol. Catal.*, 2017, **436**, 164–173.
324 T. H. Kim, K. H. Kang, M. Baek, J. H. Song, U. G. Hong, D. S. Park, W. C. Choi, Y. K. Park and I. K. Song, *Mol. Catal.*, 2017, **433**, 1–7.
325 S. Chen, L. Zeng, R. Mu, C. Xiong, Z.-J. Zhao, C. Zhao, C. Pei, L. Peng, J. Luo, L.-S. Fan and J. Gong, *J. Am. Chem. Soc.*, 2019, **141**, 18653–18657.
326 C. A. Carrero, R. Schloegl, I. E. Wachs and R. Schomaecker, *ACS Catal.*, 2014, **4**, 3357–3380.
327 C. H. Bartholomew and R. J. Farrauto, *Catalytic Oxidations of Inorganic and Organic Compounds*, John Wiley & Sons, Inc., 2010.
328 J. R. Monnier, *Appl. Catal., A*, 2001, **221**, 73–91.
329 S. J. Khatib and S. T. Oyama, *Catal. Rev.*, 2015, **57**, 306–344.
330 A. Chongterdtoonskul, J. W. Schwank and S. Chavadej, *J. Mol. Catal. A: Chem.*, 2013, **372**, 175–182.
331 M. O. Ozbek and R. A. van Santen, *Catal. Lett.*, 2013, **143**, 131–141.
332 R. M. Lambert, F. J. Williams, R. L. Cropley and A. Palermo, *J. Mol. Catal. A: Chem.*, 2005, **228**, 27–33.
333 C. J. Bertole and C. A. Mims, *J. Catal.*, 1999, **184**, 224–235.
334 A. Chongterdtoonskul, J. W. Schwank and S. Chavadej, *J. Mol. Catal. A: Chem.*, 2012, **358**, 58–66.
335 P. T. Connor, S. Kovenklioglu and D. C. Shelly, *Appl. Catal.*, 1991, **71**, 247–263.
336 S. S. Hassani, M. R. Ghasemi, M. Rashidzadeh and Z. Sobat, *Cryst. Res. Technol.*, 2010, **44**, 948–952.

337 A. Chongterdtoonskul, J. W. Schwank and S. Chavadej, *Catal. Lett.*, 2012, **142**, 991–1002.
338 L. Zhu, W. Zhang, J. Q. Zhu and D. J. Cheng, *Appl. Catal., A*, 2017, **538**, 27–36.
339 E. J. Marek, S. Gabra, J. S. Dennis and S. A. Scott, *Appl. Catal., B*, 2020, **262**, 118216.
340 G. L. Montrasi, G. R. Tauszik, M. Solari and G. Leofanti, *Appl. Catal.*, 1983, **5**, 359–369.
341 G. Boskovic, N. Dropka, D. Wolf, A. Bruckner and M. Baerns, *J. Catal.*, 2004, **226**, 334–342.
342 G. Boskovic, D. Wolf, A. Brückner and M. Baerns, *J. Catal.*, 2004, **224**, 187–196.
343 Y. Pang, X. Chen, C. Xu, Y. Lei and K. Wei, *ChemCatChem*, 2014, **6**, 876–884.
344 T. Chukeaw, A. Seubsai, P. Phon-in, K. Charoen, T. Witoon, W. Donphai, P. Parpainainar, M. Chareonpanich, D. Noon, B. Zohour and S. Senkan, *RSC Adv.*, 2016, **6**, 56116–56126.
345 A. Seubsai, M. Kahn, B. Zohour, D. Noon, M. Charoenpanich and S. Senkan, *Ind. Eng. Chem. Res.*, 2015, **54**, 2638–2645.
346 M. P. Dudukovic, *Science*, 2009, **325**, 698–701.
347 G. S. Patience and R. E. Bockrath, *Appl. Catal., A*, 2010, **376**, 4–12.
348 R. Contractor, R. J. Dry, C. White, Q. M. Mao, S. Konstantinidis and O. E. Potter, *Powder Technol.*, 2000, **111**, 132–144.
349 R. M. Contractor, *Chem. Eng. Sci.*, 1999, **54**, 5627–5632.
350 H. G. Lintz and A. Reitzmann, *Catal. Rev.*, 2007, **49**, 1–32.
351 R. R. Hudgins, P. L. Silveston, C.-Y. Li and A. A. Adesina, in *Periodic Operation of Chemical Reactors*, ed. P. L. Silveston and R. R. Hudgins, Butterworth-Heinemann, Oxford, 2013, pp. 79–122.
352 J. G. Yates and P. Lettieri, *Catalytic Processes*, 2016, vol. 26, pp. 23–65.
353 A. Godefroy, G. S. Patience, R. Cenni and J.-L. Dubois, *Chem. Eng. Sci.*, 2010, **65**, 261–266.
354 G. S. Patience and R. E. Bockrath, *Appl. Catal., A*, 2010, **376**, 4–12.
355 M. G. Rosmaninho, F. C. C. Moura, L. R. Souza, R. K. Nogueira, G. M. Gomes, J. S. Nascimento, M. C. Pereira, J. D. Fabris, J. D. Ardisson, M. S. Nazzarro, K. Sapag, M. H. Araujo and R. M. Lago, *Appl. Catal., B*, 2012, **115**, 45–52.
356 E. Hormilleja, P. Duran, J. Plou, J. Herguido and J. A. Pena, *Int. J. Hydrogen Energy*, 2014, **39**, 5267–5273.
357 R. Campo, P. Duran, J. Plou, J. Herguido and J. A. Pena, *J. Power Sources*, 2013, **242**, 520–526.
358 C. Trevisanut, M. Mari, J. M. M. Millet and F. Cavani, *Int. J. Hydrogen Energy*, 2015, **40**, 5264–5271.
359 J. V. Ochoa, C. Trevisanut, J. M. M. Millet, G. Busca and F. Cavani, *J. Phys. Chem. C*, 2013, **117**, 23908–23918.
360 C. Trevisanut, F. Bosselet, F. Cavania and J. M. M. Millet, *Catal. Sci. Technol.*, 2015, **5**, 1280–1289.
361 O. Vozniuk, S. Agnoli, L. Artiglia, A. Vassoi, N. Tanchoux, F. Di Renzo, G. Granozzi and F. Cavani, *Green Chem.*, 2016, **18**, 1038–1050.
362 N. V. R. A. Dharanipragada, V. V. Galvita, H. Poelman, L. C. Buelens, C. Detavernier and G. B. Marin, *Appl. Catal., B*, 2018, **222**, 59–72.
363 C. Wang, B. L. Dou, B. Jiang, Y. C. Song, B. G. Du, C. Zhang, K. Q. Wang, H. S. Chen and Y. J. Xu, *Int. J. Hydrogen Energy*, 2015, **40**, 7037–7044.
364 P. Pimenidou, G. Rickett, V. Dupont and M. V. Twigg, *Bioresource Technol.*, 2010, **101**, 6389–6397.
365 A. Hoteit, A. Forret, W. Pelletant, J. Roesler and T. Gauthier, *Oil Gas Sci. Technol.*, 2011, **66**, 193–199.
366 P. Moldenhauer, M. Ryden, T. Mattisson and A. Lyngfelt, *Int. J. Greenhouse Gas Control*, 2012, **9**, 1–9.
367 T. Mendiara, J. M. Johansen, R. Utrilla, P. Geraldo, A. D. Jensen and P. Glarborg, *Fuel*, 2011, **90**, 1049–1060.
368 M. Keller, H. Leion, T. Mattisson and H. Thunman, *Energy Fuels*, 2014, **28**, 3833–3840.
369 M. Keller, D. P. Anderson, H. Leion and T. Mattisson, *Appl. Catal., A*, 2018, **550**, 105–112.
370 Z. Q. Wang, M. Zhu, T. He, J. Z. Zhang, J. L. Wu, H. J. Tian and J. H. Wu, *Fuel*, 2018, **222**, 375–384.
371 Y. Sun, E. Jiang, X. Xu, J. Wang and Z. Li, *ACS Sustainable Chem. Eng.*, 2018, **6**, 14660–14668.
372 Q. Hu, Y. Shen, J. W. Chew, T. Ge and C.-H. Wang, *Chem. Eng. J.*, 2020, **379**, 122346.
373 T. Shen, H. Ge and L. Shen, *Int. J. Greenhouse Gas Control*, 2018, **75**, 63–73.
374 Z. Sun, X. Wu, C. K. Russell, M. D. Dyar, E. C. Sklute, S. Toan, M. Fan, L. Duan and W. Xiang, *J. Mater. Chem. A*, 2019, **7**, 1216–1226.
375 J. S. Dennis and S. A. Scott, *Fuel*, 2010, **89**, 1623–1640.
376 M. Keller, H. Leion, T. Mattisson and A. Lyngfelt, *Combust. Flame*, 2011, **158**, 393–400.
377 Q. Imtiaz, D. Hosseini and C. R. Müller, *Energy Technol.*, 2013, **1**, 633–647.
378 G. Luo, X. Wang, M. R. Zachariah and R. Mishra, *J. Phys. Chem. C*, 2019, **123**, 17644–17649.
379 P. Wang, N. Means, B. H. Howard, D. Shekhawat and D. Berry, *Fuel*, 2018, **217**, 642–649.
380 M. Jafarian, M. Arjomandi and G. J. Nathan, *Chem. Eng. Res. Des.*, 2017, **120**, 69–81.
381 X. Ao, H. Wang and Y. Wei, *Energy Convers. Manage.*, 2008, **49**, 2063–2068.
382 M. M. Sarafraz, M. Jafarian, M. Arjomandi and G. J. Nathan, *Int. J. Hydrogen Energy*, 2017, **42**, 16396–16407.
383 M. M. Sarafraz, M. Jafarian, M. Arjomandi and G. J. Nathan, *Appl. Energy*, 2017, **195**, 702–712.
384 M. M. Sarafraz, M. Jafarian, M. Arjomandi and G. J. Nathan, *Int. J. Hydrogen Energy*, 2018, **43**, 4195–4210.
385 D. C. Upham, Z. R. Snodgrass, M. T. Zavareh, T. B. McConnaughy, M. J. Gordon, H. Metiu and E. W. McFarland, *Chem. Eng. Sci.*, 2017, **160**, 245–253.
386 F. Li, L. Zeng and L.-S. Fan, *Fuel*, 2010, **89**, 3773–3784.
387 J. S. D. a. A. N. Hayhurst, *Chem. Eng. Sci.*, 1990, **45**, 1175–1187.
388 J. A. H. Oates, *Gaseous Effluents*, Wiley-VCH Verlag GmbH, 2007.
389 E. S. Rubin, S. Yeh, D. A. Hounshell and M. R. Taylor, Institute of Transportation Studies Working Paper, 2007, vol. 2, pp. 52–69.

390 J. R. Hufton, S. G. Mayorga and S. Sircar, *AIChE J.*, 1999, **45**, 248–256.
391 D. P. Harrison, *Ind. Eng. Chem. Res.*, 2008, **47**, 6486–6501.
392 B. Marcin, M. Vasilije, I. Qasim, A. M. Kierzkowska, E. J. Anthony and C. R. Müller, *Environ. Sci. Technol.*, 2013, **47**, 6007–6014.
393 D. P. Hanak, S. Michalski and V. Manovic, *Energy Convers. Manage.*, 2018, **177**, 428–452.
394 C. Han and D. P. Harrison, *Chem. Eng. Sci.*, 1994, **49**, 5875–5883.
395 B. Balasubramanian, A. Lopez Ortiz, S. Kaytakoglu and D. P. Harrison, *Chem. Eng. Sci.*, 1999, **54**, 3543–3552.
396 S. M. Kim, A. Armutlulu, A. Kierzkoska, D. Hosseini, F. Donat and C. R. Müller, *Sustainable Energy Fuels*, 2019, DOI: 10.1039/C9SE00619B.
397 A. Wang, N. Deshpande and L. S. Fan, *Energy Fuels*, 2015, **29**, 321–330.
398 D. P. Connell, D. A. Lewandowski, S. Ramkumar, N. Phalak, R. M. Statnick and L.-S. Fan, *Fuel*, 2013, **105**, 383–396.
399 N. Phalak, W. Wang and L.-S. Fan, *Chem. Eng. Technol.*, 2013, **36**, 1451–1459.
400 W. Peng, Z. Xu and H. Zhao, *Fuel*, 2016, **170**, 226–234.
401 D. P. Hanak, E. J. Anthony and V. Manovic, *Energy Environ. Sci.*, 2015, **8**, 2199–2249.
402 B. Duhoux, P. Mehrani, D. Y. Lu, R. T. Symonds, E. J. Anthony and A. Macchi, *Energy Technol.*, 2016, **4**, 1158–1170.
403 L. Zhou, L. Duan and E. J. Anthony, *Appl. Energy*, 2019, **235**, 480–486.
404 M. Samari, F. Ridha, V. Manovic, A. Macchi and E. J. Anthony, *Mitigation and Adaptation Strategies for Global Change*, 2019.
405 F. Donat and C. R. Müller, *Chem. Eng. J.*, 2018, **336**, 544–549.
406 B. Arias, G. S. Grasa, M. Alonso and J. C. Abanades, *Energy Environ. Sci.*, 2012, **5**, 7353–7359.
407 C. C. Dean, J. Blamey, N. H. Florin, M. J. Al-Jeboori and P. S. Fennell, *Chem. Eng, Res. Des.*, 2011, **89**, 836–855.
408 R. V. Kumar, R. K. Lyon and J. A. Cole, in *Advances in Hydrogen Energy*, ed. C. E. Grégoire Padró and F. Lau, Springer US, Boston, MA, 2002, pp. 31–45.
409 J. Kremer, A. Galloy, J. Ströhle and B. Epple, *Chem. Eng. Technol.*, 2013, **36**, 1518–1524.
410 B. Arias, M. E. Diego, J. C. Abanades, M. Lorenzo, L. Diaz, D. Martínez, J. Alvarez and A. Sánchez-Biezma, *Int. J. Greenhouse Gas Control*, 2013, **18**, 237–245.
411 M.-H. Chang, W.-C. Chen, C.-M. Huang, W.-H. Liu, Y.-C. Chou, W.-C. Chang, W. Chen, J.-Y. Cheng, K.-E. Huang and H.-W. Hsu, *Energy Procedia*, 2014, **63**, 2100–2108.
412 J. R. Fernández, J. M. Alarcón and J. C. Abanades, *Catal. Today*, 2019, **333**, 176–181.
413 I. Martínez, J. R. Fernández, M. Martini, F. Gallucci, M. van Sint Annaland, M. C. Romano and J. C. Abanades, *Int. J. Greenhouse Gas Control*, 2019, **85**, 71–85.
414 J. Chen, L. Duan, F. Donat, C. R. Müller, E. J. Anthony and M. Fan, *Chem. Eng. J.*, 2018, **351**, 1038–1046.
415 J. R. Fernández and J. C. Abanades, *Curr. Opin. Chem. Eng.*, 2017, **17**, 1–8.
416 J. M. Alarcón and J. R. Fernández, *Chem. Eng. Sci.*, 2015, **137**, 254–267.
417 F. N. Ridha, D. Lu, A. Macchi and R. W. Hughes, *Fuel*, 2015, **153**, 202–209.
418 V. V. Galvita, H. Poelman and G. B. Marin, *Top. Catal.*, 2011, **54**, 907–913.
419 V. V. Galvita, H. Poelman and G. B. Marin, *J. Power Sources*, 2015, **286**, 362–370.
420 L. C. Buelens, V. V. Galvita, H. Poelman, C. Detavernier and G. B. Marin, *Science*, 2016, **354**, 449–452.
421 J. Chen, L. Duan, T. Shi, R. Bian, Y. Lu, F. Donat and E. J. Anthony, *J. Mater. Chem. A*, 2019, **7**, 21096–21105.
422 M. Vasilije and E. J. Anthony, *Environ. Sci. Technol.*, 2011, **45**, 10750–10756.
423 K. Wang, P. T. Clough, P. Zhao and E. J. Anthony, *J. Mater. Chem. A*, 2019, **7**, 9173–9182.
424 F. N. Ridha, V. Manovic, A. Macchi, M. A. Anthony and E. J. Anthony, *Fuel Process. Technol.*, 2013, **116**, 284–291.
425 K. Wang, F. Gu, P. T. Clough, P. Zhao and E. J. Anthony, *Energy Fuels*, 2019, **33**, 7550–7560.
426 X. Ma, Y. Li, L. Duan, E. Anthony and H. Liu, *Appl. Energy*, 2018, **225**, 402–412.
427 L. Díez-Martín, J. M. López, J. R. Fernández, I. Martínez, G. Grasa and R. Murillo, *Chem. Eng. J.*, 2018, **350**, 1010–1021.
428 J. C. Abanades, R. Murillo, J. R. Fernandez, G. Grasa and I. Martínez, *Environ. Sci. Technol.*, 2010, **44**, 6901–6904.
429 J. R. Fernández and J. C. Abanades, *Chem. Eng. Sci.*, 2017, **166**, 144–160.
430 I. Martínez, M. C. Romano, J. R. Fernández, P. Chiesa, R. Murillo and J. C. Abanades, *Appl. Energy*, 2014, **114**, 192–208.
431 J. R. Fernández, J. C. Abanades, R. Murillo and G. Grasa, *Int. J. Greenhouse Gas Control*, 2012, **6**, 126–141.
432 M. Martini, A. van den Berg, F. Gallucci and M. van Sint Annaland, *Chem. Eng. J.*, 2016, **303**, 73–88.
433 L. Tan, C. Qin, Z. Zhang, J. Ran and V. Manovic, *Energy Technol.*, 2018, DOI: 10.1002/ente.201700894.
434 C. Qin, B. Feng, J. Yin, J. Ran, Z. Li and V. Manovic, *Chem. Eng. J.*, 2015, **262**, 665–675.
435 L. Diez-Martin, G. S. Grasa, R. Murillo, A. Scullard and G. Williams, *Ind. Eng. Chem. Res.*, 2018, **57**, 2890–2904.
436 A. L. García-Lario, M. Aznar, I. Martinez, G. S. Grasa and R. Murillo, *Int. J. Hydrogen Energy*, 2015, **40**, 219–232.
437 V. Manovic and E. J. Anthony, *Energy Fuels*, 2011, **25**, 4846–4853.
438 V. Manovic, Y. Wu, I. He and E. J. Anthony, *Ind. Eng. Chem. Res.*, 2011, **50**, 12384–12391.
439 A. M. Kierzkowska and C. R. Müller, *Energy Environ. Sci.*, 2012, **5**, 6061–6065.
440 A. M. Kierzkowska and C. R. Müller, *ChemPlusChem*, 2013, **78**, 92–100.
441 C. S. Martavaltzi and A. A. Lemonidou, *Chem. Eng. Sci.*, 2010, **65**, 4134–4140.
442 M. R. Cesário, B. S. Barros, C. Courson, D. M. A. Melo and A. Kiennemann, *Fuel Process. Technol.*, 2015, **131**, 247–253.
443 A. L. García-Lario, G. S. Grasa and R. Murillo, *Chem. Eng. J.*, 2015, **264**, 697–705.
444 M. V. Navarro, J. M. López, T. García, G. Grasa and R. Murillo, *J. Power Sources*, 2017, **363**, 117–125.

445 G. Grasa, M. V. Navarro, J. M. López, L. Díez-Martín, J. R. Fernández and R. Murillo, *Chem. Eng. J.*, 2017, **324**, 266–278.
446 P. S. Fennell, R. Pacciani, J. S. Dennis, J. F. Davidson and A. N. Hayhurst, *Energy Fuels*, 2007, **21**, 2072–2081.
447 J. Wang and E. J. Anthony, *Ind. Eng. Chem. Res.*, 2005, **44**, 627–629.
448 J. C. Abanades and D. Alvarez, *Energy Fuels*, 2003, **17**, 308–315.
449 C. Qin, J. Yin, W. Liu, H. An and B. Feng, *Ind. Eng. Chem. Res.*, 2012, **51**, 12274–12281.
450 S. S. Kazi, A. Aranda, L. D. Felice, J. Meyer, R. Murillo and G. Grasa, *Energy Procedia*, 2017, **114**, 211–219.
451 M. A. Naeem, A. Armutlulu, Q. Imtiaz, F. Donat, R. Schäublin, A. Kierzkowska and C. R. Müller, *Nat. Commun.*, 2018, **9**, 2408.
452 C. Dang, Y. Li, S. M. Yusuf, Y. Cao, H. Wang, H. Yu, F. Peng and F. Li, *Energy Environ. Sci.*, 2018, **11**, 660–668.
453 O. Kwon, S. Sengodan, K. Kim, G. Kim, H. Y. Jeong, J. Shin, Y.-W. Ju, J. W. Han and G. Kim, *Nat. Commun.*, 2017, **8**, 15967.
454 J. Y. Do, N. Son, N.-K. Park, B. S. Kwak, J.-I. Baek, H.-J. Ryu and M. Kang, *Appl. Energy*, 2018, **219**, 138–150.
455 J. Hu, V. V. Galvita, H. Poelman, C. Detavernier and G. B. Marin, *Appl. Catal., B*, 2018, **231**, 123–136.
456 D. Hosseini, P. M. Abdala, F. Donat, S. M. Kim and C. R. Müller, *Appl. Catal., B*, 2019, **258**, 117946.
457 https://www.iea.org/etp/tracking2017/chemicalsandpetrochemicals/.
458 T. Shimamura, K. Okumura, K. Nakagawa, T. Ando, N. O. Ikenga and T. Suzuki, *J. Mol. Catal. A: Chem.*, 2004, **211**, 97–102.
459 A. P. V. Soares, M. F. Portela and A. Kiennemann, *Catal. Rev.*, 2005, **47**, 125–174.
460 C. Brookes, P. P. Wells, N. Dimitratos, W. Jones, E. K. Gibson, D. J. Morgan, G. Cibin, C. Nicklin, D. Mora-Fonz, D. O. Scanlon, C. R. A. Catlow and M. Bowker, *J. Phys. Chem. C*, 2014, **118**, 26155–26161.
461 P. Forzatti, E. Tronconi, G. Busca and P. Tittarelli, *Catal. Today*, 1987, **1**, 209–218.
462 M. Ai, *J. Catal.*, 1982, **77**, 279–288.
463 V. V. Kaichev, Y. A. Chesalov, A. A. Saraev, A. Y. Klyushin, A. Knop-Gericke, T. V. Andrushkevich and V. I. Bukhtiyarov, *J. Catal.*, 2016, **338**, 82–93.
464 V. R. Chumbhale and P. A. Awasarkar, *Appl. Catal., A*, 2001, **205**, 109–115.
465 A. Kaddouri, C. Mazzocchia and E. Tempesti, *Appl. Catal., A*, 1999, **180**, 271–275.
466 M. D. Allen, S. Poulston, E. G. Bithell, M. J. Goringe and M. Bowker, *J. Catal.*, 1996, **163**, 204–214.
467 C. Zhao and I. E. Wachs, *J. Phys. Chem. C*, 2008, **112**, 11363–11372.
468 A. Chetouani, B. Taouk and E. Bordes-Richard, *Catal. Today*, 2004, **91–92**, 73–77.
469 W. E. Campbell, E. L. McDaniel, W. H. Reece, J. E. Williams and H. S. Young, *Product R&D*, 1970, **9**, 325–334.
470 J. M. López Nieto, P. Concepción, A. Dejoz, H. Knözinger, F. Melo and M. I. Vázquez, *J. Catal.*, 2000, **189**, 147–157.
471 P. M. Michalakos, M. C. Kung, I. Jahan and H. Kung, *J. Catal.*, 1993, **140**, 226–242.
472 J. Schulze and M. Homann, *C4-Hydrocarbons and Derivatives: Resources, Production, Marketing*, Springer Berlin Heidelberg, Berlin, Heidelberg, 1989, pp. 5–8.
473 J. M. Herrmann, J. Disdier, F. G. Freire and M. F. Portela, *J. Chem. Soc., Faraday Trans.*, 1995, **91**, 2343–2348.
474 N. C. Ramani, D. L. Sullivan, J. G. Ekerdt, J.-M. Jehng and I. E. Wachs, *J. Catal.*, 1998, **176**, 143–154.
475 X. Xia, R. Jin, Y. He, J.-F. Deng and H. Li, *Appl. Surf. Sci.*, 2000, **165**, 255–259.
476 W. Zhang, G. Innocenti, P. Oulego, V. Gitis, H. Wu, B. Ensing, F. Cavani, G. Rothenberg and N. R. Shiju, *ACS Catal.*, 2018, **8**, 2365–2374.
477 P. F. Zhang, H. F. Lu, Y. Zhou, L. Zhang, Z. L. Wu, S. Z. Yang, H. L. Shi, Q. L. Zhu, Y. F. Chen and S. Dai, *Nat. Commun.*, 2015, **6**, 10.
478 X. K. Yang, L. S. Yang, W. Fan and H. F. Lin, *Catal. Today*, 2016, **269**, 56–64.
479 K. T. V. Rao, J. L. Rogers, S. Souzanchi, L. Dessbesell, M. B. Ray and C. Xu, *ChemSusChem*, 2018, **11**, 3323–3334.
480 A. Bielański and M. Najbar, *Appl. Catal., A*, 1997, **157**, 223–261.
481 H. K. Matralis, C. Papadopoulou, C. Kordulis, A. Aguilar Elguezabal and V. Cortes Corberan, *Appl. Catal., A*, 1995, **126**, 365–380.
482 T. Li, F. Liu, Y. Tang, L. Li, S. Miao, Y. Su, J. Zhang, J. Huang, H. Sun, M. Haruta, A. Wang, B. Qiao, J. Li and T. Zhang, *Angew. Chem. Int. Ed.*, 2018, **57**, 7795–7799.
483 M. Biswal, V. V. Dhas, V. R. Mate, A. Banerjee, P. Pachfule, K. L. Agrawal, S. B. Ogale and C. V. Rode, *J. Phys. Chem. C*, 2011, **115**, 15440–15448.
484 S. S. Negi, A. T. Venugopalan, T. Raja, A. P. Singh and C. S. Gopinath, *RSC Adv.*, 2014, **4**, 57087–57097.
485 Y. I. Pyatnitskii and G. I. Golodets, *React. Kinet. Catal. Lett.*, 1976, **5**, 345–351.
486 A. F. D'Alessandro and A. Farkas, *J. Colloid Sci.*, 1956, **11**, 653–670.
487 S. Biswas, B. Dutta, K. Mullick, C. H. Kuo, A. S. Poyraz and S. L. Suib, *ACS Catal.*, 2015, **5**, 4394–4403.
488 J.-C. Lin, J. Chen, S. L. Suib, M. B. Cutlip and J. D. Freihaut, *J. Catal.*, 1996, **161**, 659–666.
489 Y. Lao, N. Zhu, X. Jiang, J. Zhao, Q. Dai and X. Wang, *Catal. Sci. Technol.*, 2018, **8**, 4797–4811.
490 J. Chen, D. Yan, Z. Xu, X. Chen, X. Chen, W. Xu, H. Jia and J. Chen, *Environ. Sci. Technol.*, 2018, **52**, 4728–4737.
491 X. Wang, W. Zhao, X. Wu, T. Zhang, Y. Liu, K. Zhang, Y. Xiao and L. Jiang, *Appl. Surf. Sci.*, 2017, **426**, 1198–1205.
492 X. Weng, W. L. Wang, Q. Meng and Z. Wu, *Catal. Sci. Technol.*, 2018, **8**, 4364–4372.
493 S. Zhao, K. Li, S. Jiang and J. Li, *Appl. Catal., B*, 2016, **181**, 236–248.
494 J. Perez-Ramirez and E. V. Kondratenko, *J. Catal.*, 2007, **250**, 240–246.
495 F. Zhang, X. Zhang, G. Jiang, N. Li, Z. Hao and S. Qu, *Chem. Eng. J.*, 2018, **348**, 831–839.
496 S. Yasyerli, G. Dogu, I. Ar and T. Dogu, *Chem. Eng. Sci.*, 2004, **59**, 4001–4009.